IMAGING THE KHEIS TERRANE CRUSTAL STRUCTURES: AN INTEGRATED MAGNETOTELLURIC – SEISMIC – MAGNETIC – GEOLOGICAL STUDY

by

Malaika Motsoai

(1604192)

Dissertation

Submitted in fulfilment of the requirements for the degree

Master of Science

in

Geophysics

in the Faculty of Science, University of the Witwatersrand, Johannesburg, South Africa

Supervisor: Prof Musa Manzi
University of the Witwatersrand

Co-Supervisor: Dr Stephanie Enslin-Scheiber
University of the Witwatersrand

Co-Supervisor: Dr David Khoza
Integrated Geoscience Solutions (IGS)

December 2024

DECLARATION

I declare that this dissertation is my own, unaided work. It is being submitted for the Degree of Master of Science at the University of the Witwatersrand, Johannesburg. It has not been submitted before for any degree or examination at any other University.

(Signature of candidate)

___12th___________day of _______December_________20______24________at__Johannesburg___

Abstract

The Kheis Province and Kaaien Terrane in the Northern Cape have challenges in understanding their substructure due to the complex subsurface and limited geophysical imaging. Recent studies advocate for revising their classification and merging them into the Kheis Terrane, yet detailed geological mapping has been insufficient to reach a consensus. Addressing this, my study employs 3D magnetotelluric (MT) inversion modelling and seismic-MT cross-sections to attempt to enhance understanding the Kheis Terrane. The MT data analysis reveals electrical anisotropy and structural complexity in the subsurface, supported by apparent resistivity plots and phase diagrams. Penetration depth analysis indicates variations in subsurface resistivity up to 200 km below the surface, with phase tensor maps showing predominantly NW-SE oriented 2-D structures. 3D inversion modelling provides insights into resistive and conductive zones, validated by integration with seismic and magnetic data. The proposed geological model confirms the Kheis Terrane's boundaries and supports the 'Kheis Event' theory, suggesting a tectonic collision between the Namaqua-Natal Metamorphic Province and the Kaapvaal Craton. This study suggests that the Kheis Terrane is interlocked with the craton and extends approximately 20 km deep. This comprehensive approach enhances our understanding of the region's geological evolution and provides valuable insights for further research.

Acknowledgements

I would first like to express my deepest gratitude to my supervisors, Prof. Musa Manzi, Dr Stephanie Enslin-Scheiber and Dr David Khoza for their support and guidance. I approached Prof. Musa Manzi about doing a magnetotelluric MSc project integrated with seismics and he gave me the resources and exposure to learn and grow during my research projects. All the field projects, consultations and advice taught me a lot about geophysics and how to be a meaningful geophysicist in society and for that I will be eternally grateful. Dr Stephanie Enslin-Scheiber worked tirelessly to make sure that I have the right assistance and resources to make sure that I finish, from the administration that came with the project to the consultations of the various directions to take, thank you for always being available to help. Dr David Khoza, for sharing your expertise with me in magnetotellurics and providing advice on the magnetotelluric theory and working with the magnetotelluric data, your advice helped me understand magnetotellurics more than I ever thought I would and for that, thank you.

I would like to thank Minenhle Khoza from the Council for Geosciences (CGS). She held my hand and supported me throughout my MSc journey. From training me in the field on how to acquire MT data, to guiding me on the various processes to follow when processing MT data. Your patience and kindness allowed me to learn and finish my research project. Thank you for your efforts in making sure I have the MT data and the consultations on how to understand and process my data. I would also like to thank the Council for Geoscience (CGS) for providing the MT data, the original seismic reflection data and the regional total field magnetic data set, that I used for my research project.

I would like to thank Prof. Ken Nixon and Nicholas Warrener from the School of Electrical Engineering and Information Engineering, for letting me to use their computer cluster which allowed me to successfully complete my 3D MT inversions. Your patience and guidance in making sure that the cluster works well for my research is appreciated.

I would like to thank the National Research Foundation (NRF) and Boart Longyear, for sponsoring this research.

I would like to thank the Wits University Geoscience Department staff and students for creating a positive working environment and providing me with advice and guidance on various problems I had. Thank you for the companionship that I found in some of you, which inspired me to keep going.

I would like to thank my friends and most importantly my family. Your support throughout this journey is appreciated.

Lastly, as uTshatshu, Tubhane, Mawuse, Qhumapase, Maphasa, Gungubele. I would like to acknowledge and thank those who come before me, and the higher powers controlled by God for guiding and protecting me. May my journey and actions inspire those who come after me to do and be great.

"If you could choose to be anything in life, choose to be kind."

Table of Contents

Table of Figures

List of Tables

List of Abbreviations and variables

Abbreviations

MT	Magnetotellurics
NNMP	Namaqua-Natal Metamorphic Province
Z	Impedance
T	Tipper
TE	Transverse Electric
TM	Transverse Magnetic
RMS	Root Mean Square
CGS	Council for Geoscience
EDI	Electromagnetic Data Interchange (format)
WAL	Weaver, Agarwal, Lilley invariants
TMI	Total Magnetic Intensity
mgal	Milligal (gravity unit)

Mathematical variables and constants

E: Electric field

B: Magnetic field

Zxx, Zxy, Zyx, Zyy: Components of the impedance tensor, (x, y) - horizontal directions.

p: Skin Depth, $p = \frac{1}{Re(q)} = \sqrt{\frac{2}{\mu_0 \sigma \omega}}$

q: Penetration depth

$\boldsymbol{\mu_0}$: Magnetic permeability of free space, $\mu_0 = 1.2566 \times 10^{-6} H/m$

σ: Electrical conductivity

ω: Angular frequency of electromagnetic waves, ω$= 2\pi f$

t: Period of the electromagnetic field

A, B: Components of the electric field

Φ: Phase angle of impedance

ρ (apprho): Apparent resistivity

θ: Angle of impedance tensor rotation

R: Cartesian rotation matrix

Introduction

The Northern Cape's Kheis Province and Kaaien Terrane have been a topic of debate in the geoscientific community (e.g. (Van Niekerk, (2006); (Cornell & Pettersson, (2007); Hanson (2003))) due to their structurally complex subsurface and limited imaging of their crustal structures. This is mainly due to the Kalahari sediment cover, making it hard to identify geological outcrops. The Kaaien Terrane is a single fault-bounded rock body situated along the eastern boundary of the Namaqua Tectonic Zone(van Niekerk & Beukes, 2019), linked through geochronology to the 'Ubendian event' (Hanson, 2003) and thus a similar age to the Magondi and Piriwiri groups in Zimbabwe. The Kheis Province is a thin-skin folded thrust belt situated along the western boundary of the Kaapvaal Craton (van Niekerk & Beukes, 2019) that was probably caused by an impending collision between the Congo and Kaapvaal-Zimbabwe cratons which caused the folding and metamorphism known as the Ubendian event (Tinker et al. (2002); Unrug (1992)).

Stratigraphic classification of this region has been met with lots of debate, with van Niekerk & Beukes (2019) highlighting the need of a careful revision of the stratigraphic subdivisons due to the discrepancies that stem from the fact that most of the mapping and intepretation of this region being done in the southernmost region of the Kheis Province and Kaaien Terrane region where there is relatively good outcrop. The area further north, although less complex, has very poor exposure, leading to less detailed mapping. This led to a very uncertain and incomplete understanding of the region as it mainly relied on the southern region's information.

Despite minimal mapping done in the northern region of the Kheis Province and Kaaien Terrane, van Niekerk & Beukes (2019) compared geology, satelite imaging , and aeromagnetic data to demonstrate a consistent and persistent lithostratigraphy of the rocks in the northern and southern region of the Kheis Province and Kaaien Terrane. van Niekerk & Beukes (2019) suggested combining the Kheis Province and the Kaaien Terrane to form what they termed the Kheis Terrane. Positioned as a highly faulted wedge, the Kheis Terrane lies along the western edge of the Kaapvaal Craton and the eastern area of the Namaqua Tectonic Zone. It comprises of rocks of the Keis supergroup and is also bounded by the

Blackridge thrust in the east, the Kalahari line in the west and the Trooilspspan shear zone in the southwest (van Niekerk & Beukes, 2019) *(see Figure 1)*.

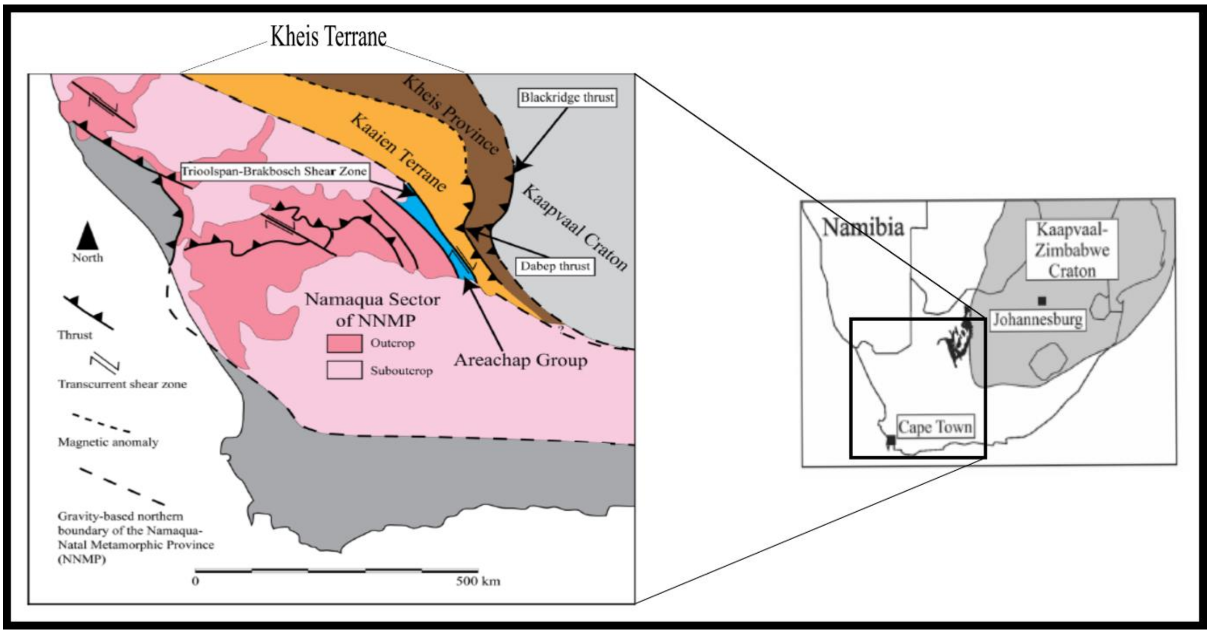

Figure 1: Modified geological map of the western portion of South Africa. The map shows the Kaaien Terrane and Kheis Province wedged between the Namaqua-Natal Metamorphic Province (NNMP) and the Kaapvaal Craton. It shows thrust and fault zones which act as boundaries between the formations, with the Blackridge thrust acting as a boundary between the Kheis Province Kaapvaal Craton, the Dabep thrust acting as a boundary between the Kaaien Terrane and Kheis Province and the Trioolspan-Brakbosch Shear Zone acting as a boundary with the Namaqua-Natal Metamorphic Province. (van Niekerk & Beukes, 2019).

However, a significant gap in the study by van Niekerk & Beukes (2019) arises from the lack of detailed mapping of the underlying structure of the Kheis Terrane to support their assertions. Various geophysical investigations have been carried out in the area, including reflection seismic surveying (Tinker et al., 2002) and a NE-SW magnetotellurics survey in the Northern Cape Province, covering the western perimeter of the Kaapvaal Craton (E. H. Stettler et al., 1999). This survey deployed stations at Inkruip, Paleisheuwel, Waaihoek, Olifantshoek, and Roscoe, spaced 20 km apart, following an existing seismic line labelled SAGS-02-91. E. H. Stettler et al. (1999) integrated magnetotelluric (MT) datasets with the seismic data from SAGS-02-91, gathered from 1989 using a vibroseis source along the main road between Sishen, Upington, and Keimoes, covering a distance of 226 km with an imaging penetration depth of approximately 50 km, to construct a 2-D model of the subsurface structure of the

Kheis Terrane. In the past, magnetotellurics (MT) and seismic acquisition and processing faced limitations like low signal strength, static shift distortions, poor spatial resolution, and 2D modelling of complex 3D structures. Seismic surveys also suffered from limited penetration depth, poor vertical and lateral resolution, and time-consuming data processing. These issues have since been improved through advancements in technology, such as more sensitive MT instruments, 3D inversion modelling, better static shift corrections, high-performance computing, and denser seismic receiver arrays, allowing for more accurate and detailed subsurface imaging. This means that old datasets containing various uncertainties, including challenges in accurately delineating the lithological complexities within the Kheis Terrane and determining the boundaries between the Kaapvaal Craton and the Kheis Terrane can now be improved upon with recent advancements in data acquisition and processing of MT and seismic data. Expanding upon the geological work of van Niekerk & Beukes (2019) and enhancing the geophysical methodology employed by E. H. Stettler et al. (1999), this study develops a scientifically grounded model of the geological crustal structures, thereby contributing to a deeper comprehension of the Kheis Terrane's crustal configuration. It investigates the nature of the boundary (geometry and depth extent) between the Kheis Province and the western edge of the Kaapvaal Craton, as well as the boundary between the Kheis Province and the eastern edge of the Kaaien Terrane. With the improvement in the technology behind the acquisition and processing of MT and seismic datasets, this study uses recently acquired MT data, the Council for Geoscience (CGS) SAGS-02-91 co-located seismic data, CGS magnetic, and CGS geological data to create a 3D MT inversion model, a 2D integrated seismic-MT cross-section and geologic model. The interpretation of this 2D cross-section aims to improve existing geoscientific data of the region. The datasets also used to provide a clear image and better understanding of the crustal and upper mantle structures along the Kheis Terrane.

Furthermore, this study probes into the established hypothesis of the 'Kheis Event,' positioning a tectonic collision between the Namaqua Natal Province and the Kaapvaal Craton, driving the genesis of the Kheis Terrane.

This thesis is structured as follows: Chapter 1 is the regional geological setting of the Kheis Terrane region. It discusses the tectonic evolution of the region, and lithologies occurring in the area and provides a stratigraphy of the area. In addition, the chapter also discusses previous geological studies made in the area.

Chapter 2 delves into the previous geophysical studies conducted in the area. Work done by Stettler et al. (1998, 1999) is discussed which aims to provide context on what geophysical work has been done and needs to be improved.

Chapter 3 provides a comprehensive overview of the magnetotelluric (MT) method. It outlines the historical background, theoretical foundations based on Maxwell's equations, and practical applications. The discussion includes a brief derivation of impedance and skin depth equations, interpretation of the MT impedance tensor for different subsurface dimensions, and considerations for analysing MT data in various geological scenarios. Additionally, it covers the sources of electromagnetic fields and the wide range of electrical resistivity/resistivity of Earth materials, underscoring MT's effectiveness in investigating lithospheric structures and composition.

Chapter 4 delves into the methodology and data acquisition process of MT surveys, drawing from practical experience in the field. It outlines the steps involved in MT acquisition, including community engagement, equipment setup, and site deployment. Various tools and equipment are detailed along with their roles in the process. The chapter also covers data analysis techniques, including quality control, dimensionality analysis, rotation, TE/TM mode assignment, and inversion methods. Furthermore, it discusses software packages used for data processing, emphasizing the importance of accurate interpretation for understanding subsurface conductivity structures. Through a comprehensive approach, the chapter provides insights into the complexities and nuances of MT surveying and analysis.

Chapter 5 presents findings from the acquired MT dataset survey revealing complex geoelectric structures. Analysis of the MT dataset is shown using depth transformations, phase tensor maps, strike analyses and dimensionality analyses, which show anisotropy and conductivity variations in the region. Based on these findings, a 3D inversion method was chosen to construct a reliable geoelectric model. Chapter 6 provides a detailed comparison of the 2D cross sections generated from two different models, emphasizing the benefits of using both impedance and tipper data in inversion for subsurface resistivity structures. Through the integration of magnetotelluric (MT) and seismic data, the chapter reveals distinct resistive and conductive zones, shedding light on the geological structures of the Kheis Terrane in Southern Africa. By correlating MT and magnetic data, linear features and lithostratigraphy are delineated, aiding in proposing geological subdivisions. A geological model is also proposed which suggests a complex terrane boundary and folding within the Kheis Terrane. Chapter 7 provides a conclusion based on the results and discussion made in chapter 6 and 5. Recommendations are also made.

Chapter 1. Geology

Tectonic evolution

The Northern Cape province in South Africa is characterized by a diverse geology shaped by hundreds of millions of years of geological processes. It is mainly known to encompass various crustal entities with complex geological formations and landscapes, including the Namaqua-Natal Metamorphic Province (NNMP), and the Kaapvaal Craton.

The Namaqua-Natal Metamorphic Province region is composed of ancient metamorphic rocks dating back to over 1.5 Ga. These rocks have undergone intense heat and pressure, resulting in their metamorphism. They include gneisses, schists, and granites. The Kaapvaal Craton forms the stable core of the Southern African continent. It consists of ancient granite-greenstone terranes and is one of the oldest geological formations on Earth, dating back over 3 billion years. During the Archean Eon, the NNMP and Kaapvaal Craton collided and formed part of a larger tectonic process that led to the formation of the Bushmanland, the Kakamas Domain, the Areachap and the Kheis Terrane (Cornell & Pettersson, 2007) *(see Figure 2)*.

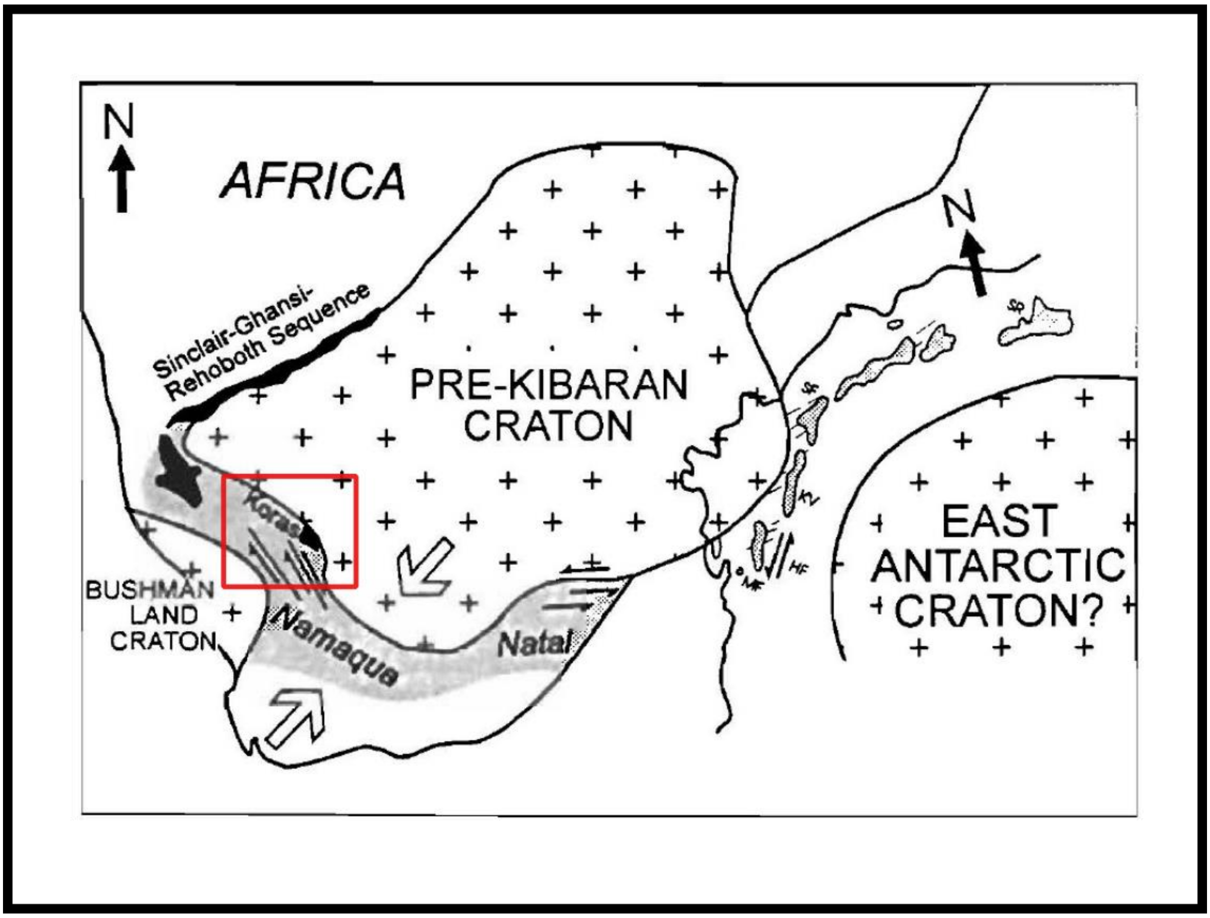

Figure 2: Modified tectonic sketch map of the Namaqua-Natal Metamorphic Province (after Jacobs et al., 1993). *In each area early thrusts are directed northeast and/or southwest, during the initial accretionary orogenic* phase (Thomas et al., 1994). *The outlined red block indicates the study area.*

The Kheis Terrane formed as part of a back-arc basin (Cornell & Pettersson, 2007), with the subduction of the oceanic crust and closure of the oceanic basins during the collision and assemblage of the Bushmanland, Kakamas, Areachap, and Kheis Terranes from east to west respectively *(see Figure 3)* between ~1300 Ma and 1180 Ma (Cornell & Pettersson, 2007). This event has been coined the 'Kheis Event'. This also resulted in a high-grade metamorphic and multiple granitoid intruded region that we now refer to as the Namaqualand Metamorphic Province (Thomas et al., 1994).

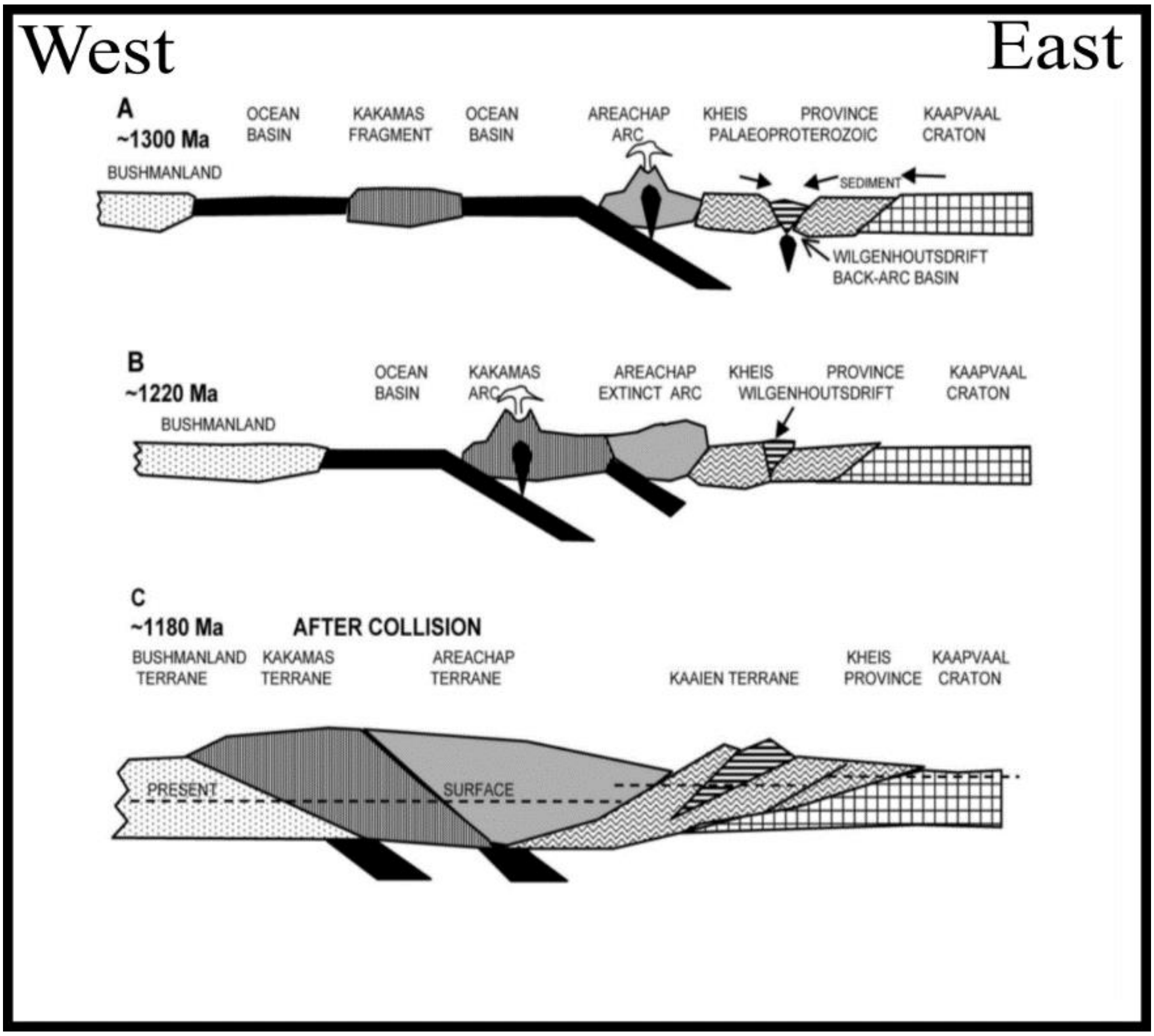

Figure 3: East-West tectonic sketch across NNMB-Kheis Province-Kaapvaal craton (See Fig 1) (A) and (B) show the configurations of crustal blocks and ocean basins at two stages of evolution between ~1300 Ma and ~1220 Ma, and (C) (enlarged by a factor two) shows how they were assembled to form the present-day configuration (Cornell & Pettersson, 2007).

Geological studies in the region

In Van Niekerk (2006), an in-depth investigation was undertaken to tackle several intricacies pertaining to the geological structure of the Kheis Terrane and its interconnection with the Areachap Group and Namaqua-Natal Metamorphic Province. This research yielded significant findings. Table 1 shows the new stratigraphic units of the proposed Keis Supergroup, as suggested by Van Niekerk (2006).

Table 1: Table showing the new stratigraphic units of the Keis Supergroup, as suggested by Van Niekerk (2006).

Wilgenhoutsdrif Group	**Keis Supergroup**
Groblershoop Group	
Olifantshoek Group	
Elim Group	

This stratigraphic interpretation, in turn, outlined the internal compositional structure of the Kheis Supergroup, which was established as comprising the Elim- Olifantshoek-, Groblershoop-, and Wilgenhoutsdrift Groups (Van Niekerk, 2006) resulting in some rock formations being moved into the Transvaal Group.

Van Niekerk (2006), suggested the Dabep fault should not be perceived as the representative terrane boundary. Instead, this research suggested that the Blackridge fault might serve as the genuine terrane boundary separating the Kheis Terrane from the Kaapvaal Craton rocks (Van Niekerk, 2006).

Furthermore, a key revelation emerged concerning the contact between the Wilgenhoutsdrif Group and the underlying Groblershoop Group. The analysis pointed towards an unconformable contact rather than a structural contact, implying that it may have acted as a low-friction fault plane separating the two rocks (Van Niekerk, 2006).

In summation, Van Niekerk (2006) made substantial contributions to the understanding of the geological structure of the Kheis Terrane and its relationships with the Areachap Group and Namaqua-Natal Metamorphic Province, reshaping stratigraphic understandings, terrane boundaries, and the nature of key geological contacts within this region. This study will therefore attempt to provide substantial evidence that supports these findings.

Stratigraphy

van Niekerk & Beukes (2019) are advocating for the stratigraphic units of this region to be grouped into the Kheis Supergroup rather than the Kheis Province as still described in Johnson et al. (2006). The group is defined as a middle Paleoproterozoic to late Mesoproterozoic succession. The supergroup is subdivided from the base into the Elim-, Olifantshoek-, Groblershoop- and Wilgenhoutsdrif Group, where the Elim- and Olifantshoek Group is part of the Kheis Province and the Groblershoop and Wilgenhoutsdrift Groups are part of the Kaaien Terrane (van Niekerk & Beukes, 2019). The metasedimentary rocks of the Olifantshoek Group and Groblershoop Group were deposited in a shallow continental margin on the western side of the Kaapvaal-Zimbabwe Craton and the rocks of the Wilgenhoutsdrift Group overlay the Groblershoop Group unconformably. Figure 4 shows the revised lithostratigraphic units of the Kheis Province and Kaaien Terrane. Figure 4 also shows the two thrust faults namely Dabep and Blackridge Thrust, which are considered to be the boundaries between the Kaaien Terrane and Kheis Province and the boundary between the Kheis Terrane (Province) and Kaapvaal Craton, respectively.

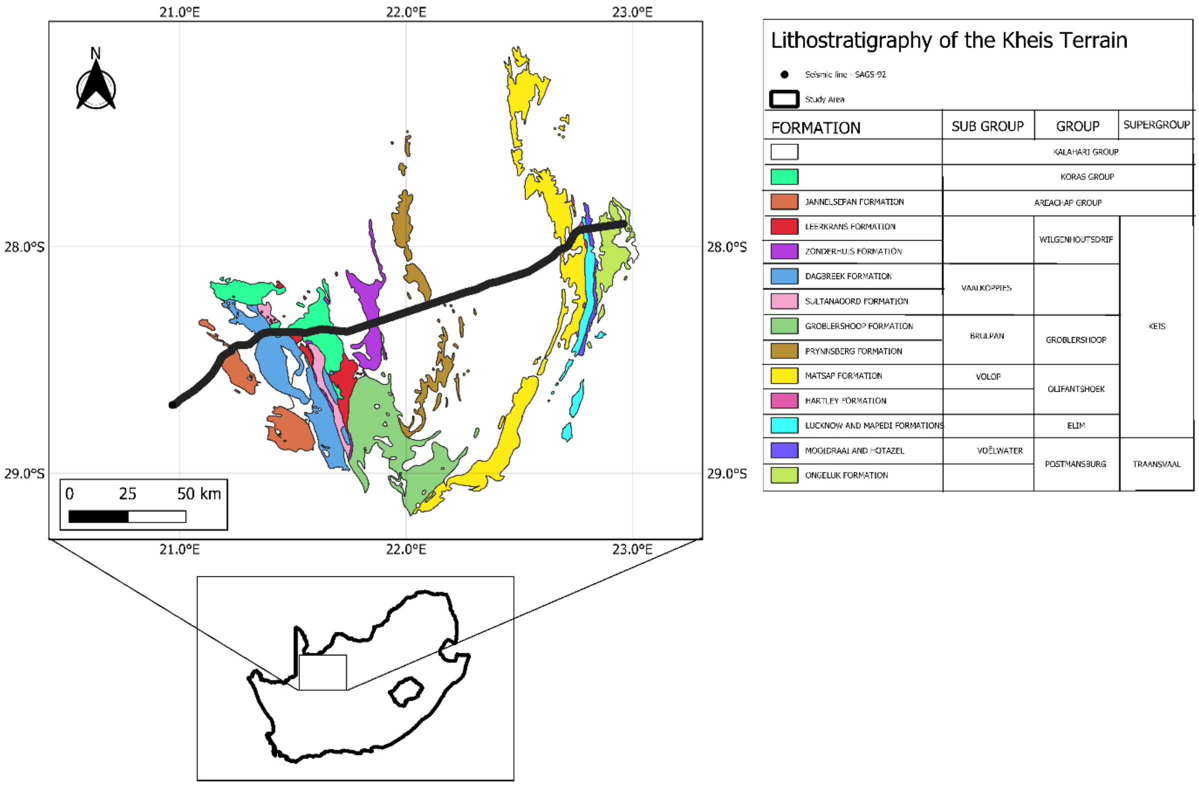

Figure 4: Geological map of the Kheis Terrane. Geological information was obtained from the Council for Geosciences.

Geological setting

When looking at the regional geology of the study area (*see* Figure 4), it is observed that the easternmost region (east of the Kheis Supergroup) consists of the dolomitic series of the Transvaal Supergroup (In the Postmansburg Group) which are succeeded conformably by a suit of banded ferruginous and siliceous sediment rocks with a considerable thickness of volcanic rocks featuring prominently (Boardman & Visser, 1958).

Resting unconformably on the rocks of the Elim Group are grey to purplish quartzite, reddish shale, and conglomerate which belong to the Olifantshoek Group that form the Langerberg Mountains. The Olifantshoek Group rocks are then overlain by a northward-plunging anticline on the Blackridge Thrust. (Boardman & Visser, 1958). Overlying the Olifantshoek Group rocks, a large section of sandstone, quartzite, and basalt is found which belongs to the Groblershoop Group but below a cover of Kalahari. This is where the main Kheis System is situated.

The Kheis System is a stratum of sedimentary and volcanic rocks. Regional deformation (up doming) occurred in the Kheis Strata and caused the Kheis rocks to fold around a fold axis with an east-west direction. This then produced intense shearing and resulted in the metamorphism of the sediments, resulting in intense folding in the N-S axes and observed quartzite outcrops towards the middle of the region. This intense folding is expected to be followed by a tensional phase; therefore, faulting would be expected in this region (Von Backstrom & De Villiers, 1972). The rocks in this middle region are characterized by regional folds with north-south trending fold-axial surfaces and consist of mostly the Faansgeluk, Faanshoop, and Vuilnek formations of the Grobblershoop Group rocks.

Towards the end of the western region, is a highly complex geological region. This is where sedimentary rocks and lavas correlated with the Kheis System, have been extensively intruded by granitic rock which resulted in metamorphism of various stages. This region is also characterized by regional folds with northwest-southwest-trending fold axial traces as indicated by the Opwag and Skurweberg fms.

Chapter 2. Previous geophysical studies

Multiple geophysical studies have been conducted over the region. These include magnetic, gravity, seismic, and electrical studies. The following are some of the geophysical studies done in the area.

J. H. De Beer (1978) conducted a magnetometer array study aimed at determining the susceptibility of tectonic provinces in Southern Africa. The results from their study argued against the hypothesis that all southern African mobile belts have traces of subduction zones for the areas investigated. They also conducted geoelectrical investigations that showed no large high conductivity structures along the boundary between the Kaapvaal Craton and the Namaqua-Natal Mobile Belt that could possibly be associated with traces of oceanic floor (De Beer, 1978).

De Beer & Meyer (1984) used regional gravity data to observe that the boundaries of the NNMP have distinct geophysical signatures. The work done by De Beer & Meyer (1984) suggests that the Bouguer values in younger provinces are consistently higher than in older provinces. This is mainly due to the crustal densities of younger provinces being higher than that of older provinces (De Beer & Meyer, 1984). In this case, Figure 5 shows that most of the NNMP has a broadly high Bouguer gravity signature, suggesting it is a younger province than the Kaapvaal Craton which shows broadly relatively lower Bouguer values. However, De Beer & Stettler (2015) show the BMA to coincide with a negative (AH30) isostatic gravity anomaly. The Kheis Terrane can be observed to act as a transitional zone as it consists of intermediate Bouguer values. Based on the evidence gathered by De Beer & Meyer (1984), they suggested that rather than being a boundary between two tectonic plates, the shear zone along the Namaqua-Natal Front (in the Kheis Terrane) could be within the Kaapvaal Craton. They also speculate that this boundary might indicate the emergence of a deeper shear zone from beneath the Namaqualand gneisses to the surface (De Beer & Meyer, 1984).

The work done by De Beer (1978) and De Beer & Meyer (1984) suggests that the boundary between the NNMP and Kaapvaal Craton may not be a subductive zone, but rather a shear zone. Subduction of an oceanic crust is suggested in the lower region of the NNMP however, that is beyond the scope of this research.

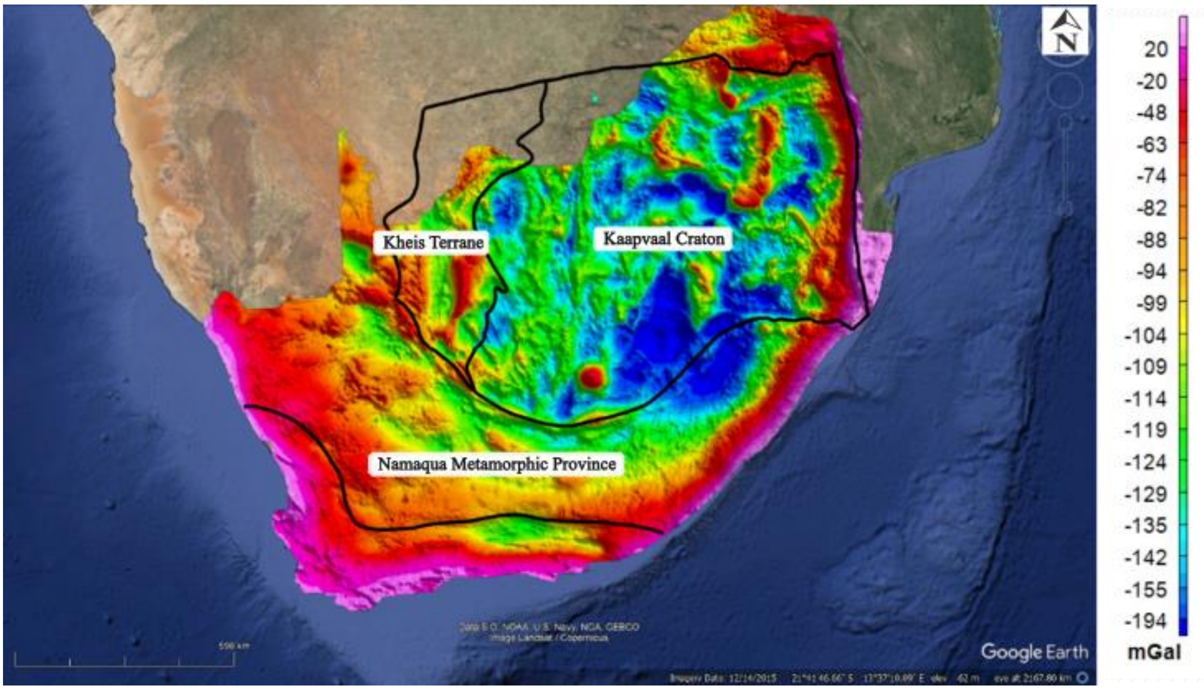

Figure 5: The CGS regional Bouguer gravity map of South Africa. The map shows the Bouguer gravity signatures of the Kaapvaal Craton, Kheis terrane, and Namaqua Metamorphic Province (NNMP) which are bounded by black lines. The maps show that younger provinces such as the NNMP have higher Bouguer gravity signatures than that of the Kaapvaal Craton. The Kheis Terrane portrays as a transition between the Kaapvaal Craton and NNMP by having intermediate Bouguer gravity signatures (Fourie & Cole, 2000).

In 1989, a deep seismic reflection survey labeled SAGS-02-91 was conducted using a vibroseis source along the main road between Sishen, Upington, and Keimoes in Northern Cape, South Africa, with a distance of 226 km (E. H. Stettler et al., 1999). Stettler et al. (1998, 1999) sought to further understand the structure and history of the Namaqua Metamorphic Province using the SAGS-02-91 reflection seismic, magnetotellurics, gravity and magnetic data over the Kheis Terrane. The geophysical dataset used in E. H. Stettler et al. (1998) study only covers the region between Keimos and Avondale *(see Figure 6 and Figure* 7*)*. Studies by E. H. Stettler et al. (1999) focused on the area between Avondale, Roscoe, and Olifantshoek, *(see Figure 6)*. The reflection seismic data were only able to provide information on the gross structure of the region. However Tinker et al. (2002) describe deep reflection seismic surveys, using the KBF01 conducted on the Kaapvaal craton, covering the Olifantshoek Supergroup and latching onto the eastern part of SAGS-02-91. Tinker et al. (2002) identified thrusting of the lower Olifantshoek and upper Griqualand strata, and their studies support the idea that the Kaapvaal Craton was once part of a significantly larger continent.

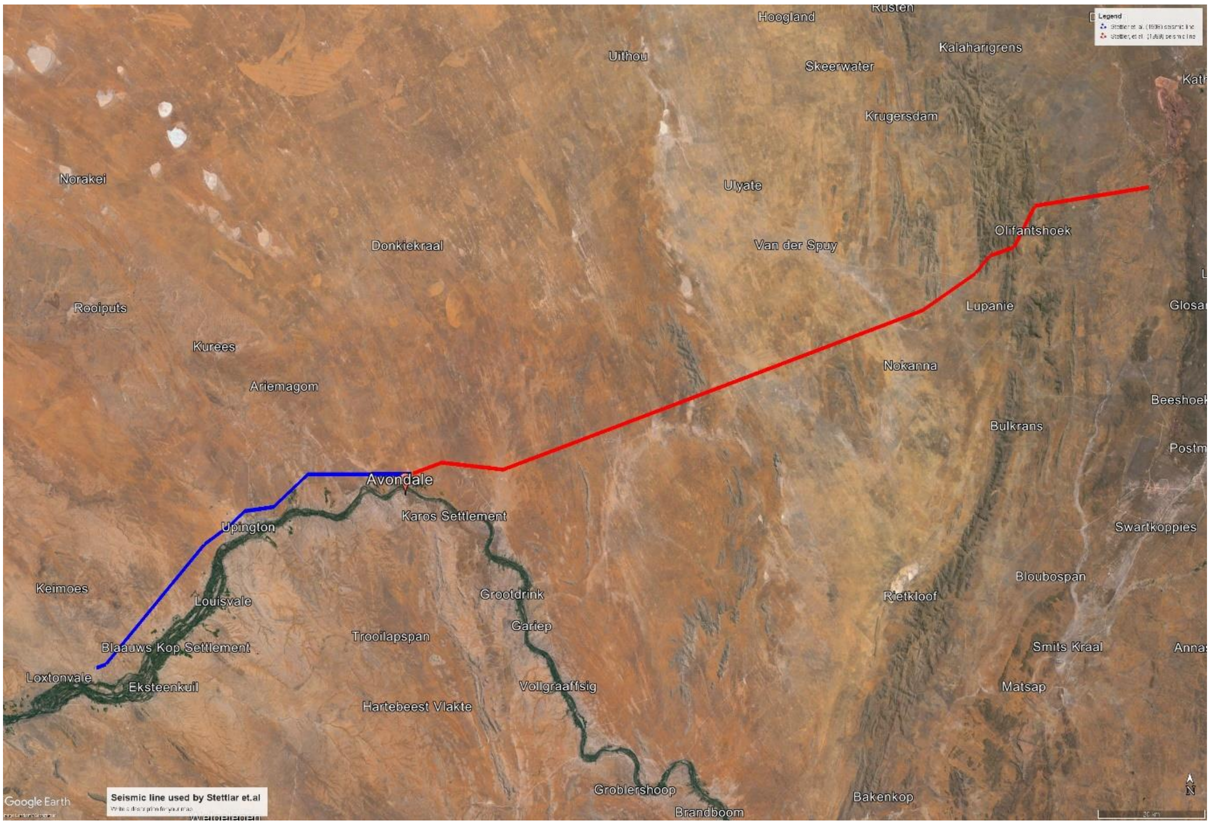

Figure 6: Google Earth map showing the seismic lines used by Stettler et al. (1998, 1999). The blue line represents the line Stettler et al. (1998) used, and the red line represents the line Stettler et al. (1999) used. The two lines combined represent the SAGS-02-91 seismic line which is also used in this study.

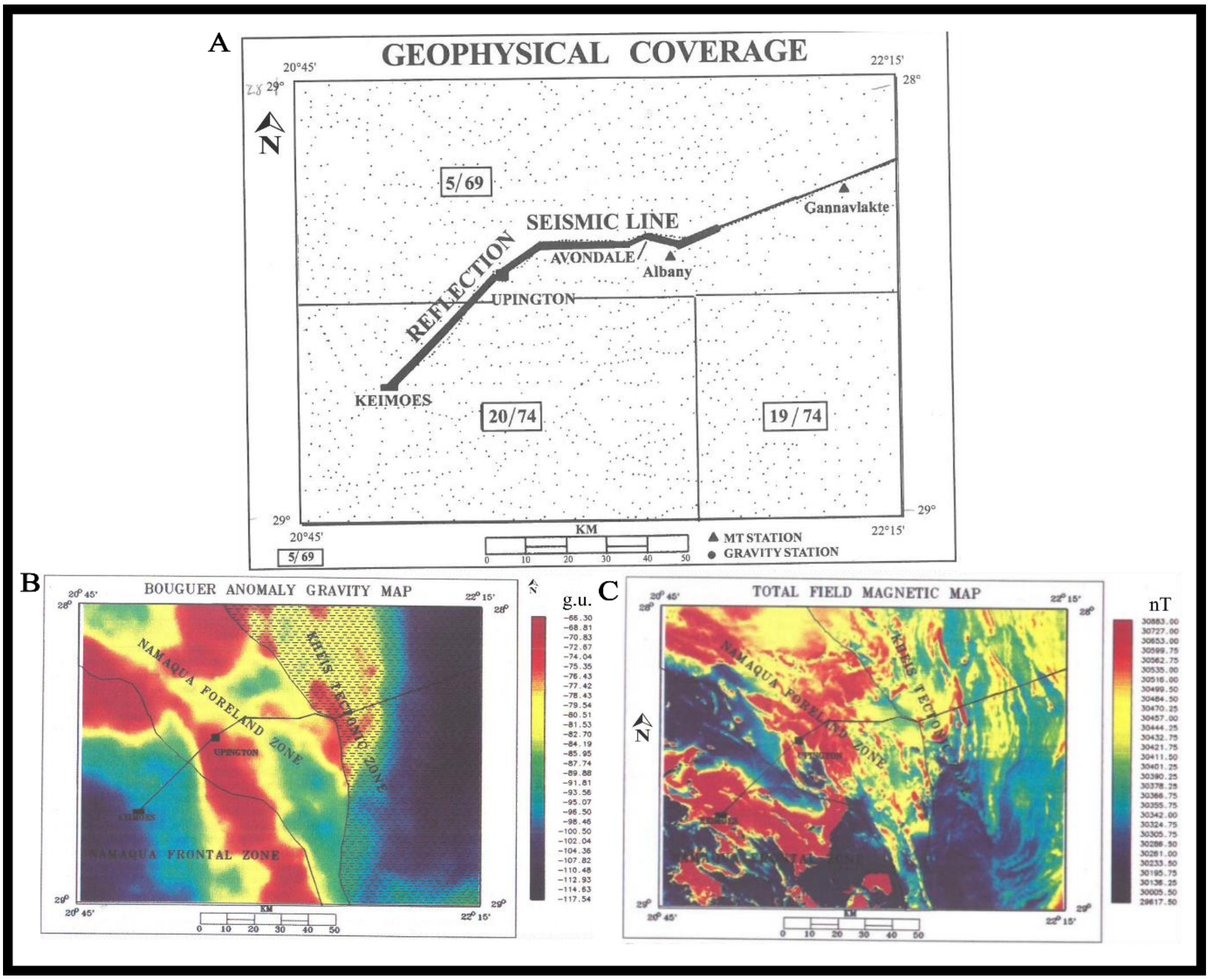

Figure 7: Geophysical coverage between Keimoes and Avondale of the (SAGS-02-91) seismic profile (E. H. Stettler et al., 1998). a) Shows the seismic line and gravity stations. b) Shows the Bouguer gravity map and c) shows the total magnetic field map.

The gravity data shown in *Figure 7b* were interpreted to define the Kheis system by a Bouger gravity low which signifies rocks of average crustal density of (2670 km/m^3) or less while the Namaqua Foreland Zone is defined by a gravity high, with a presence of higher density material (Stettler et al., 1998).

The magnetic data shown in *Figure 7c* was interpreted to be semi-vertical, moderately magnetic units with north-northeast to northeast fold axes typical of low and medium grade metamorphic terrains. The Namaqua Foreland Zone contains highly magnetic units with a pattern indicative of high grade metamorphism (Stettler et al., 1998).

On the SAGS-02-91 reflection seismic section between Keimos and Avondale *(see Figure 8b),* reflectors marked with an A indicate the presence of a basin like feature which possibly may contain Wilgenhoutsdrift Group material. Reflectors at B are interpreted to indicate the contact between a sedimentary basin and the floor rock, while the reflector at C may indicate a younger basin outline (Stettler et al., 1998). One of the most interesting reflectors which are located at D, are interpreted to indicate the presence of a body with either large density or velocity contrast or both. Further west of the seismic section, reflectors E and F are interpreted to indicate the presence of the Trooilapspan shear, while reflectors marked H and I are interpreted to be associated with thrust units because of their lens-like features (Stettler et al., 1998). There are a number of deep reflectors such as those marked K which may indicate the crustal mantle boundary (Stettler et al., 1998).

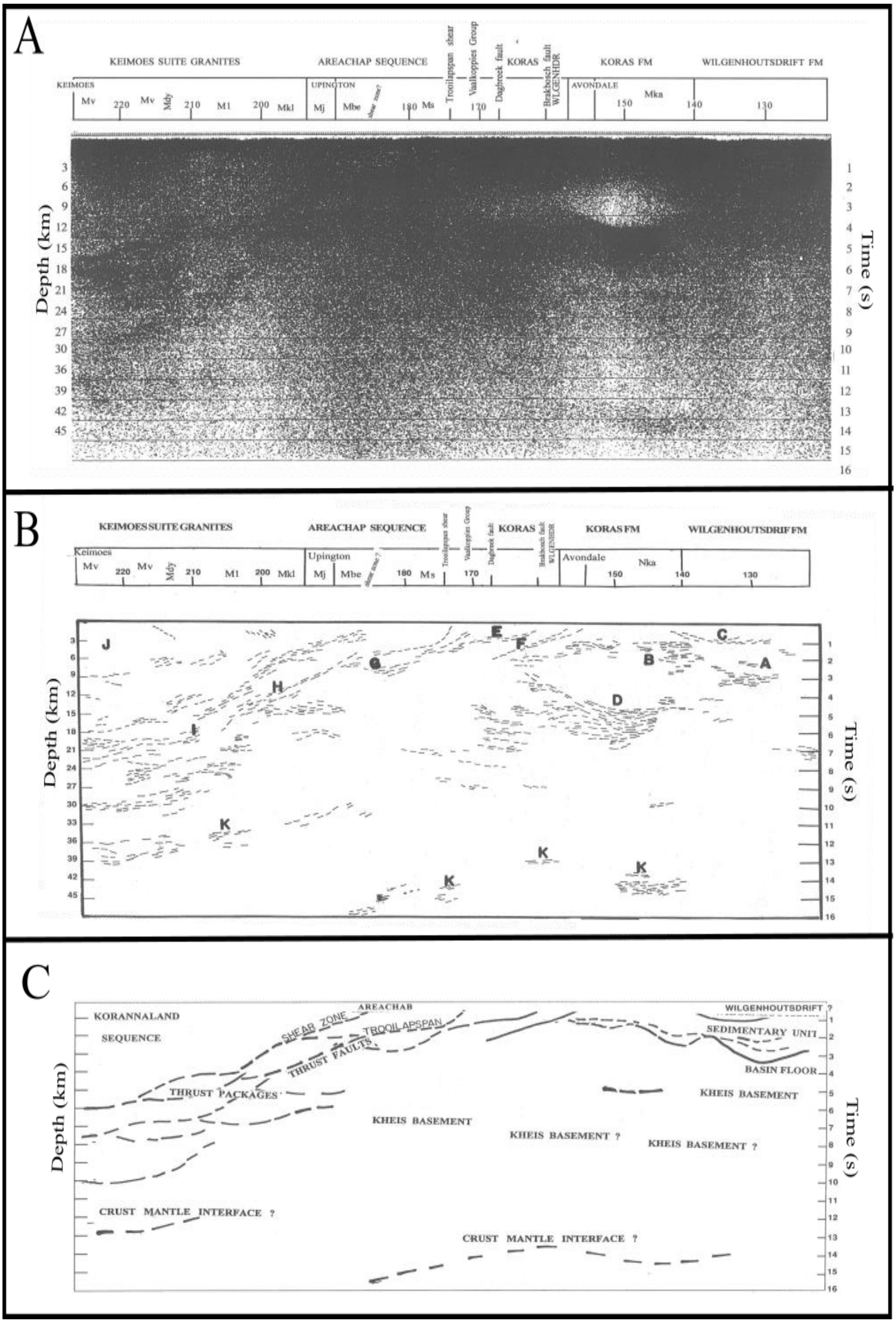

Figure 8: A) Migrated reflection seismogram between Keimos and Avondale of line (SAGS-02-91). B) Line drawing important reflectors. C) Interpretation of the seismogram (Stettler et al., 1998).

Stettler et al. (1999) focused on the region of the previously collected SAGS-02-91 reflection seismics line between Avondale and Olifantshoek/Roscoe and carried out a magnetotelluric (MT) survey in the Northern Cape Province, positioning sequentially five stations at Inkruip, Paleisheuwel, Waaihoek, Olifantshoek, and Rosecoe. The survey line was oriented in a northeast-southwest direction, traversing the boundary of the Kaapvaal Craton. These stations were spaced 20 km apart and arranged in a magnetic north-south, east-west direction.

Similarly to Stettler et al. (1998), reflection seismics, magnetic and gravity data were processed and interpreted on the rest of the 260 km seismic line between Avondale and Roscoe *(see Figure 9)*.

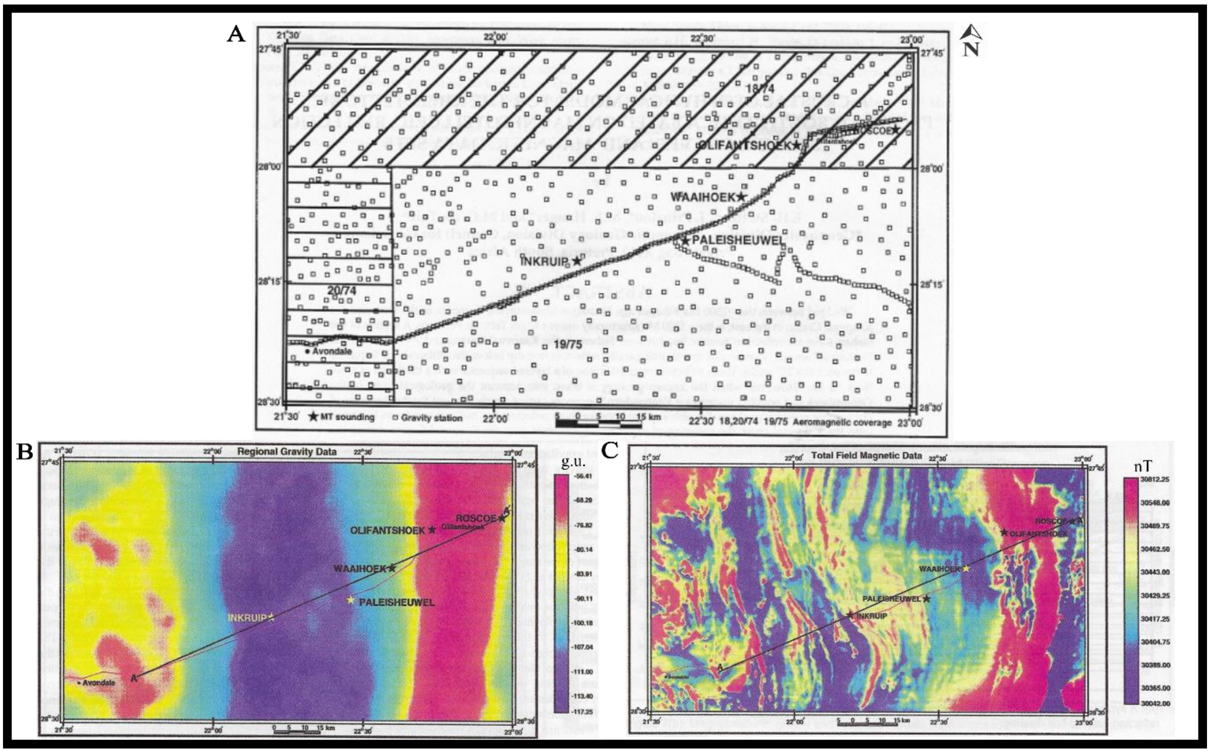

Figure 9: Taken from Stettler et al. (1999) A) Geophysical coverage of the 226km seismic line between Avondale and Roscoe. The stars represent MT stations, the small squares represent gravity stations, and the line connecting the small squares represent the seismic line (Stettler et al., 1999). B) CGS Bouguer gravity map and C) shows the CGS total field magnetic map.

The gravity map in Figure 9b displays prominent north-south striking features, notably a significant gravity high in the eastern area exceeding -30 milligals (mgal), followed by a broad gravity low in the central region, and a lower amplitude gravity high in the western perimeter. This anomaly has been previously studied and associated with westward dipping seismic reflectors and high conductivity bodies. Similarly, the total field magnetic data in Figure 9c reveals distinct magnetic patterns, including a major magnetic high coinciding with the eastern gravity high attributed to magnetic units in the Voëlwater Formation, while the central and western regions depict folded units of the Olifantshoek Sequence and the Namaqua Metamorphic Complex, respectively (Stettler et al., 1999).

The migrated section in Figure 10a depicts numerous reflection patterns that originate from sharp acoustic impedance contrast in the subsurface, caused by discontinuous geological entities.

Using geological evidence Stettler et al. (1999) observed that further east, the eastern section of the Kheis Terrane consists of the west dipping Olifantshoek Sequence which is characterized by steep tight folding. Reflection seismic data indicate that the thickness of the Olifantshoek Sequence could reach a maximum of about 3 km. The sedimentary Olifantshoek Sequence is overlain by the sedimentary Groblershoop Formation which is in turn overlain by the Wilgenhoutsdrift Group lavas. This sedimentation that is present on the Kheis basement suggests that the basement is stable to at least the start of the Namaqua event (Stettler et al., 1998). The geophysical evidence presented in the paper also indicate that the Kaapvaal Craton interlocked at depth with the Kheis basement, indicative of a collision tectonic event between the Namaqua Metamorphic Province, Kheis Terraine and the Kaapvaal Craton.

The reflector package marked A on Figure 10b is interpreted to show deepening reflector packages with a dip of ~22° to the west. The region is seen to have reflector packages resembling a layered sequence of an unconfirmed geological sequence (Stettler et al., 1999). The reflector package marked A is also seen to indicate elongated lens-like reflector patterns that could indicate thrusting which can be interpreted as presenting the boundaries of sheared geological units that are due to a thrusting event in the basement on the edge of the Kaapvaal Craton (Stettler et al., 1999). The reflector package marked B is interpreted to mark the base of the Olifantshoek Sequence which is estimated to have a maximum thickness of about 2 km (Stettler et al., 1999). The reflectors marked C are interpreted to strongly indicate the presence of thrusting which are considered separate to those from the ones dipping down in the package marked A (Stettler et al., 1999). The reflector package marked D is interpreted to mark the possible boundary between the Kaapvaal Craton and the Kheis basement (Stettler et al., 1999). While the reflector package at E is suggested to indicate the presence of the Kheis Terrane (Stettler et al., 1999).

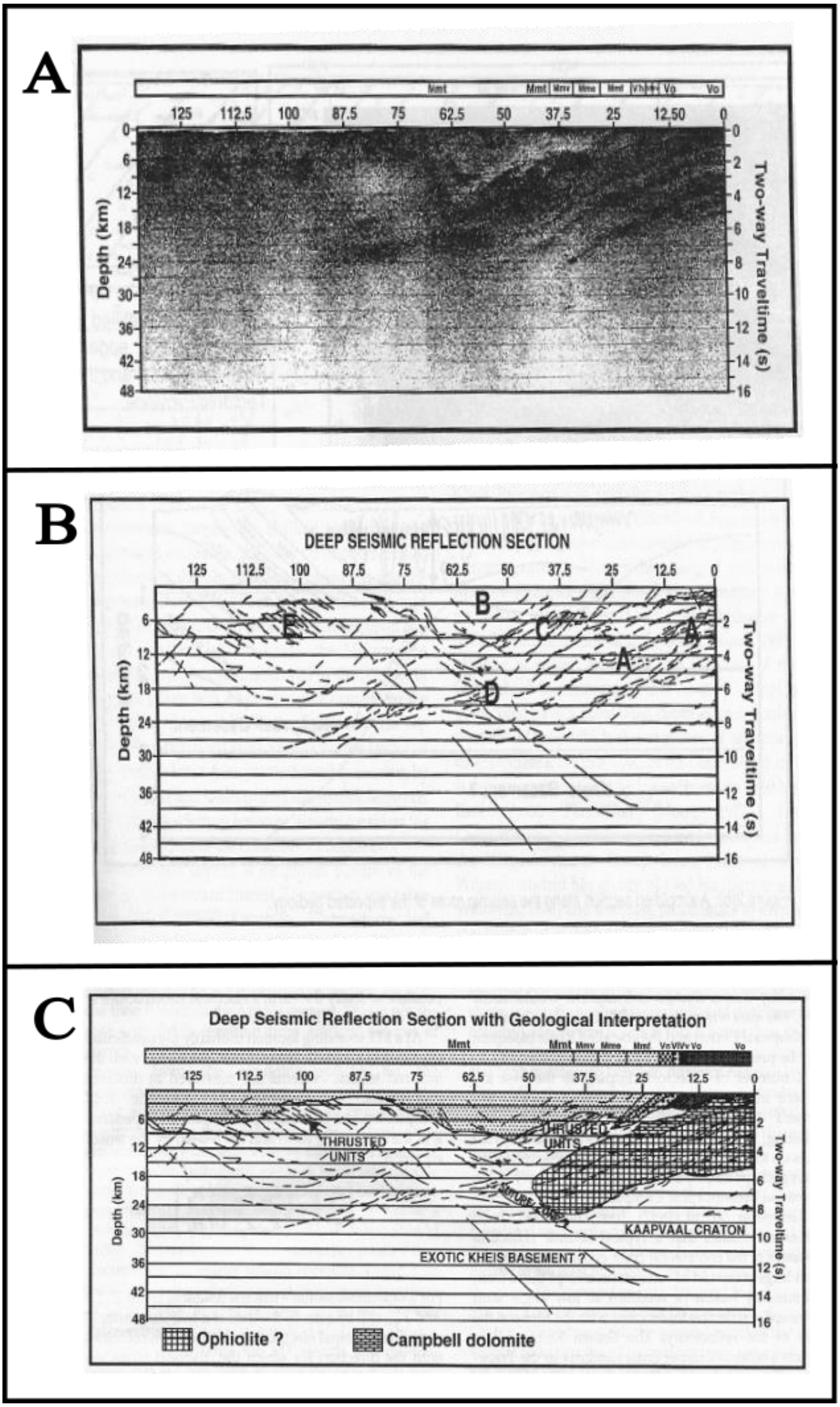

Figure 10: A) Migrated seismic section between Avondale and Sishen. B) Seismic section showing lines drawn of the most important reflectors. C) Interpretation of seismic line (Stettler et al., 1999).

Figure 11 shows the MT soundings and one dimensional models from the five MT stations that were used Figure 9. These were then used as inputs for a two dimensional modeling software that provided the model in Figure 12. Figure 12 shows a model consisting of resistive material (20000 Ωm) in the east and west sandwiching less resistive material (6700 Ωm) and a 100 Ωm conductor (Stettler et al., 1999). The resistive material in the east was interpreted as belonging to the Kaapvaal Craton while the 6700 Ωm and 100 Ωm conductive material may belong to the Kheis Province.

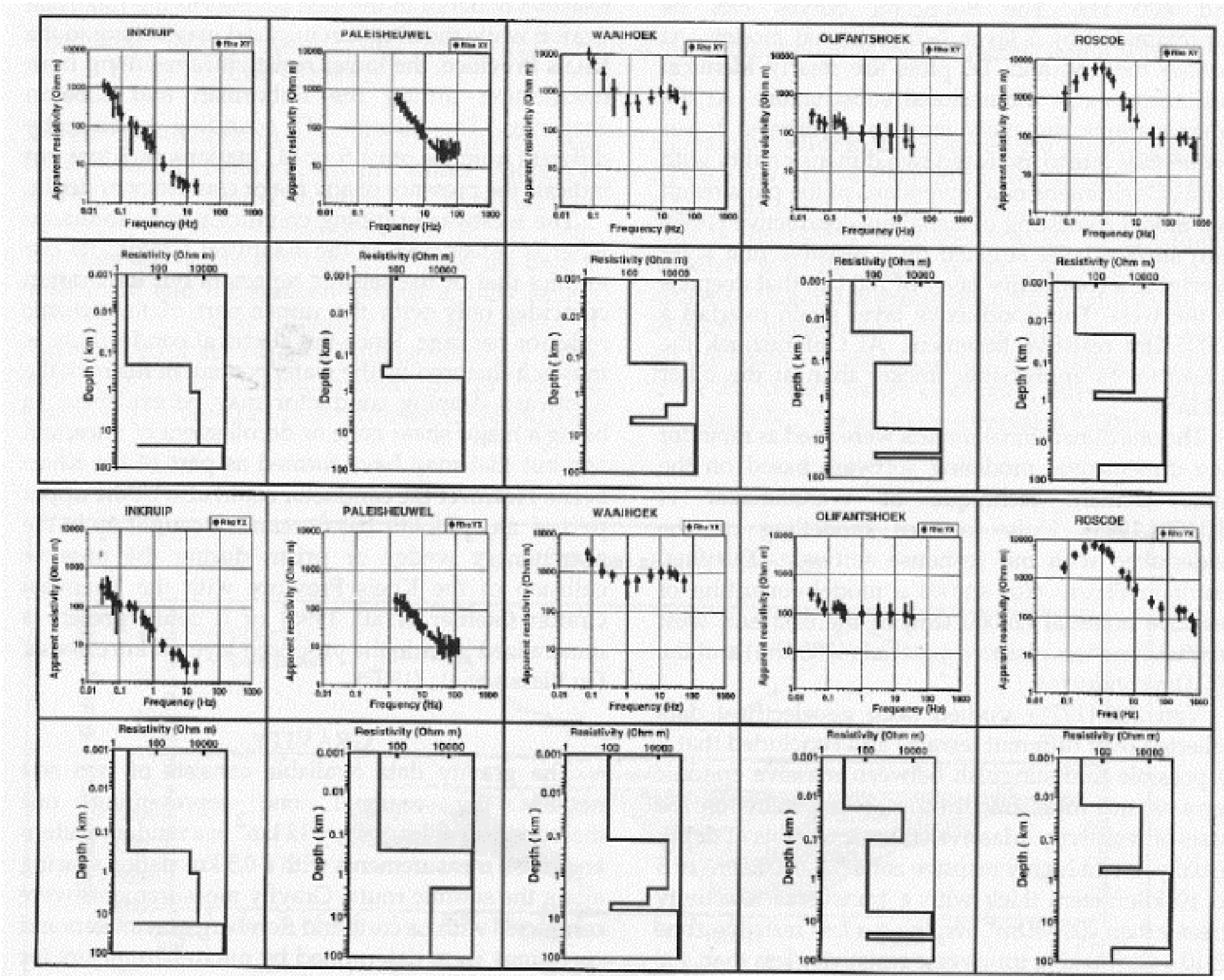

Figure 11: MT soundings and 1-D models of the five MT stations used in. The soundings and 1-D models in the top row represents the XY component of the apparent resistivity, and the bottom row soundings represent the YX component apparent resistivity (Stettler et al., 1999).

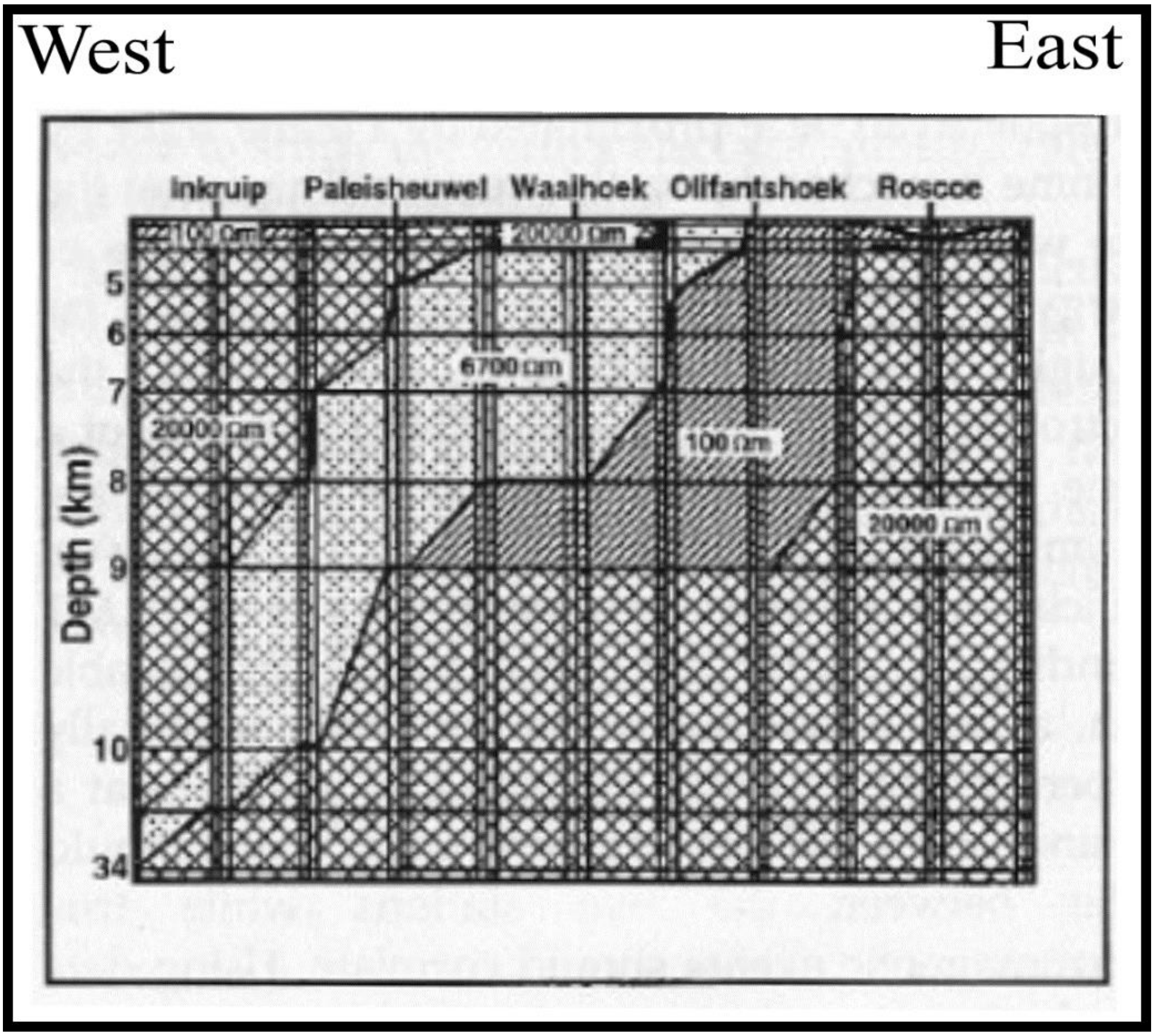

Figure 12: Approximately 70 km long 2-D magnetotelluric model section of the five stations (Stettler et al., 1999)

The data were combined into a susceptibility and density model over the region. The gravity data *(see Figure 13)* was interpreted as indicating the presence of dense material on the Kaapvaal Craton region westward of the seismic profile. To fit the observed data, a 2840 kg/m^3 material is identified as a combination of the Ongeluk lava and Campbell dolomites and possible Ventersdorp, and is estimated to be 3 km thick, with an additional 8 km dipping ultramafic material below. Furthermore, west of the profile in Figure 13b suggests a thick succession of either sedimentary or another granitic material present that is present below the Olifantshoek Sequence (Stettler et al., 1999).

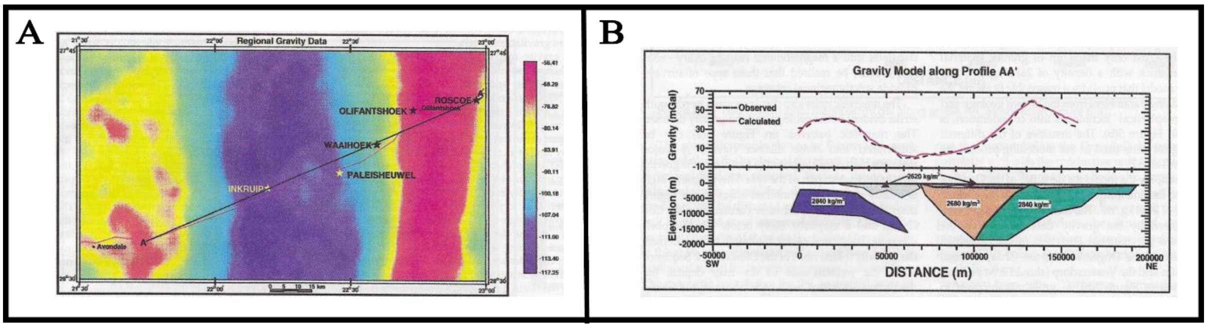

Figure 13: A) Gravity contour map covering the seismic profile region between Avondale and Roscoe. B) 2-D gravity model along profile AA' as shown in (A) (Stettler et al., 1999).

The magnetic data as shown in Figure 14 is interpreted to indicate the existence of dipping layers which are partially magnetic and have a possibility of mineralization (Stettler et al., 1999).

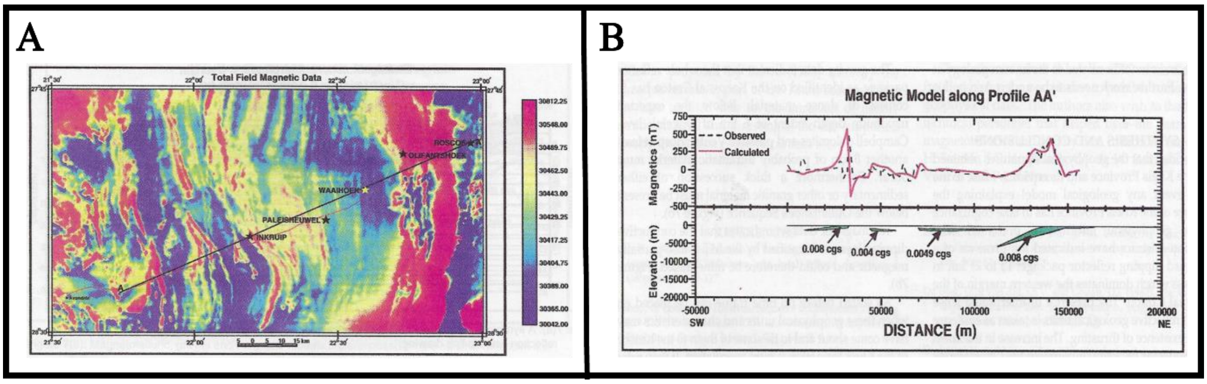

Figure 14: A) Magnetic contour map covering the seismic profile between Avondale and Roscoe. B) 2-D magnetic model along profile AA' as shown in (A) (Stettler et al., 1999).

Combining seismic profiles from Stettler et al. (1998, 1999) we can get an idea of how the whole 226 km seismic profile looks like *(see Figure 15 and Figure* 16*)*. The data from Stettler et al. (1998, 1999), proposed a model whereby the Kheis formed by a continental collision and a thick ophiolitic sequence being emplaced onto the Kaapvaal Craton margin either by intrusion or thrusting or both into the accretionary wedge that formed between the Kheis terrain and the Kaapvaal Craton.

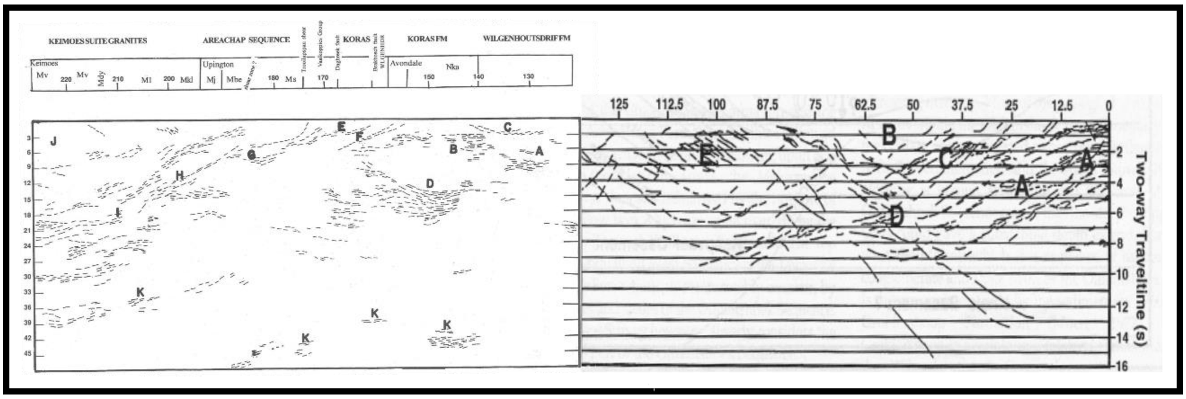

Figure 15: Seismic reflector packages from Stettler et al. (1999) (left) and Stettler et al. (1998) (right) showing the whole SAGS-02-91 seismic profile.

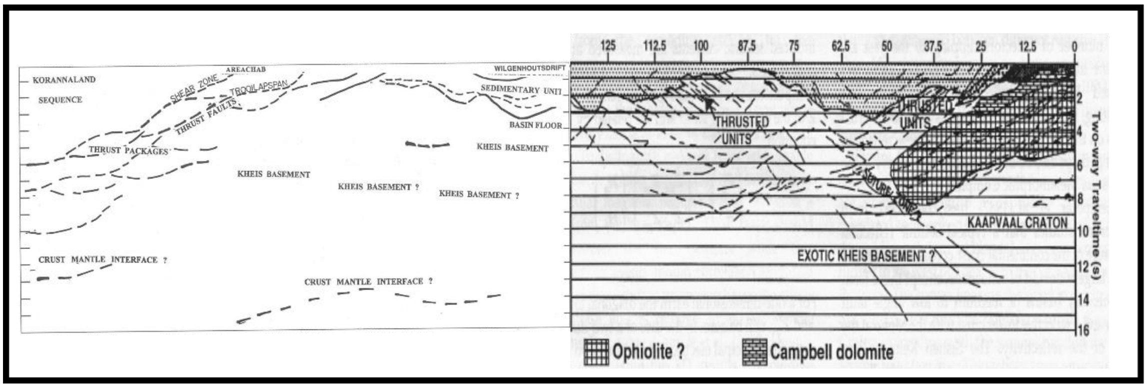

Figure 16: Seismic interpretation packages from Stettler et al. (1999) (left) and Stettler et al. (1998) (right) showing the whole seismic profile.

Chapter 3. The magnetotelluric method

Brief MT history

The magnetotelluric (MT) technique is an electromagnetic approach that utilizes a passive source to detect variations in the natural magnetic and electric fields, which are perpendicular to each other on the Earth's surface (Simpson & Bahr, 2005). Variations in solar activity and lightning generate currents in the ionosphere, inducing telluric currents that are harnessed to assess the conductivity characteristics of subsurface materials, spanning from surface layers to depths of several hundred kilometres (Stettler et al., 1999). MT represents a relatively recent addition to geophysical methods, initially proposed in its foundational theory by Tikhonov (1950) and further elaborated upon by Cagniard (1953). They observed that simultaneous calculation of electric and magnetic field variances allows for describing the penetration of the electromagnetic field by the ratio of electric to magnetic field (impedance) (Simpson & Bahr, 2005).

MT theory

MT is based on Maxwell's electromagnetics equations, namely Faraday's Ampere's Laws listed below respectively.

$$\nabla \times \vec{E} = -\frac{\partial \vec{B}}{\partial t} = -i\omega\mu\vec{H} \qquad (1)$$

$$\nabla \times \vec{H} = \vec{J} + \frac{\partial \vec{D}}{\partial t} = (\sigma + i\omega\varepsilon)\vec{E} \qquad (2)$$

Where ω is the angular frequency, i is the complex variable, σ is the conductivity, ε is the electric permeability, μ is the magnetic permeability, E and H are the electric and magnetic fields respectively. The Fourier transform is used to analyse the behaviour of the electromagnetic fields in the frequency domain rather than the time domain, this is done because when deriving the Helmholtz equation, it is an advantage to turn derivations with respect to time into algebraic expressions in frequency domain. The same holds for the transition into wavenumber domain. Due to the plane wave assumption that tells us that the medium through which the wave propagates is assumed to be homogenous and that the electromagnetic fields propagate in a single direction (in this case z-axis), then the solutions to

Maxwells equations for a plane wave result in the electric and magnetic field being perpendicular to the direction of wave propagation. This means that the inducing magnetic field will only have horizontal components, which drive the currents that responds to subsurface resistivity variations. We therefore get the following solutions for E and H respectively.

$$\vec{E} = Ae^{-i\omega\mu_0\sigma t} + Be^{i\omega\mu_0\sigma t} \tag{3}$$

$$\vec{H} = \frac{\sqrt{\omega\mu_0\sigma}}{\omega\mu_0}(Ae^{-i\omega\mu_0\sigma t} + Be^{i\omega\mu_0\sigma t}) \tag{4}$$

Using these equations, we can then calculate the impedance (Z) which describes the ratio the of electric and magnetic field.

$$Z_{xy} = \frac{E_x}{H_y} = \frac{\omega\mu_0}{\sqrt{\omega\mu_0\sigma}} = \frac{\omega\mu_0}{k} \tag{5}$$

Where $k = \sqrt{\omega\mu_0\sigma}$ is our wave propagation term.

To help us understand the relationship between the applied telluric current and the potential difference for a half-space we calculate the apparent resistivity can be calculated as.

$$\rho_{xy} = \frac{1}{\omega\mu_0}\left|\frac{E_x}{H_y}\right|^2 \tag{6}$$

Where ρ is the apparent resistivity.

The phase lag between the electric and magnetic field is given by.

$$\varphi_{xy} = \tan^{-1}\left(\frac{E_x}{H_y}\right) \tag{7}$$

Where φ is the phase difference. $Z, \rho\ and\ \varphi$ are analogous for components yx, yy and xx.

Maxwell's equations also yield the diffusion equation governing the propagation of an electric field within the Earth's interior, offering insights into the conductivity distribution within the Earth. This equation is given by (Simpson & Bahr, 2005);

$$\nabla^2 E = \mu_0\sigma\frac{\partial E}{\partial t} \tag{8}$$

Where E is the electromagnetic field, $\mu_0 = 1{,}2566 \times 10^{-6} Hm^{-1}$ (magnetic permeability of free space), σ is the conductivity of the rocks in the half space. This equation describes the electromagnetic induction within the interior of the earth. Electromagnetic induction within the earth is governed by the capacity of current to spread across its surface, exhibiting a phenomenon known as the 'skin effect,' which results in a rapid decrease in intensity with increasing depth of penetration (Simpson & Bahr, 2005).

For the electromagnetic induction in the earth to be possible, the following assumptions are considered (Cagniard, 1953; Keller & Frischknecht, 1966):

- The adherence to Maxwell's electromagnetic equations, which establish the relationship between the derivative of the horizontal magnetic field component H and the vertical electric field component E, is imperative.
- The Earth's structure and atmosphere are only capable of absorbing and dissipating electromagnetic energy; they do not generate it.
- Both electric and magnetic fields maintain their conservation properties as they propagate away from their sources.
- In mid-latitude regions, electromagnetic fields generated naturally from ionospheric currents can function as homogeneous, plane-polarized waves, penetrating the Earth with near-vertical incidence.
- While free charges tend to dissipate as they traverse through the layered structure of the Earth, the accumulation of charges may occur at discontinuities within the Earth's layers, leading to a non-inductive alteration in the MT apparent resistivity response, known as static shift.
- Charge conservation persists as it traverses through the Earth's interior, acting akin to an ohmic conductor.
- During MT sounding periods, the electric displacement fields exhibit near-static behaviour. Consequently, electromagnetic induction within the Earth can be approximated as a diffusion process.

In electromagnetic methods such as magnetotellurics, the earth's electrical conductivity is a crucial factor influencing how deep an electromagnetic signal can penetrate and the level of detail it can provide. High electrical conductivity essentially absorbs or weakens the electromagnetic wave by harnessing the movement of electrical charge. Materials with high conductivity effectively absorb electromagnetic energy and restrict its ability to penetrate deeper into the earth. This weakening of the electromagnetic signal becomes more pronounced with increasing depth, a phenomenon explained by the skin depth relationship.

The skin depth is the depth at which the electromagnetic signal diminishes to 1/e or roughly one-third of its initial strength. This parameter is typically quantified in meters and depends on both the frequency (f) of the electromagnetic wave and the electrical conductivity (σ) of the medium (such as geological materials) through which the EM wave is propagating. It is also important to note that we use an Ansatz of an up-going and down-going wave and that the up-going wave can be neglected in the case of 1D (in which the concept of penetration depth is only strictly valid).

Using Maxwell's Faraday Law alongside Ampere's Law of electromagnetism we can get the following equation to describe the electromagnetic field to derive the skin depth.

$$E = Ae^{i\omega t - qz} + Be^{i\omega t + qz} \tag{9}$$

Where t is the period of the electromagnetic field E, A and B are the components of the electromagnetic field, $q = \sqrt{\frac{\mu_0 \sigma \omega}{2}} + i\sqrt{\frac{\mu_0 \sigma \omega}{2}}$ and z is the penetration depth. Earth is incapable of sustaining arbitrarily large electric field amplitudes because it solely dissipates and absorbs electromagnetic energy, without generating it (Simpson and Bahr, 2005). Consequently, the electromagnetic field weakens as the penetration depth approaches the radius length of the Earth. Giving us:

$$E = E_1 e^{i\omega t - qz} \tag{10}$$

We then derive the electromagnetic penetration depth or skin depth of an electric field from taking the real part of q, which gives (Simpson and Bahr, 2005).

$$p = \frac{1}{Re(q)} = \sqrt{\frac{2}{\mu_0 \sigma \omega}} \qquad (11)$$

The MT impedance tensor

The impedance tensor portrays the concept of delineating fields in orthogonal directions by decomposing the horizontal electric and magnetic fields into their independent components along the x and y axes. Due to the Maxwell's equations, it turns out that the general 2D Maxwell's equations decouple into equations either having only the Ex or the Hx component. In doing so, it preserves the independence (orthogonality) of these field components, helping to understand how different directions of the subsurface affect the propagation of electromagnetic waves. Since the MT technique involves measuring the fluctuations in the natural electric and magnetic fields which are orthogonal to each other, the impedance tensor (Z) is then used to describe the relationship between the horizontal components of the electric and magnetic fields. The impedance tensor is, **Z** is given by,

$$\begin{pmatrix} E_x \\ E_y \end{pmatrix} = \begin{pmatrix} Z_{xx} & Z_{xy} \\ Z_{yx} & Z_{yy} \end{pmatrix} \begin{pmatrix} \frac{B_x}{\mu_0} \\ \frac{B_y}{\mu_0} \end{pmatrix} \; or \; \boldsymbol{E} = \underline{Z}\boldsymbol{B}/\mu_0 \qquad (12)$$

The impedance tensor **Z,** which is also defined as the observed estimated MT impedance tensor (Z_{obs}), contains information about dimensionality and direction.

If the half-space under the MT stations is 1-D (i.e., conductivity varies only with depth), then the tensor is expressed as

$$Z_{1D} = \begin{pmatrix} 0 & Z_{xy} \\ -Z_{yx} & 0 \end{pmatrix} \qquad (13)$$

The two estimates (Z_{xy} and $-Z_{yx}$) of apparent resistivity curves should lie on top of each other, and the phases should be exactly 180° apart. The XY phase should lie in the first quadrant, and the YX phase should lie on the third quadrant.

If the half-space under the MT stations is 2-D, then the tensor should look like

$$Z_{2D} = \begin{pmatrix} 0 & Z_{xy} \\ Z_{yx} & 0 \end{pmatrix} \quad (14)$$

Therefore, to observe the impedance tensor to appear as 2-D as possible, meaning Z_{xx}=Z_{yy}=0 along electromagnetic strike, we need to derive the best angle to rotate the impedance tensor. Thus, the observed impedance tensor is given by

$$Z_{obs} = RZ_{2D}R^T \quad (15)$$

Where R is the Cartesian rotation matrix, given by

$$R = \begin{pmatrix} \cos\theta & \sin\theta \\ -\sin\theta & \cos\theta \end{pmatrix} \quad (16)$$

Where θ denotes the best angle to rotate the impedance tensor. The primary goal in this scenario is to derive the appropriate strike angle and rotate the data into the interpretation reference frame.

In 2-D, since the electric and magnetic field are orthogonal, the equations split into two different modes of propagation. In one mode, the electric currents flow parallel to the geological strike and is termed the transverse-electric (TE) mode. The other mode is when the electric currents are orthogonal to the geological strike or structures and is called the transverse-magnetic (TM) mode. When processing and analysing MT data in 2-D one needs to assign components of the impedance tensor to either the TE or TM mode.

If the conductivity distribution varies with depth and in both lateral directions the electrical structure is 3-D, and the tensor is expressed as

$$Z_{3D} = \begin{pmatrix} Z_{xx} & Z_{xy} \\ Z_{yx} & Z_{yy} \end{pmatrix} \quad (17)$$

Source fields

Electromagnetic fields exceeding 1 Hz in frequency are induced by worldwide lightning discharges (Simpson and Bahr, 2005). Fields below 1 Hz are induced by ionospheric current systems, giving rise to electromagnetic variations that induce telluric currents (Simpson and Bahr, 2005).

Electrical conductivity/resistivity of the Earth's materials

MT is effective in investigating and delineating lateral changes in the conductivity structures of the lithosphere at all depths and it can help determine the thickness of various layers in the lithosphere (Muller et al., 2009). The MT models provide insight into the composition and metasomatism of the lithosphere in the survey area.

The electrical resistivity of Earth materials varies due to the vast variation of the rocks formed on earth. The resistivity varies by more than 10 orders of magnitude throughout the range of rocks. This is a result of variations in temperatures and pressure during formation in weathered and unweathered igneous and metamorphic rocks, to the porosity, clay content, water saturation and dissolved material of sedimentary rocks. Figure 17 shows the resistivity and conductivity ranges of Earth materials (Palacky, 1988), the figure shows how vast the range of resistivity is and how due to this level of variation, MT can take advantage of this, especially in a geologically complex region.

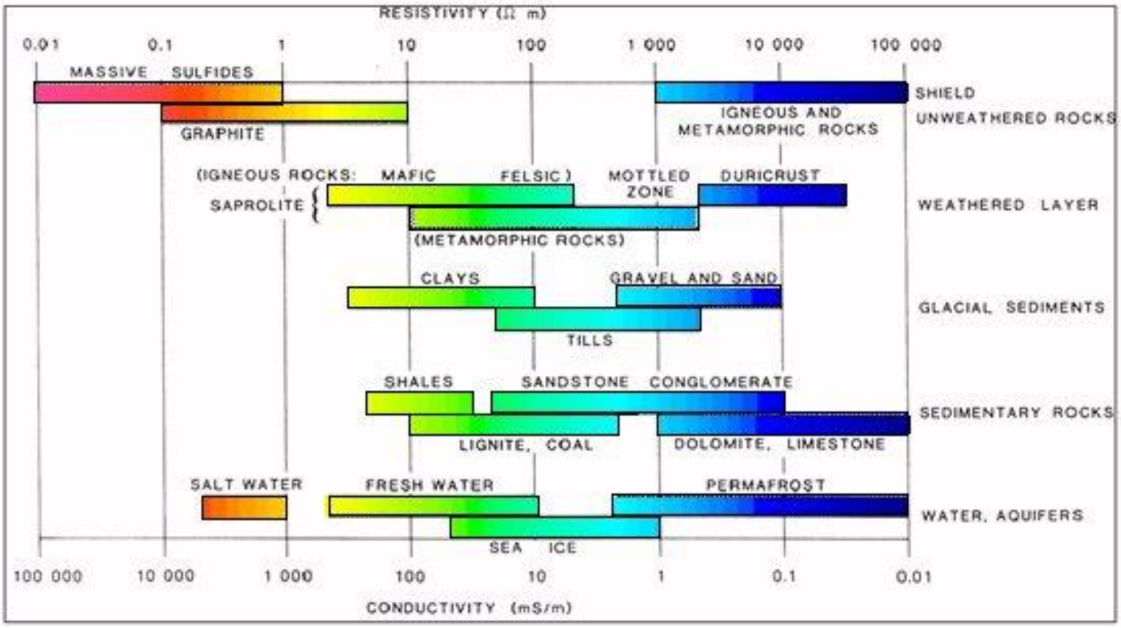

Figure 17: Typical ranges of resistivity and conductivities of earth materials(Palacky, 1988).

Chapter 4. Data and Methodology

Data

Seismic data

SAGS-02-91 seismic profile *(see Figure 18)* was collected from 14 March 1991 to 15 April 1991 by Geoseis (Pty) Limited for The Council for Geosciences. The seismic profile was collected using a 4 Hertz Vibrators (vibroseis) source west of Upington in the Northern Cape Province. Acquisition parameters of the survey are provided in Table 2 as extracted from the observer's report, and the details regarding processing workflow are not known. The seismic data was then reprocessed by Wits Seismic Research Centre in 2020 and is now being used in this study to further constrain the MT data. This is the same profile used by Stettler et al. (1998, 1999), and it will be the same seismic profile that will be used for this research.

Table 2: Reflection seismic survey parameters.

Vibrator station interval	150m
Vibrator pattern	4 vibrators in-line, 12.5 m pad separation and 4.2 m move up after each sweep. Centre of gravity of pattern equidistant between the two adjacent geophone stations.
Sweeps/Vibrator point	7
Sweep frequency	8-64 Hz
Sweep length	19 s
Listening time	32 s
Sample interval	4 ms
Multiplicity	32-fold
Geophone station interval	50 m
Geophone pattern	2 sets of 12 geophones linear in line per station centred on group centre with 50 m spacing

	between group centres. 2 m spacing between geophones. Receiver array length= 46 m.
Spread geometry	-4775-25-0+25+4775

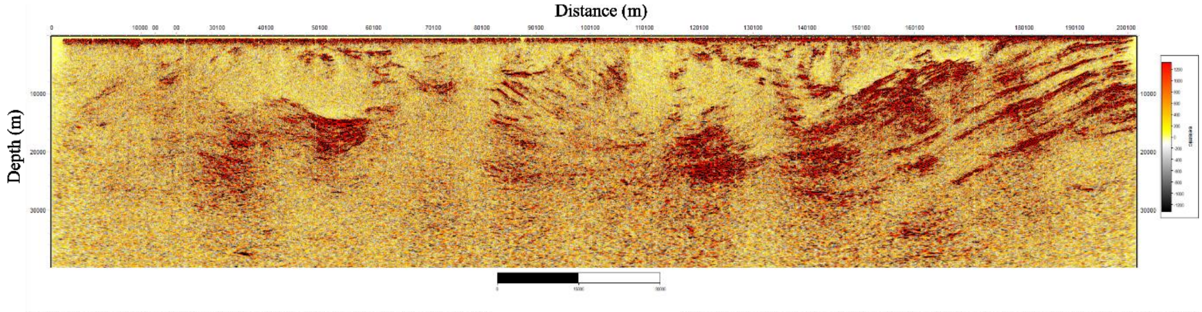

Figure 18: Migrated SAGS-02-91 reflection seismic profile along the Kheis Terrane Transact.

Magnetic data

Figure 19a shows the cropped regional magnetic data (TMI) of South African as provided by the Council for Geoscience to show the study area. Magnetic data is bi-polar and for purely induced magnetism only the edges of a magnetic body give a magnetic high (northern and western) or magnetic low (southern and eastern perimeter) in southern Africa. The centre of a magnetic body if it is sill-like in shape has no elevated magnetic field, in contrast to the gravitational field of the same body, where the highest amplitude is found in the centre of the body with a positive density contrast with respect to the surrounding rocks. The green coloured regions may therefore approximately, represent areas of low magnetic susceptibility, and the red (magnetic high)/blue (magnetic low) regions represent areas with bodies of smaller lateral dimensions with possibly high magnetic susceptibility and/or strong remanent magnetisation. Figure 19b shows the same magnetic data with the vertical derivative applied to enhance the presence of linear features. These magnetic data were collected between the 1980s and late 1990s by the Geological Survey (now the Council for Geoscience). Flight lines are 1 km apart, with tie lines collected very 10 km, and the plane flying at approximately 100 to 150 m height (Stettler et al., 2000).

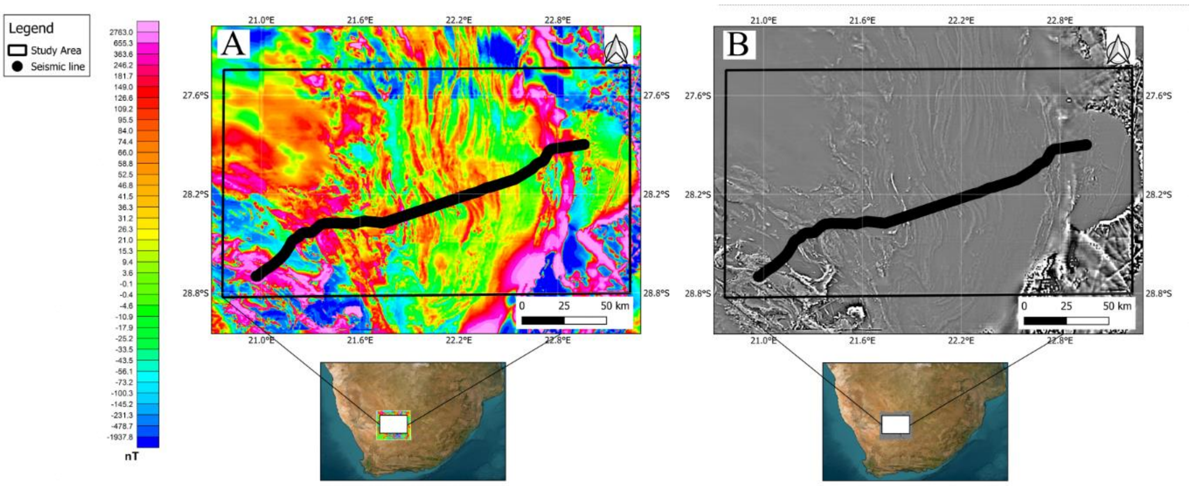

Figure 19: Magnetic data of the study area. A) Total Magnetic Intensity (TMI) over the study area and B) magnetic vertical derivative of the dataset (E. Stettler et al., 2000).

Magnetotelluric data

In 2019, the Council for Geosciences (CGS) conducted a regional MT survey in Southern Africa to investigate the resistivity structure of Southern Africa. For the purposes of this research, the organization provided MT data from 14 MT stations that are within the area of interest. The 14 MT stations consist of MT soundings with periods that range from 10^{-4}s to 10^{4}s (MT practitioners tend to swap period and frequency however, one is the inverse of the other.)Each station was deployed to collect data for up to 3 nights using the MTU5A and Phoenix MT equipment. The dataset is in an equally spaced rectangular grid with a station spacing and line spacing of 10km. Within this grid is the SAGS-02-91 seismic line, which was acquired in 1989. The study area/grid spans a length of approximately 230 km W-E and approximately 140 km N-S, giving an approximate surface area of the study area/grid to be 32200 km^2.

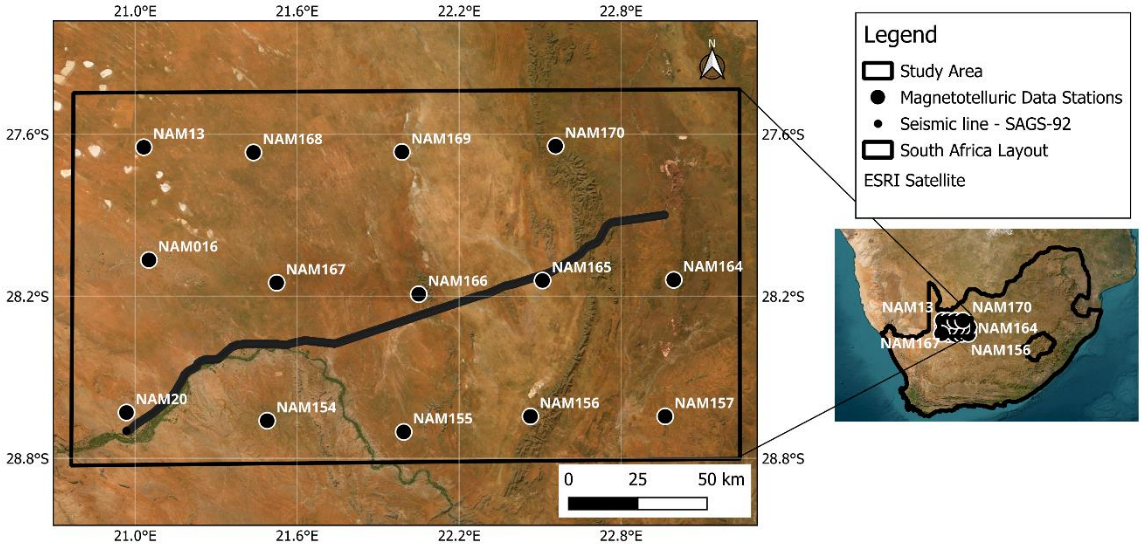

Figure 20: Map of study area showing location and names of the MT stations. The black in in the study area represents the SAGS-02-91 seismic line.

Data acquisition training

Between 21 July 2023 and 18 August 2023, I had the opportunity to acquire MT data which gave me the skillset to acquire MT data practically in the field. I will be using this experience to illustrate the MT acquisition process. I joined the Council for Geoscience (CGS) in South Africa to acquire MT data in Geselskapbank, Northern Cape between 21 July 2023 and 18 August 2023.

MT acquisition starts with doing a field investigation of the survey area. Communities around the survey area need to be informed and in some cases be involved during the acquisition by being casual workers to assist in deploying the MT stations. This is an important step as in some cases you may not have permission from the locals to conduct your survey. After reaching an agreement with the local community, preparation of MT equipment begins.

For a successful MT acquisition, the following equipment was used during my field survey with CGS:

- Three magnetic induction coils, accompanied by three magnetic induction coil cables per MT station:

  The three magnetic coils are used to measure variations in the Earth's magnetic field at different frequencies. These coils are typically oriented in three orthogonal directions (x, y, and z) to capture the full vector components of the magnetic field. The horizontal coils (x and y direction) measure the horizontal variations in the Earth’s magnetic field and vertical coils (z direction) measure the vertical variations in the Earth's magnetic field. The magnetic induction coil cables connect the induction coils to the datalogger (data acquisition system).

- Five electrodes accompanied by five telluric cables per MT station:

  The electrodes measure the resulting electric potential differences associated with passive telluric currents. Each electrode represents the geographic location it will be placed at i.e., East, West, South, North, and a reference electrode that is normally placed in the centre:

- The datalogger used was the MTU 5C:

  The MTU 5C data logger records the electric potential differences between the pairs of electrodes and the Earth's magnetic field response from the induction coils. It has advanced signal processing capabilities, data filters filtering techniques and amplifies the recorded signals, ensuring high-quality data free from noise and interference.

- One Global Positioning System (GPS) per MT station:

  Global Positioning System (GPS) technology is often used to precisely determine the geographic locations of the measurement stations where electrodes and recording equipment are deployed. GPS receivers are typically installed at each station, allowing for accurate positioning data to be collected as well as most importantly the time reference.

- One battery per MT station.

  The batteries are typically used to power the data acquisition systems, including the recording units such as the MTU 5C, GPS receivers, and other electrical equipment deployed in the field. The equipment is normally left in remote areas where there is no power grid supply and the batteries act as a power supply.

- One solar panel:

  The solar panel is used to harness solar energy to charge batteries that power the data acquisition systems and other electronic equipment used in the survey (normally for the reference station), ensuring continuous operation even in remote locations without access to grid power.

- Computer/laptop:

The laptop is used to interface with the data acquisition system to monitor data collection, adjust settings, and download recorded data for analysis using specialized software designed for processing MT survey data.

- 50 litre storage container:

  The container is used to cover the datalogger and other sensitive equipment and protect it from harsh weather conditions like very hot weather conditions.

- Digging equipment (shovel, garden shovel, fork spade, auger digger, garden, pick):

  Digging equipment is used to prepare the ground for installing electrodes and grounding systems, ensuring proper contact with the Earth for accurate measurement of electromagnetic signals.

- Compass:

  A compass is used to orient the electrode layout according to the desired survey geometry, ensuring accurate positioning of measurement stations and alignment with geographic coordinates.

- Nappies/diapers:

  Nappies or diapers are sometimes used as absorbent material to keep moisture in the electrodes, allowing for better contact into the ground.

- Packets of salt:

  Salt packets are used to create a conductive electrolyte solution when preparing electrodes for insertion into the ground, ensuring good electrical contact between the electrodes and the Earth for accurate measurements.

- 20 litre plastic drums with water:

  The water in these 20 litre drums is used to keep moisture betweent the electrodes and the ground, making for a more efficient electrical contact.

- PPE (safety gloves, safety googles, sun hat, safety boots):

Personal protective equipment (PPE) is worn by survey personnel to ensure safety during fieldwork, protecting against hazards such as sharp objects, falling debris, sun exposure, and chemical exposure.

- Plastic buckets or pots per electrode:

  Plastic buckets or pots are used to place the electrodes. Cat litter and diaper covered electrodes are inserted inside the pot plants. This is to make sure that no foreign substances are left in the field after the equipment has been removed and to make it easier for the moisture to be retained as the study area contained porous rocks that made keeping the electrodes moist and saturated hard..

- Cat litter:

  The cat litter is used to retain moisture for as long as possible around the electrodes. Due to its unique property, water is retained in the soil for an extended period.

- Spirit level:

  A spirit level is used to ensure the horizontal alignment of the induction coils and stability of equipment such as tripods, ensuring accurate and consistent measurements by maintaining proper orientation relative to the Earth's surface.

A typical MT field crew will consist of the following members:

- Operators: They are resposible for setting up the site. They look for the best location to place the station in order to avoid noise.
- Field assistants: They are responsible for digging and laying out the equipment, they are sometimes hired from the local community.
- Processors: They are responsible retrieving the data from the data logger and pre-processing the field data , making sure it is good quality data which does not need to be re-taken.

Upon arrival at the survey area, all equipment needs to be calibrated. This is to make sure that all of the equipment is working properly and are reading correct measurements. Figure 21 shows the magnetic sensors being calibrated and tested by placing all of them parallel to each other and connecting them to the data loggers and checking if a response is measured.

Figure 21: Image showing the magnetic induction coils being prepared for calibration.

Once the calibration has been completed, deployment of the stations can begin. We used the remote reference acquisition technique. This is when a reference/remote station is planted at any distance away from the survey area (approx. 0.5km to 100's of km's) for the duration of the whole survey. This is done to reduce noise, as noise at a given site can be reduced by cross-correlating it with the appropriate field components between the local and remote/reference site. This is because electromagnetic noise between two sites are not correlated, however the plane wave MT fields between two fields are correlated. Due to the reference station being planted at a site for a considerably long time, a solar panel is used to charge the battery.

Once the appropriate location to place the site is found a tripod with a compass is placed at the preferred site location in order to determine the north, east, west and south direction as shown in Figure 22.

Figure 22: Image showing a geophysicist using a compass and tripod to locate the north, south, east, and west direction.

Once the bearings have been identified, four electrodes are placed 50m away from the tripod in the east, west, south and north direction respectively. The electrodes need to be buried on a surface that has low resistance, therefore we need to ensure that the electrodes are buried in a moist area. This done by covering the electrodes with a nappy/diaper in order to retain moisture for longer, and buring it in a pot plant that has a salt water and cat litter mud solution as shown in Figure 23.

Figure 23: Image showing electrodes being placed inside a salt water and cat litter mud solution while covered with diapers for moisture retention.

The electrodes are buried 60 cm below the surface and are covered with the saltwater mud solution *(see Figure 24)*.

Figure 24: Image showing an electrode being buried in a salty water mud solution.

Once all of the electrodes have been buried, the magnetic coils are then laid out. The magnetic coils are buried at least 40 cm below the surface and are oriented in the north-south and west-east direction. A third magnetic coil is buried in the up-down direction to represent the Z-component. A compass and spirit level are used to ensure that the sensors are perfectly horizontal *(see Figure 25b)*.

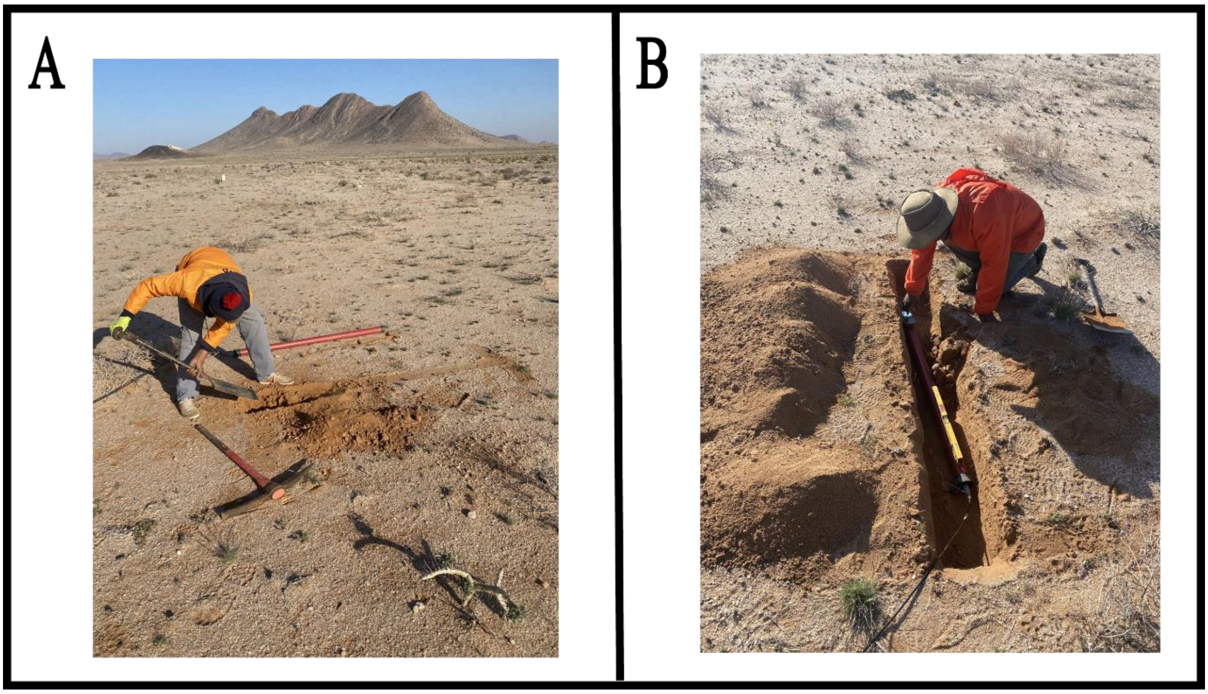

Figure 25: Image showing the magnetic coils being buried (A). Image showing the magnetic coils being accurately measured with a compass and spirit level to ensure it lays flat on the ground and in the correct direction(B).

Once the electrodes and magnetic sensors are buried correctly, they are then connected to the data logger which is placed at the centre (where the tripod was). The data logger is placed inside a casing alongside a battery to avoid overheating from the sun and damage from rain *(see Figure 26)*.

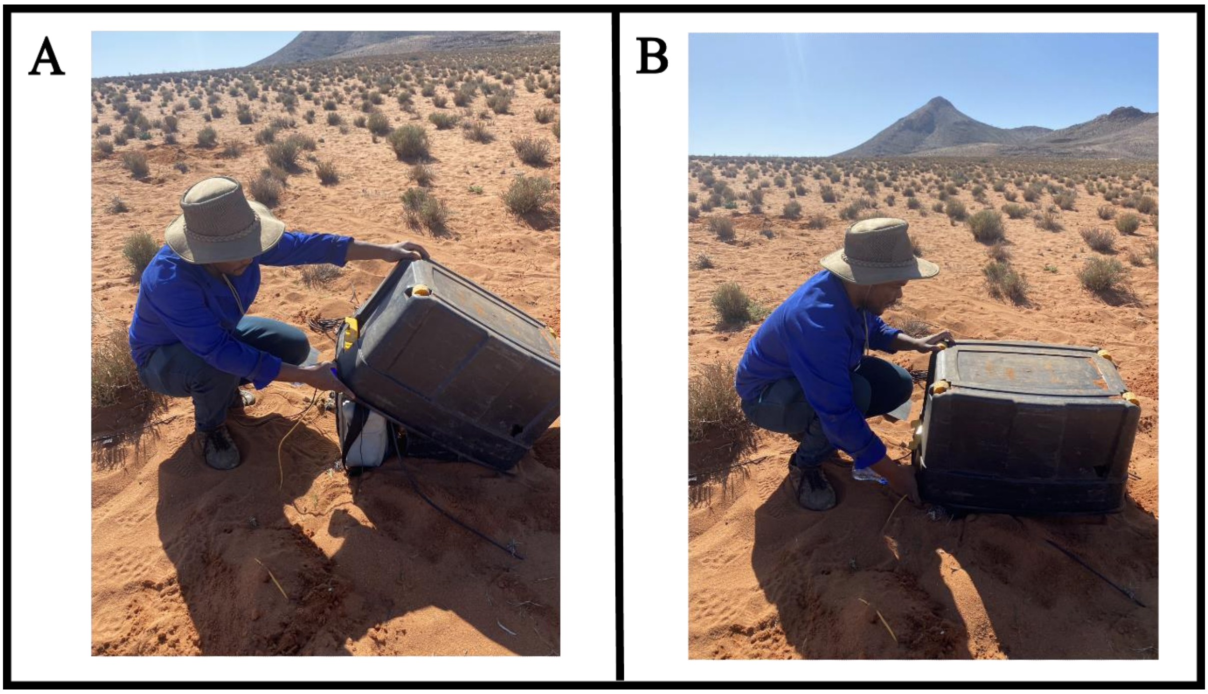

Figure 26: Image showing the data logger and battery being started up and place inside a casing.

There are various ways to layout your site but they all follow the same principle as mentioned above. There different MT arrays/layouts one can use such as the L-shaped *(see Figure 27a)* and the X-shaped *(see Figure 27b)*.

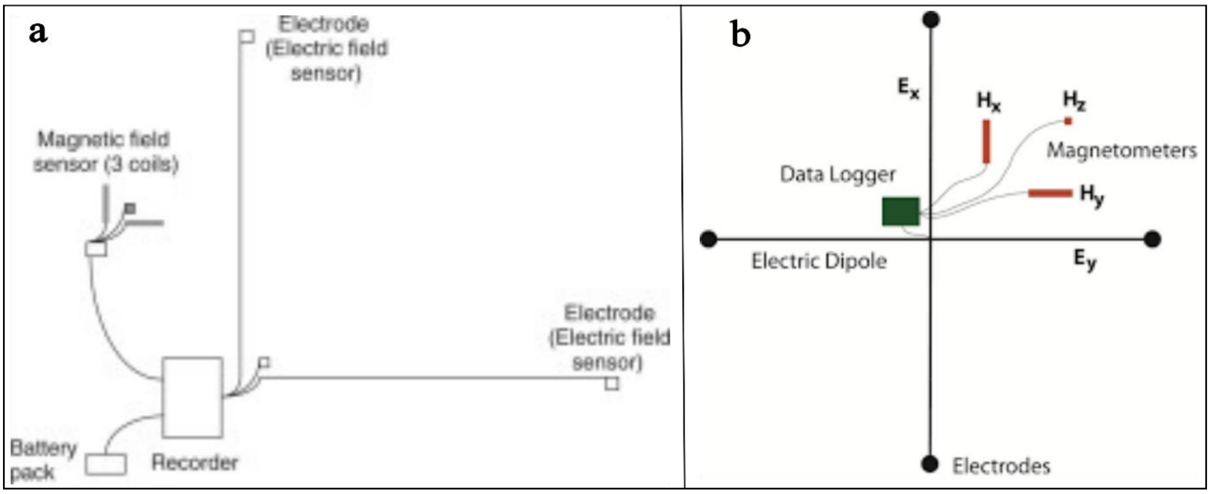

Figure 27: Typical MT station layout. (a) Shows the L-shape array and (b) shows the x-shaped array.

For the purpose of this survey the stations were left to record for two days, after which they were retrieved before being deployed to another site. Figure 28 shows the crew I had the opportunity to work with when acquiring the MT data.

Figure 28: MT crew that took part in the MT data acquisition.

Data analyses

The processing of the MT data involves the analysis and filtering of the time series data acquired from the datalogger to determine the MT impedance tensor response estimates. This is done by converting the time series data which is in the time domain into the frequency domain using Fourier Analysis. Data used in this research was obtained having already been processed and saved in .edi formatted files which contain MT impedance tensor response information; therefore, we will mainly discuss the interpretation and analyses of that data.

Data analyses and interpretation is done in the following steps:

- Data quality control
- Data dimensionality
- Editing/masking data

- Rotation
- Assigning TE and TM
- 3-D inversion

Data quality control

MT dataset is considered good quality when the apparent resistivity and phase curves have small error bars that show little to no distortion. The apparent resistivity curves should obey the 45° rule, meaning the curves should not rise or fall on a log-log plot by more than 45°, however, this is generally true for 1D structures and not 3D structures. Although it cannot be mathematically proven, in case of far field induction this holds true in 3D as well. The phase curves should be within one of the four quadrants. In this case the first quadrant (0°- 90°).

Editing/masking data

Data is edited to remove bad points in the apparent resistivity and phase curves. Some data points may indicate large error bars and would therefore need to be masked to avoid giving a misrepresentation of the dataset during inversion.

Data dimensionality

Dimensionality analysis is important in understanding what model (1-D, 2-D, 3-D) describes the Earth under the MT station. Dimensionality analyses is important in understanding what model (1-D, 2-D, 3-D) describes the Earth under the MT station. One of the most common ways to determine the dimensionality is by using the MT skew, which was first introduced by (Swift, 1967). The skew is defined by a 2x2 tensor, namely:

$$skew = \left| \frac{Z_{xx} + Z_{yy}}{Z_{xy} - Z_{yx}} \right|$$

The skew is a measure of the ratio of the amplitudes of the diagonal impedance elements to the off-diagonal impedance elements. In 1-D and 2-D cases, the skew should be zero (or less than 0.3 due to the Earth’s heterogeneous nature). Values that are far larger than zero (greater than 0.3) would be considered as indicating 3-dimensionality. However, it is possible to get a skew of 0 along symmetry axes.

There are also several other parameters to analyse data dimensionality such as: Ellipticity, Tipper Magnitude and Polar Diagrams.

Before an inversion procedure can be done on MT data, the process of MT data decomposition is required which deduces the geoelectric strike direction and the dimensionality of each MT site (whether the site response is 1-D, 2-D or 3-D in character)(Muller et al., 2009). Before an inversion procedure can be done on MT data, the process of MT data decomposition is required which deduces, the geoelectric strike direction and the dimensionality of each MT site (whether its site response is 1-D, 2-D or 3-D in character) (Muller et al., 2009). Once the best geological strike direction and dimension is determined, the MT site responses at each site can be modelled in that coordinate system and model dimension approach.

To perform the dimensionality analyses, (Weaver et al., 2000) dimensionality study based on invariants of the MT tensor has been used . These are sets of scalars that are computed from the observed MT site response and do not depend on the orientation of the axes considered (Martí et al., 2009). They are a set of eight invariants which are referred to as WAL invariants where seven are independent (I_1, I_2, I_3, I_4, I_5, I_6, I_7 and one is dependent (Q)) (Martí et al., 2009). Invariants I_1 and I_2 are the fundamental pair and are expressed by dividing the impedance by the factor μ_0. The invariants I_3, I_4, I_5, I_6, I_7 and (Q) can be identified geometrically on a Mohr circle diagram (Lilley, 1993) and can be expressed as the sine of an easily identifiable angle (Weaver et al., 2000). Invariants I_3 to I_7 and Q allow us to establish a criterion that determines the type of dimensionality and identify galvanic distortion and anisotropy in the half space. Invariants I_3 to I_7 and Q allow us to establish a criterion that determines the type of dimensionality and identify galvanic distortion and anisotropy in the half space. Galvanic distortion is the totality of changes in the electromagnetically induced electric field direction and amplitudes due to the heterogeneous nature of the electrical conductivity in the Earth’s subsurface (Bahr, 2007). Electric anisotropy is the varying conductivity of the Earth’s crust as you increase penetration depth and vary orientation of the earth's half space (Martí et al., 2010). The use of these invariants provides a full dimensionality analysis and the parameters necessary to correct for galvanic distortion, and it is for this reason that the WAL invariants were chosen as suitable to perform the dimensionality analyses. Table 3 and Table 4 shows a summary of the criteria each invariant has to follow for each geoelectric dimensionality.

Table 3: Dimensionality criteria according to the WAL invariants values of the magnetotelluric tensor (Martí et al., 2009).

Case	I_3 to I_7 and Q values	Geoelectric dimensionality
1	$I_3 = I_4 = I_5 = I_6 = 0$	**1D** $\rho_{1D} = \mu_0((I_1^2+I_2^2)/\omega)$, $\varphi_{1D} = \arctan(I_2/I_1)$
2	$I_3 \neq 0$ or $I_4 \neq 0$; $I_5 = I_6 = 0$; $I_7 = 0$ or $Q = 0$ ($\xi_4 \neq 0$ and $\eta_4 \neq 0$)	**2D**
3a	$I_3 \neq 0$ or $I_4 \neq 0$; $I_5 \neq 0$; $I_6 = 0$; $I_7 = 0$	**3D/2D twist** 2D affected by galvanic distortion (only twist)
3b	$I_3 \neq 0$ or $I_4 \neq 0$; $I_5 \neq 0$; $I_6 = 0$; $Q = 0$	**3D/1D 2D** Galvanic distortion over a 1D or 2D structure (non-recoverable strike direction)
3c	$I_3 \neq 0$ or $I_4 \neq 0$; $I_5 = I_6 = 0$; $I_7 = 0$ or $Q = 0$ ($\xi_4 = 0$ and $\eta_4 = 0$)	**3D/1D 2D diag** Galvanic distortion over a 1D or 2D structure resulting in a diagonal MT tensor
4	$I_3 \neq 0$ or $I_4 \neq 0$; $I_5 \neq 0$; $I_6 \neq 0$; $I_7 = 0$	**3D/2D** General case of galvanic distortion over a 2D structure
5	$I_7 \neq 0$	**3D** (affected or not by galvanic distortion)

Table 4: An extension of the dimensional criteria to anisotropic structures (Martí et al., 2010).

<table>
<tr><th>I_3 to I_7 and Q</th><th colspan="4">GEOELECTRIC DIMENSIONALITY (“2D cases”)</th></tr>
<tr><td rowspan="5">$I_3 \neq 0$ or $I_4 \neq 0$;
$I_5 = I_6 = 0$;
$I_7 = 0$ or Q = 0</td><td rowspan="3">$\theta_{2D} = \theta_1 = \theta_2 = \theta_{3D/2D}$</td><td rowspan="2">Identical tensors at all sites (period dependent)</td><td>$\theta_{2D} = 0$</td><td>1D MEDIUM WITH ONE ANISOTROPIC LAYER or 2D ISOTROPIC MEDIUM WITH MEASUREMENTS ALONG STRIKE</td></tr>
<tr><td>$\theta_{2D} \neq 0$</td><td>1D MEDIUM WITH ONE ANISOTROPIC LAYER</td></tr>
<tr><td colspan="2">Different tensors at each site (period dependent)</td><td>2D ISOTROPIC MEDIUM</td></tr>
<tr><td>$\theta_{2D} \neq \theta_{3D/2D}$</td><td colspan="2">Identical tensors at all sites (period independent)</td><td>HOMOGENEOUS ANISOTROPIC MEDIUM</td></tr>
<tr><td>$\theta_{2D} \neq \theta_{3D/2D}$
or
$\theta_1 \neq \theta_2$</td><td colspan="2">Different tensors at each site (period dependent)</td><td>ANISOTROPIC STRUCTURE IN A 2D MEDIUM</td></tr>
</table>

A FORTRAN code called WALDIM was utilized to perform the MT analysis using the Weaver et al. (2000) criteria. When running the program, the following inputs are needed:

- A file that has input parameters, these input parameters include:

- Units for impedances in EDI files $\left(M = \frac{m}{s}; F = \frac{km}{s}; Z = Ohm\right)$
- Threshold value for invariants I3 to I7
- Q threshold value
- Whether the EDI files contain errors or not (YES/NO)
- Using errors in EDI files (YES/NO)
- Whether to average in bands (YES/NO)
- Minimum period to average
- Maximum period to average
- Number of bands per decade
- Root name for output files
- Writing file with all parameters and errors

- A file containing a list of all names of the sites with their accompanied coordinates.
- EDI files of each site.

The code outputs the type of dimensionality corresponding to each site and frequency, and computes related parameters, such as strike direction and distortion parameters, with their errors. Figure 29 shows an example of one of the output files obtained when entering an MT station EDI file (kim001) into the WALDIM code. The output files provide a summary of the overall results as it shows the dimensions, relevant strike direction, twist and shear angle of each measured period of the MT site response.

Writing main dimensionality analysis results for site kim001

Table with results for each frequency

Site	Longitude	Latitude	F(Hz)	Per(s)	DIM	Strike(º)	errStrike(º)	Twist(º)	errTwist(º)	Shear(º)	errShear(º)
kim001	23.1706	-27.6581	0.360E+03	0.278E-02	3D						
kim001	23.1706	-27.6581	0.300E+03	0.333E-02	3D						
kim001	23.1706	-27.6581	0.260E+03	0.385E-02	3D						
kim001	23.1706	-27.6581	0.220E+03	0.455E-02	3D						
kim001	23.1706	-27.6581	0.180E+03	0.556E-02	3D						
kim001	23.1706	-27.6581	0.150E+03	0.667E-02	3D						
kim001	23.1706	-27.6581	0.130E+03	0.769E-02	3D						
kim001	23.1706	-27.6581	0.110E+03	0.909E-02	ANIS-HINT1	74.8791	0.0498				
kim001	23.1706	-27.6581	0.900E+02	0.111E-01	ANIS-HINT2	47.7576	0.0000				
kim001	23.1706	-27.6581	0.750E+02	0.133E-01	ANIS-HINT2	38.4568	0.0000				
kim001	23.1706	-27.6581	0.650E+02	0.154E-01	3D						
kim001	23.1706	-27.6581	0.550E+02	0.182E-01	3D						
kim001	23.1706	-27.6581	0.450E+02	0.222E-01	ANIS-HINT2	20.3506	0.0000				
kim001	23.1706	-27.6581	0.370E+02	0.270E-01	ANIS-HINT2	18.1009	0.0000				
kim001	23.1706	-27.6581	0.330E+02	0.303E-01	ANIS-HINT2	15.5410	0.0000				
kim001	23.1706	-27.6581	0.275E+02	0.364E-01	ANIS-HINT2	14.1871	0.0000				
kim001	23.1706	-27.6581	0.225E+02	0.444E-01	3D						
kim001	23.1706	-27.6581	0.188E+02	0.532E-01	ANIS-HINT2	12.9132	0.0000				
kim001	23.1706	-27.6581	0.162E+02	0.617E-01	3D						
kim001	23.1706	-27.6581	0.137E+02	0.730E-01	3D						
kim001	23.1706	-27.6581	0.112E+02	0.893E-01	3D						
kim001	23.1706	-27.6581	0.940E+01	0.106E+00	3D						
kim001	23.1706	-27.6581	0.810E+01	0.123E+00	3D						
kim001	23.1706	-27.6581	0.690E+01	0.145E+00	3D						
kim001	23.1706	-27.6581	0.560E+01	0.179E+00	3D						
kim001	23.1706	-27.6581	0.490E+01	0.204E+00	3D						
kim001	23.1706	-27.6581	0.410E+01	0.244E+00	3D						
kim001	23.1706	-27.6581	0.340E+01	0.294E+00	3D						
kim001	23.1706	-27.6581	0.281E+01	0.356E+00	3D						
kim001	23.1706	-27.6581	0.244E+01	0.410E+00	3D						
kim001	23.1706	-27.6581	0.206E+01	0.485E+00	3D						
kim001	23.1706	-27.6581	0.169E+01	0.592E+00	3D/2Dtw	36.9317	0.0707	-7.5736	0.0322	-4.6644	0.0544
kim001	23.1706	-27.6581	0.141E+01	0.709E+00	3D/2Dtw	34.8953	0.0742	-8.0804	0.0383	-6.2418	0.0602
kim001	23.1706	-27.6581	0.122E+01	0.820E+00	3D/2Dtw	31.7432	0.1079	-8.0177	0.0486	-7.3708	0.0790
kim001	23.1706	-27.6581	0.103E+01	0.971E+00	2D	38.3574	0.0324				

Figure 29: An example of the output files obtained from the WALDIM code for a site labelled kim001.

Rotation

When conducting magnetotelluric surveys, the electric and magnetic fields are measured in multiple directions and frequencies. These measurements can be represented as a set of impedance tensors for each frequency and direction. However, the inherent anisotropy of the Earth's subsurface can make the interpretation of these tensors complex.

To simplify the analysis and interpretation of the data, we often rotate the impedance tensors. The rotation involves applying appropriate mathematical transformations to the impedance tensors to be parallel or perpendicular to the impedance strike. This can make it easier to identify the dominant geological features and conductivity structures in the subsurface.

Assigning TE and TM

After rotating the impedance tensors, it's possible to assign the Transverse Electric (TE) and Transverse Magnetic (TM) modes from the rotated tensors. TE should be parallel to the predominant current flow and TM should be perpendicular to it.

The tipper strike would generally indicate the geological strike in which the TE should be directed. The tipper is a measure of the ratio of the horizontal and vertical components of the magnetic fields.

Inversion 1-D/3-D

In order to better understand the dataset, it will need to be visualized. We use numerical models to provide us with inversion models of how the dataset looks like probabilistically. This is called inversion, and it can be done in 1-D, 2-D, or 3-D.

Phase tensor maps

The phase tensor is derived from the (MT) impedance tensor, it provides additional information about the variation of subsurface conductivity. It is also a good dimensionality indicator as it does not require any assumptions about the dimensionality of the subsurface (Caldwell et al., 2004).

The phase tensor can be represented graphically as an ellipse, with the orientation of the principal axes of the phase tensor ellipse reflecting the lateral variations in the regional conductivity structure and the direction of greatest inductive response which is also closely related to the 2-D geoelectric strike direction (Caldwell et al., 2004). The shape of the ellipse can also describe the dimensionality of the structure where a circular phase tensor relates to a 1-D structure, a more elliptical shape phase tensor relates to a 2-D or 3-D structure.

The phase tensor can be characterized by three coordinate invariants, namely the maximum phase value (Φ_{max}), the minimum phase value (Φ_{min}) and the skew angle (β). Φ_{max} and Φ_{min} provide information about the orientation of the maximum and minimum conductivity directions, respectively, while β indicates the degree of skewness or misalignment between the minor and major axes (Caldwell et al., 2004).

Data processing

Using the data analyses mentioned in the methodology chapter, an analysis was conducted on the MT data. For data processing the following software packages have been utilized:

- MTpy: An open-source Python toolbox software that contains modules for basic processing and analysis that can be applied to MT data. The software bases its codes on existing and widely accepted research papers on MT data processing and analysis (Krieger & Peacock, 2014:

Kirkby et al., 2019). This software was used to create penetration depth, phase tensor and strike analyses maps.

- Geotools: An MT data analyses licensed software that has QC, data editing, data analyses and 1D to 3D inversion modelling. It is currently owned by and commercially available from CGG.
- ModEM: An electromagnetic modelling and inversion software, written in Fortran 95 (Egbert & Kelbert, 2012; (Kelbert et al., 2014)). This software was used to conduct the 3D inversion model.
- WALDIM: This is a code written in Fortran that calculates the various dimensionalities below the stations at various periods (Weaver et al., 2000).

Chapter 5. Results

The MT data used in this section are the 14 station MT dataset from CGS that was collected in my study area in the Northern Cape. This dataset is explained in detail in the data section of the methodology chapter.

Raw data visualisation

Data visualization is essential in MT for its ability to provide insights into the quality, interpretation, and communication of complex geological data. Apparent resistivity plots and phase diagrams offer initial assessments of data quality, revealing patterns and anomalies that may indicate noise or interference. Pseudo-sections provide a comprehensive view of subsurface resistivity and phase variations. Penetration depth maps offer insights into how deep the MT measurements penetrate the Earth's subsurface, guiding the understanding of geological features' depth extent.

Data examples shown in Figure 30 for selected sites, NAM155, NAM168, NAM166, NAM20, show their respective apparent resistivity and phase curves. The apparent resistivity in these sites show varying behaviour along the profiles, indicating the complexity of the geoelectric structure. Sites NAM155, NAM166, NAM20 show high apparent resistivity values reaching up to approximately 10^4 Ohm.m for the Z_{xy} and Z_{yx} components. A quality check was conducted where highly scattered MT estimates were masked to guarantee a smooth MT response function for further analyses and modelling. Site NAM168 shows an example of good quality data in terms of the Z_{xy} and Z_{yx} components with a smooth curve and small error bar values, as compared to the Z_{xx} and Z_{yy} components of the same site where the phase values have larger error bar values.

The raw edi plots of the 14 MT stations *(see Appendix A: Raw Edi Plots)* indicates a generally good quality dataset, with the apparent resistivity plots depicting generally smooth curves. However, there is a consistent trend amongst all plots where the apparent resistivity and phase values of the Z_{xy} and Z_{yx} component appear to have smoother curves and smaller error bar values, as compared to those of the Z_{xx} and Z_{yy} components which have values that have larger error bar values.

The Z_{xx} and Z_{yy} components correspond to diagonal elements of the impedance tensor, which involve the electric field and magnetic field being parallel to each other. This then makes measurements in this direction/component more sensitive to the anisotropy and heterogeneity of the subsurface, as compared to the Z_{xy} and Z_{yx} components which correspond to off-diagonal elements of the impedance tensor, which involves the electric field and magnetic field being in different directions from each other, making them less sensitive to the anisotropy variations in the subsurface. This and the behaviour of the curves suggests the possibility of 2-D and 3-D structures.

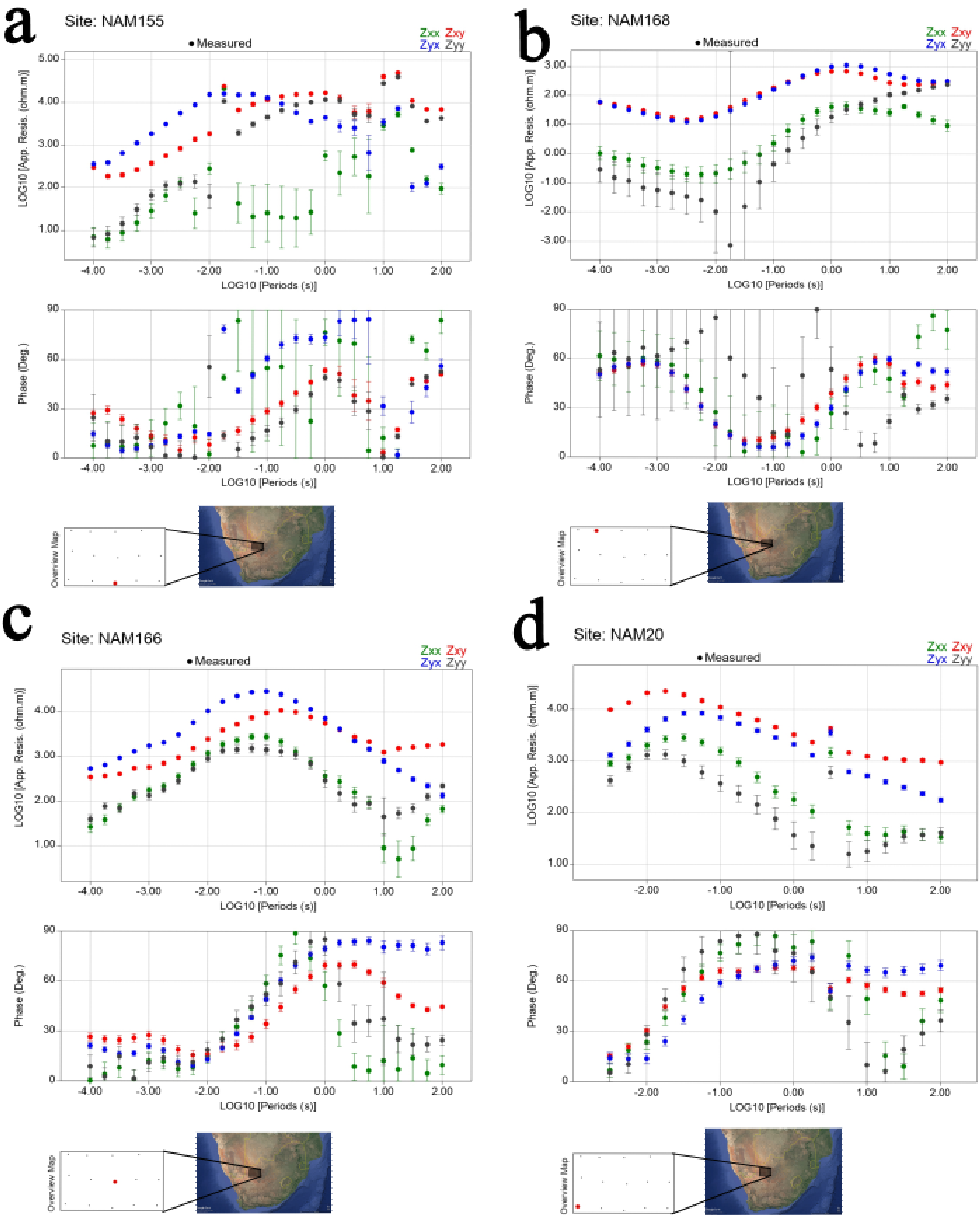

Figure 30: EDI plots of four stations: NAM155, NAM168, NAM166, NAM20. The plots show the apparent resistivity and phase of all four components. The overview map at the bottom of each plots shows the relative location of the site.

Before any inversion processes are carried out, preliminary analyses of the MT data must be done to gather a preliminary understanding of resistivity variations of the subsurface and to know which inversion method to use between 2D and 3D. Starting with using pseudo-sections, which are apparent resistivity and phase data against increasing period sections that provide a quick analysis of the resistivity variation.

The MT data have been divided into 3 profiles. The direction of these profiles is E-W, this direction was chosen because it is perpendicular to the strike of the geological features of the study area, which should make it easier to observe any resistivity variations. The pseudo-sections were created using the Geotools software package using 10 periods per decade, a tolerance of 0.5, a horizontal distance (x) of 300km, a cell size of 10 km, an interpolation radius of 5 km and a smoothing factor of 2 in the x direction and 1 in the y direction.

Apparent resistivity pseudo-sections

Profile 1

The TE and TM pseudo-sections *(see Figure 31)* indicate an overall conductive structure with a resistive (averaging 15000 Ohm.m) structure transcending from the east, with the TM section showing a large resistive structure transcending westerly.

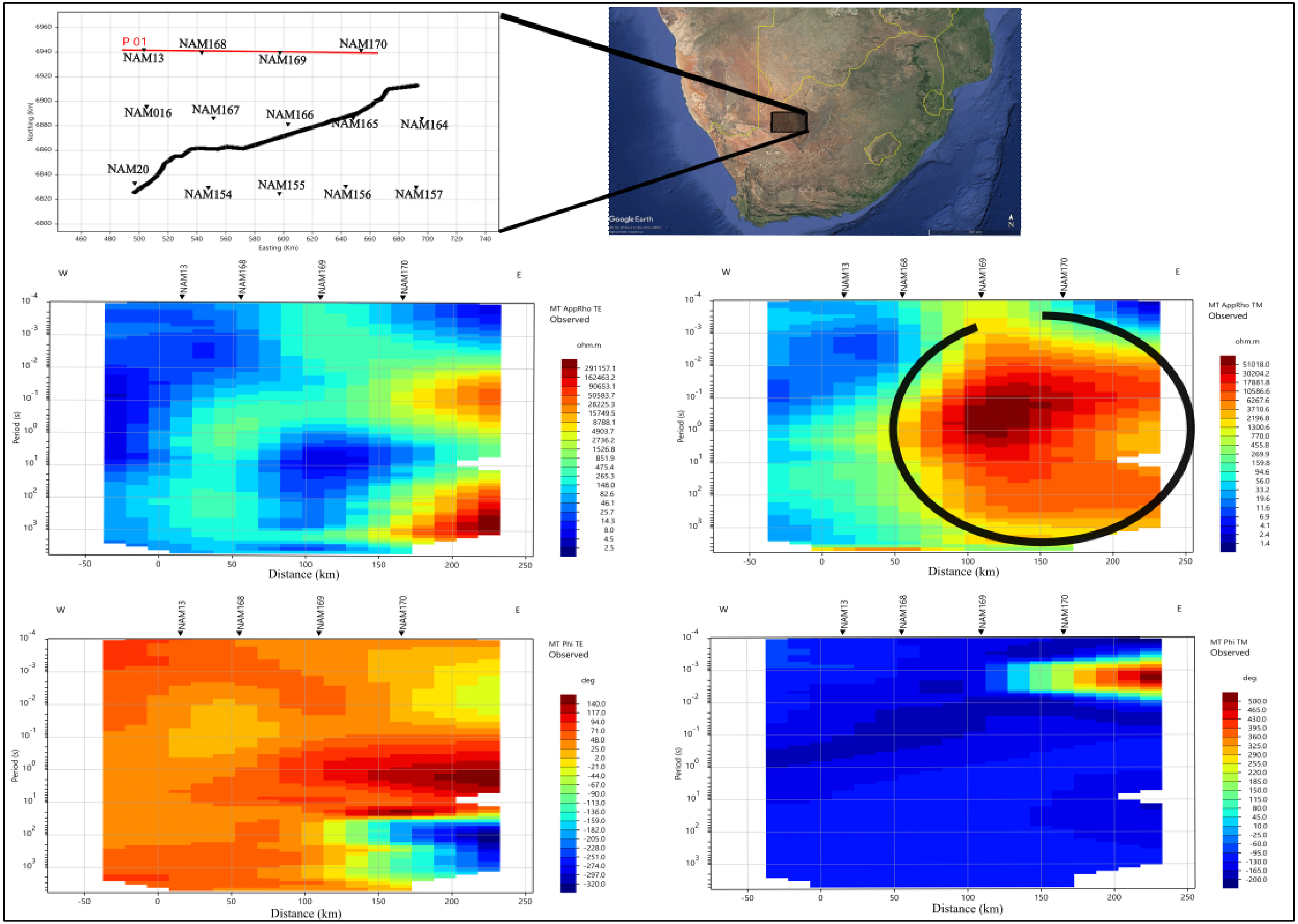

Figure 31: Pseudo section plot of Profile 1, showing the TE and TM mode of the apparent resistivity (AppRho) and phase (Phi) variations. The red colour indicates resistive structures, and the blue colour indicates conductive structures in the AppRho plots. The blue colour shows the lower phase angles of impedance, while the red colour indicates the higher phase angles of impedance in the phase diagrams. The region marked with a black circle indicates the large resistive region transcending westerly. The triangles above the sections indicate the MT stations. The black line on the location map indicates the seismic line and black triangles the MT sites.

Profile 2

Profile 2 pseudo-sections *(see Figure 32)* show relatively identical apparent resistivity sections for the TE and TM modes. The apparent resistivity sections indicate a region with an overall resistive subsurface in the region of 3000 Ohm.m.

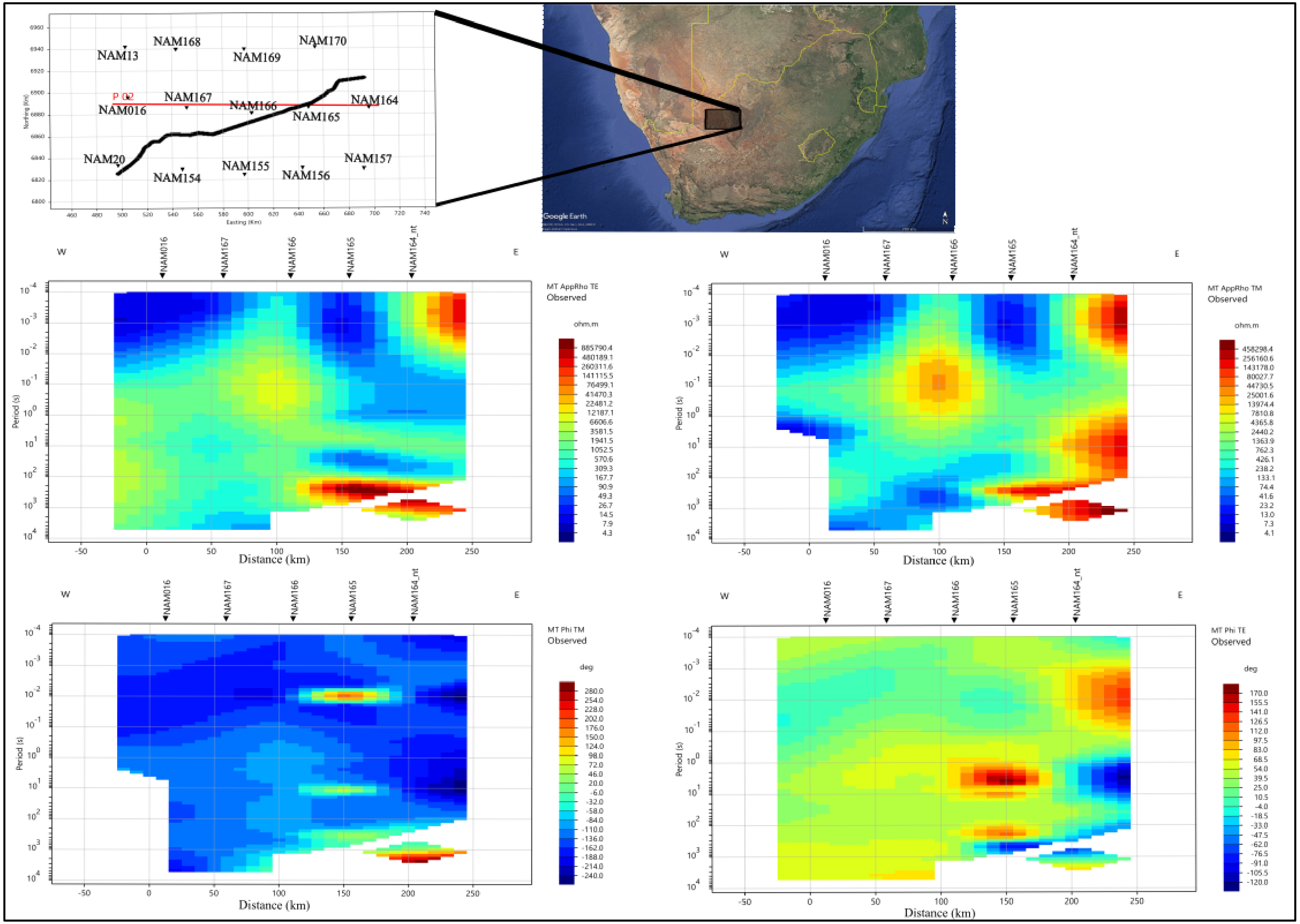

Figure 32: Pseudo section plot of Profile 2, showing the TE and TM mode of the apparent resistivity (AppRho) and phase (Phi) variations. The red colour indicates resistive structures, and the blue colour indicates conductive structures in the AppRho plots. The blue colour shows the lower phase angles of impedance, while the red colour indicates the higher phase angles of impedance in the phase diagrams. The triangles above the sections indicate the MT stations. The black line on the location map indicates the seismic line and black triangles the MT sites.

Profile 3

Profile 3 pseudo-sections (see Figure 33) shows relatively identical TE and TM mode sections for apparent resistivity and the phase tensor, with an overall resistivity of 6000 Ohm.m.

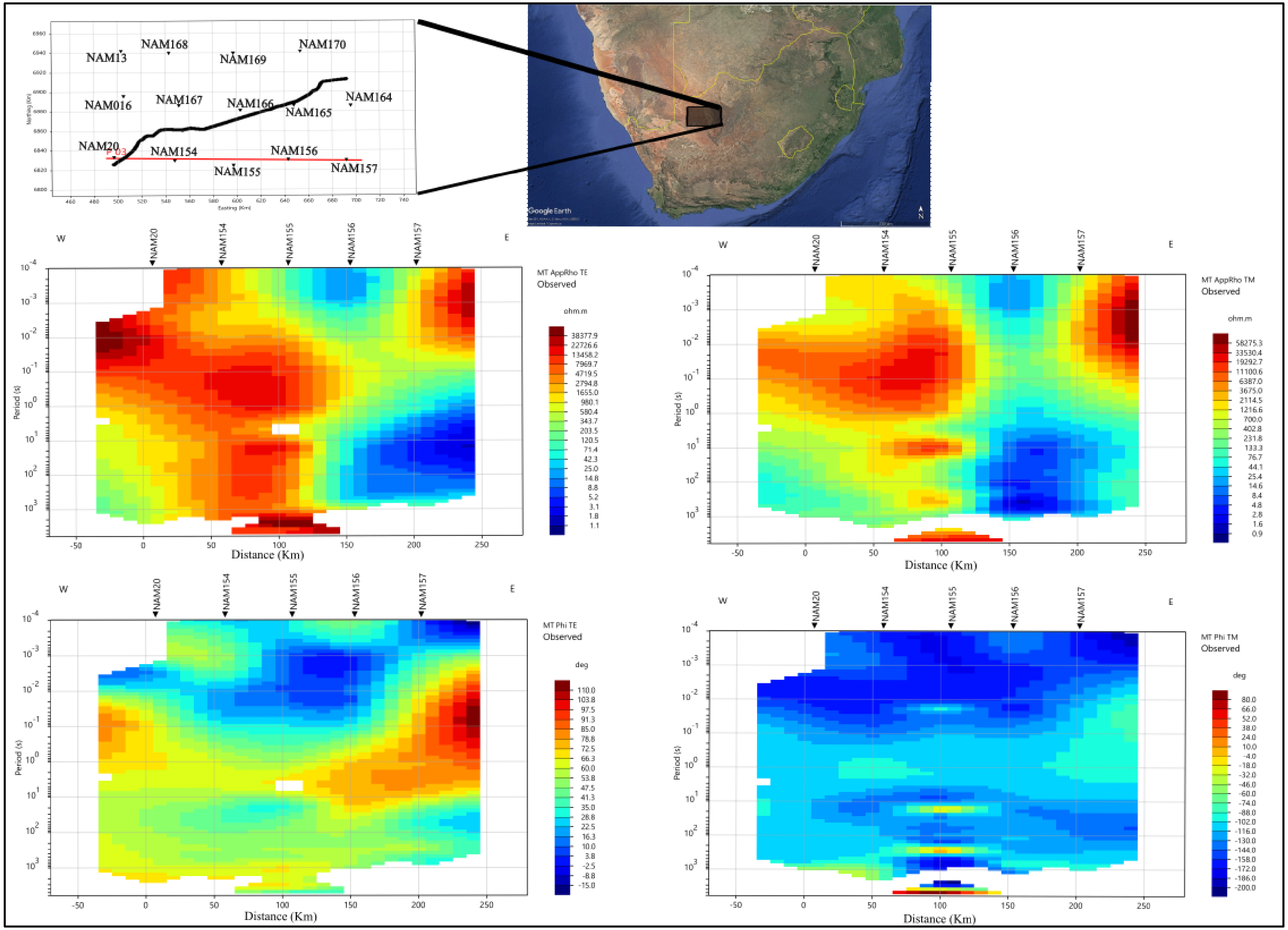

Figure 33: Pseudo section plot of Profile 3, showing the TE and TM mode of the apparent resistivity and phase variations. The red colour indicates resistive structures, and the blue colour indicates conductive structures in the AppRho plots. The blue colour shows the lower phase angles of impedance, while the red colour indicates the higher phase angles of impedance in the phase diagrams. The triangles above the sections indicate the MT stations. The black line on the location map indicates the seismic line and black triangles the MT stations.

Penetration Depth

During pre-data analyses, it is important to understand the penetration depths beneath the recording stations. This is to make sure that the right initial model parameters for 2-D or 3-D inversion are used.

The Niblett-Bostick Depth Transformation gives a resistivity-depth distribution in a half space medium of resistivity equal to the apparent resistivity in relation to its respective period (Niblett & Sayn-Wittgenstein, 1960); Bostik, 1977).

Figure 34 shows the Niblett-Bostick depth using MTpy. It shows plots for four periods: 0.1 s, 2.4 s, 109.2 s, and 252.1 s. The first thing that can be seen is that there is a variation in the penetration depths along the stations in each frequency, this can be related to the fact that due to the variation in the subsurface resistivity structure (as suggested by the pseudo-sections) below the stations it can be expected to have a variation in penetration depth, since this calculation of the penetration depth is dependent on apparent resistivity. Looking at the map with period 252.1 s in Figure 34, the maximum penetration depth of majority of the stations, 10 out of 14 stations, is approximately 200 km, with one station having a penetration depth of 600 km.

The one station (NAM165) with a penetration depth of approximately 600 km could indicate that it is in a region that has higher resistivity than the other regions. It could also indicate that there may be something wrong with that specific station and will require further investigation. The desired penetration depth for this study is 40 km, as it is approximately the same penetration depth as the seismic data which will be used in this study. A depth of 40 km is well within the overall penetration depth of the stations, good quality inversion approximation results can be expected at this depth.

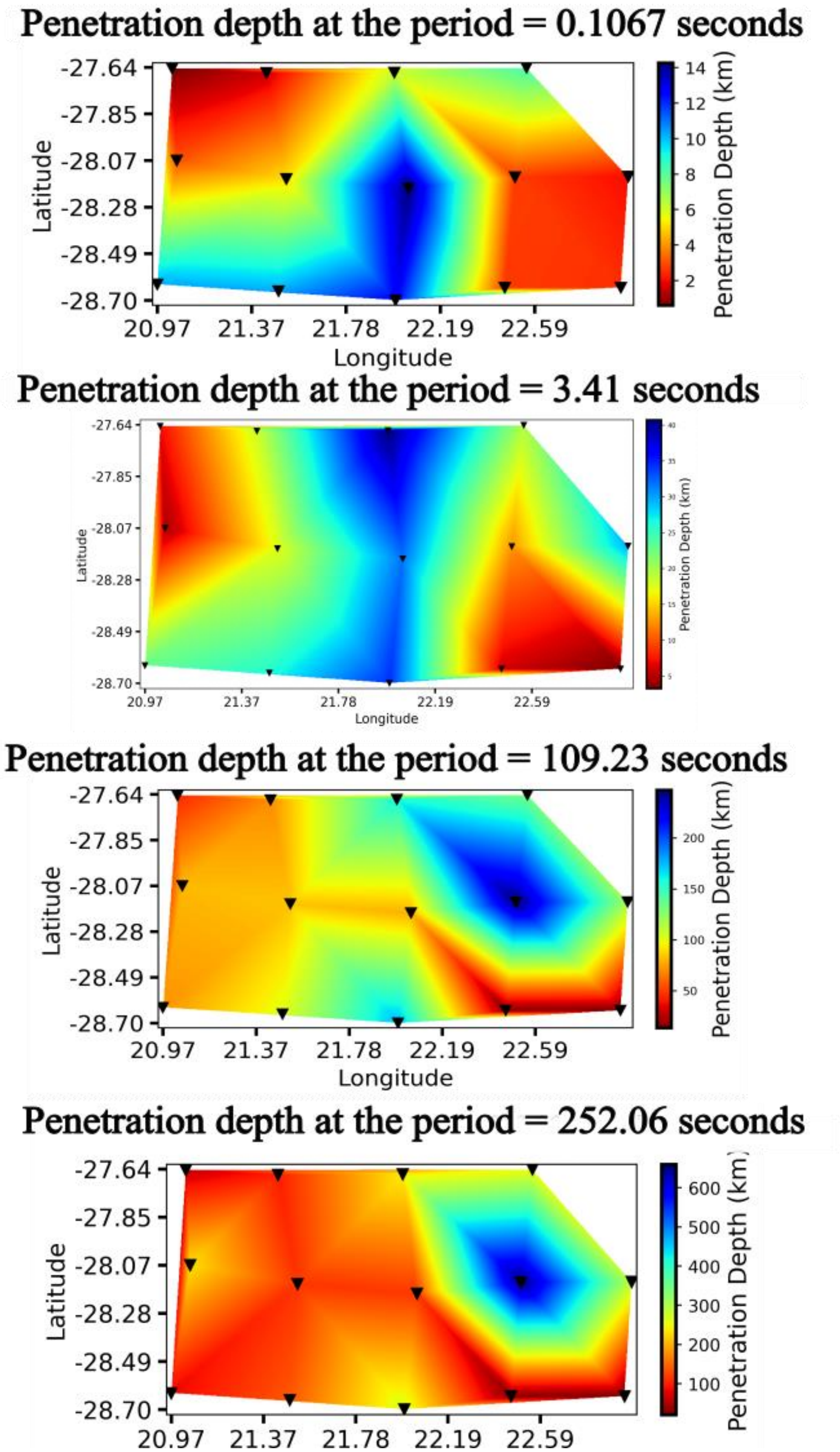

Figure 34: Niblett-Bostick depth estimates map for all stations at periods 0.1 s, 2.4 s, 109.2 s, and 252.1 s

Phase Tensor Maps

Figure 35 shows the phase tensor maps of this study's MT stations. Phase tensor maps for the maximum phase value (Φ_{max}), the minimum phase value (Φ_{min}) and the skew angle (β) are plotted for the respective periods 0.1s, 3.3s and 100s. The imaginary (blue arrow) and real (black arrow) parts of the induction arrows of the tipper are also plotted, they are used to define the major and minor axes of the phase tensor ellipse where the real part of the impedance tensor is parallel to the major axes which also indicates the preferred direction of flow as it is in the direction of maximum conductivity. The imaginary part is parallel to the minor axes and is in the direction of the minimum conductivity (Caldwell et al., 2004). The length of these arrows is proportional to the magnitude of the real and imaginary tipper. If the two arrows are perpendicular, it suggests that the subsurface is isotropic, meaning the conductivity is the same in all directions however if the two arrows are not perpendicular, there is a variation in the subsurface conductivity.

The phase tensor is derived from the MT impedance tensor, it provides additional information about the variation of subsurface conductivity. It is also a good dimensionality indicator as it does not require any assumptions about the dimensionality of the subsurface (Caldwell et al., 2004). Looking at Figure 35, there is a variation in the maximum phase value (Φ_{max}), the minimum phase value (Φ_{min}) and the skew angle (β) values, with changes in the period. However, the phase tensor ellipse shape and tipper directions remain the same with change in period with few stations showing variations. Majority of the phase tensor ellipses are elliptically shaped, suggesting at least 2-D structures being present in the half-space. The phase tensor ellipse shape varies with all the stations and all three periods. However, they appear to be orienting in the NW-SE direction. This suggest that the geological structure of the region is complex with geological features facing different directions.

The skew angle shows the relationship between the major and minor axes, with a skew angle closer to zero indicating that the major and minor axes are close to being orthogonal and a larger value indicating an increase in the deviation between the two axes. Looking at the skew values in Figure 35 the major and minor axes are not orthogonal in all periods based on the relatively high values of the tilt in all three observed periods. Although there is a variation, the minimum phase values indicate that, generally, the azimuth direction of the least conductive geological features is in the region of approximately 20° - 40°. The maximum phase values indicate that generally the azimuth direction of the most conductive geological features is in the region of approx. 40° - 80°. The tipper values (real and imaginary) are not observed to be perpendicular to each other, which suggests that the subsurface conductivity is anisotropic.

The direction of the real tipper arrow uses the Parkinson convention (Parkinson, 1959) which means it points towards the conductive zone. The real tipper arrow points in the south to south-westerly direction on most stations especially in the southern region of the map suggesting that there might be a region of high conductance in that region. The large magnitude of the tipper in the southeasterly region of the tipper is suggestive of how close the conductive zone is from those stations; with the very small magnitude of the real tipper values in the northwest region of the map suggesting a less conductive zone in that region.

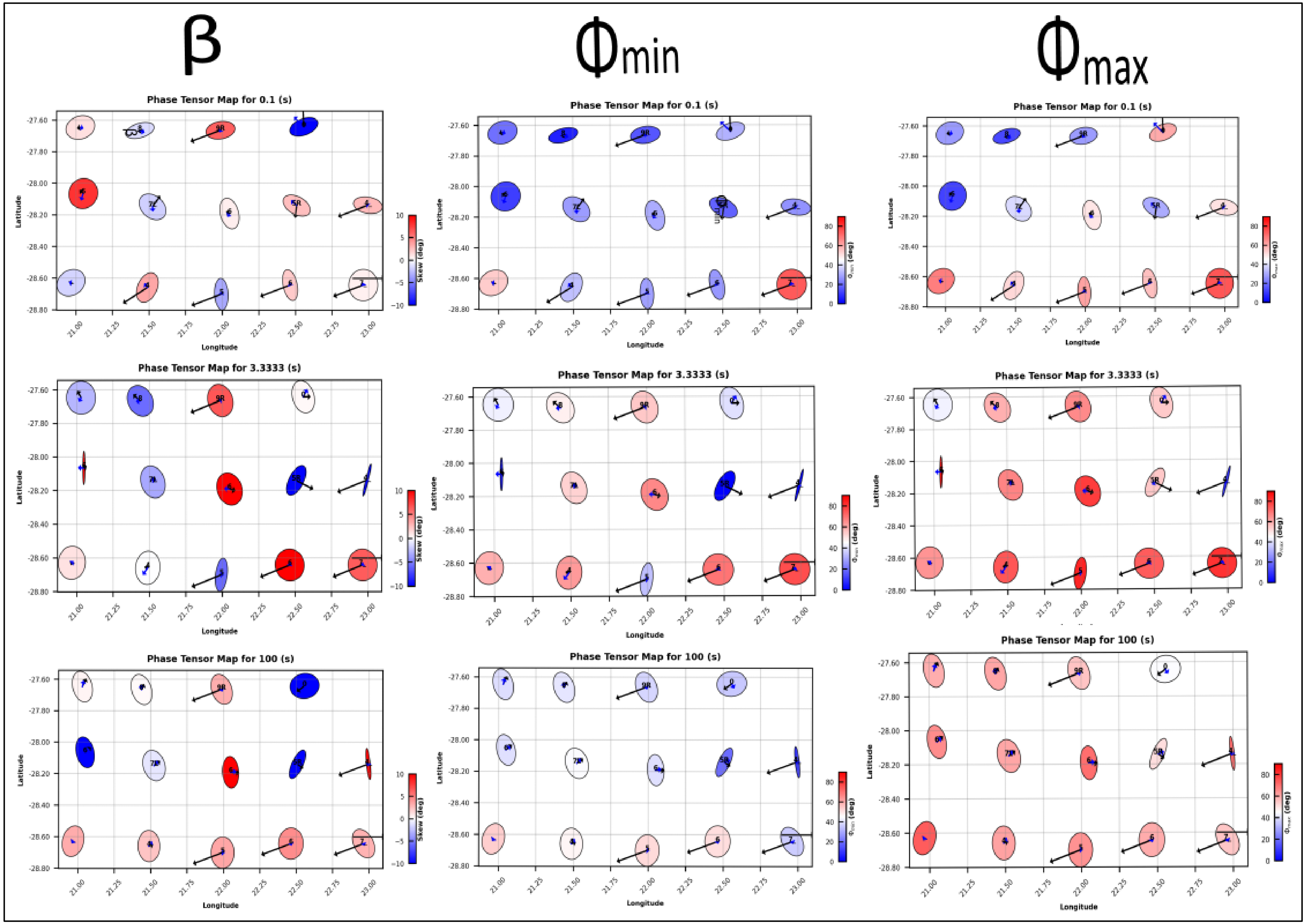

Figure 35: Image showing the phase tensor maps of this study's MT stations. The phase maps are for periods 0.1s, 3.3s and 100s. Phase tensor maps for the maximum phase value (Φ_{max}), the minimum phase value (Φ_{min}) and the skew angle (β) are plotted for the respective periods. The imaginary (blue arrow) and real (black arrow) parts of the induction arrows of the tipper, are used to define the major and minor axes of the ellipses.

Strike and dimension analyses

Figure 36 shows the calculated strike angles plotted as rose diagrams. The impedance (Z) strike was calculated based on Weaver et al. (2000), the phase tensor azimuth and tipper strike were calculated based on Caldwell et al. (2004). The geology of the region appears to have a NW-SE trend in the west and N-S around the Kheis Terrane. The results of the impedance strike and phase tensor strike angle supports this analysis as it shows varied strike angles that are between the NW and NE direction. A 90° ambiguity remains when determining the strike directions, this is due to the condition of a 2D case where its strike is either parallel or perpendicular to the impedance tensor which determines the maximum or minimum current flow Caldwell et al. (2004). However, this ambiguity can be solved using the real induction arrows, using the fact that in a 2D case the induction arrows are perpendicular to the strike direction. The strike from these three methods is equivalent which shows the reliability of the strike value provided as it is consistent throughout all three methods. Using the calculated strike angle and the real induction arrows, the suggested strike direction is approx. 75° NW or 15° West of North. A general NE-SW strike direction is therefore invoked, given that the tipper strike is generally oriented in the NW direction *(see Figure 35).*

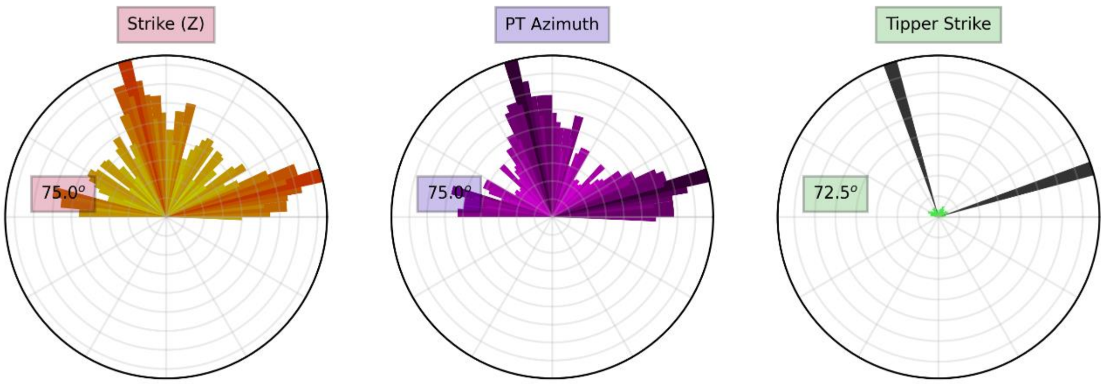

Figure 36: Rose diagrams of the mean strike angles, phase tensor (PT) azimuth and tipper strike of all stations.

A dimensionality analyses was carried out for selected periods at each site using the WALDIM code (Martí et al., 2009). Table 5 shows the parameters used for the parameter input file in order to run the program:

Table 5: Inputs used to run the WALDIM program.

Parameter	Input used
Units for impedances	M
Threshold value for invariants I3 to I7	0.150
Q threshold value	0.100
EDI files contain errors	Yes
Using errors in EDI files	Yes
Average in bands	Yes
Minimum period to average	0.1×10^{-4}
Maximum period to average	0.1×10^{4}
Number of bands per decade	1.0
Root name for output files	OUT
Writing file with all parameters and errors	Yes

Threshold values were required as they represent boundary conditions to which the invariants are minimized. Therefore any invariant value below this value will be considered to be zero. The recommended literature threshold of 0.15 was used for invariants I3 to I7 and a threshold value of 0.1 was used for the Q invariant. The minimum and maximum periods used at each site was 10^{-6}s to 10^{6}s respectively.

Figure 37 shows a visualized plot of the WALD outputs. A one-dimensional (1D) case is representative of earth as a horizontally layered medium, a two-dimensional (2D) case is suggestive of a layered earth containing a significant portion of medium aligned to a strike. Three dimensional (3D) cases suggest an entirely structurally complex medium with structural bodies of various shapes and sizes. Twist and shear outputs are due to galvanic distortions caused by near surface inhomogeneities with inductive effects that decay to long periods.

The following are the dimensionality types used in Figure 37:

- UNDETERMINED
- 1D
- 2D
- 3D/2D only twist
- 3D/2D general
- 3D
- 3D/2D with diagonal regional tensor
- 3D/2D or 3D/1D indistinguishable
- Anisotropy hint 1: homogeneous anisotropic medium
- Anisotropy hint 2: anisotropic body within a 2D medium

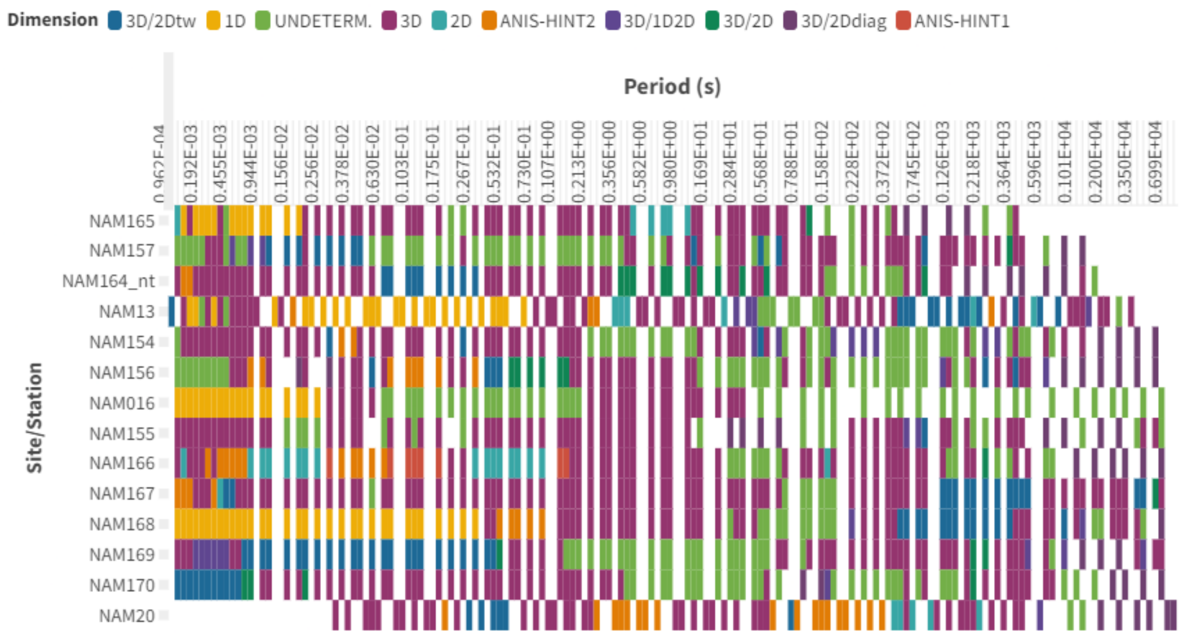

Figure 37: Plots of the WALD outputs visualized, where the dimensionality parameters (1D, 2D, 3D, 3D/2Dtw, 3D/1D2D, ANIS-HINT2, ANIS-HINT1, 3D/2D, 3D/2Ddiag, UNDETERM are plotted with respect to period (s) for each site. One dimensional (1D) outputs are representative of earth as a horizontally layered medium where the diagonals of the MT tensor are zero and the non-diagonal components are equal with opposite signs. A two-dimensional case (2D) occurs when an axis aligns to a geoelectric strike where the diagonal components remain zero and the non-diagonal components are no longer equal or opposite; suggestive of a layered earth containing a significant portion of medium aligned to a strike. Three dimensional cases (3D) are representative of the MT tensor where diagonal and off diagonal components are non-zero; an entirely structurally complex medium. Twist and shear outputs are due to galvanic distortions caused by near surface

inhomogeneities with inductive effects that decay to long periods. The undetermined outputs are due to those periods not meeting the threshold.

Figure 38 shows a graph which will allow us to numerically quantify the occurrence of each dimensionality. Understanding the dominant dimensionality will help provide an appropriate reason to choose the best method to use in the inversion process (2D or 3D inversion). Based on the graph in Figure 38, it can be seen that there is a majority of 3D cases within all stations. 3D cases account for approximately 47% of all dimensionality cases. This means that the substructure below the stations is structurally complex, with structural bodies of various shapes and sizes.

From Figure 37 the subsurface is shown to be structurally complex due to its variety of all 10 dimensions at various periods. There is observed evidence of galvanic distortion and electric anisotropy, which means that the subsurface has varying conductivity structures which also have varying directions of the electric field direction at different periods. There is observed evidence of 1D structures near surface (up to 10^2s) mainly in stations NAM13, NAM168, NAM165 and NAM016. Although, there is also evidence of 2D structures there is an observed dominance of 3D structures within the whole substructure.

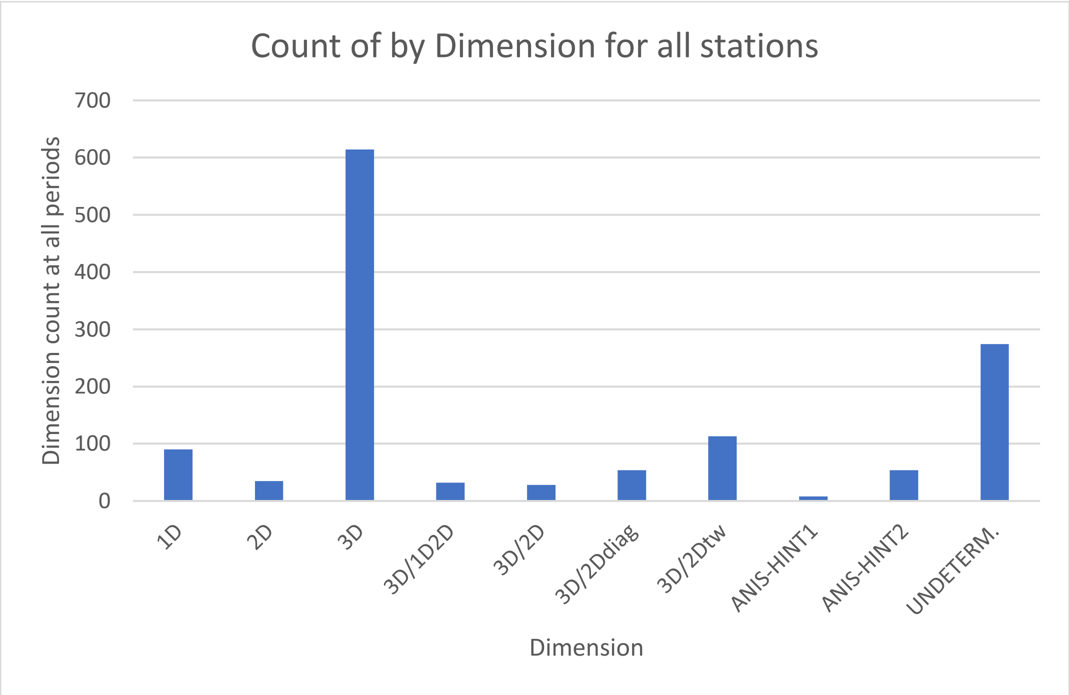

Figure 38: Graph showing the occurrence/count of all 10 dimensions for all stations at various periods.

3D MT inversion data

Based on all the preliminary analyses done, we can confidently say that due to the 3D structurally complex nature of our study area, the most appropriate inversion method to use would be a 3D inversion. Using all four components (Z_{xx}, Z_{yy}, Z_{xy}, Z_{yx}) will provide added information of the electric resistivity structure. This inversion method also requires few assumptions as compared to 2D inversion such as having no assumption of the strike direction in a 3D inversion.

To create a 3D model, MTpy was used to build a model, data and covariance file for the inversion and ModEM was used to run the 3D inversion. All 14 MT stations were used to produce the 3D inversion model. The MTpy software produces the following input files which are compulsory for the ModEM code:

- Model file: Contains information on the mesh size and starting resistivity.
- Data file: Contains the impedance tensor and tipper data at each frequency and station locations.
- Covariance file: Contains model covariance parameters, which control smoothing.

The inversion software uses the non-linear conjugate gradients (NLCG) algorithm, which is the preferred algorithm in this study as it increases relatively less rapidly with problem size, allowing for larger model grids and datasets compared to other algorithms like the Gauss-Newton (GN) algorithm. Two inversion models were produced. One with the full impedance tensor (Z_{xx}, Z_{yy}, Z_{xy}, Z_{yx}) plus the tipper, and another one without the tipper. The model consists of a total of 144 cells, of which 32 cells are in the x-direction, 50 cells are in the y-direction and 62 are in the vertical direction. Table 6 shows the input and output parameters used to produce the model files for both inversion models as well as the output results and parameters. Mackie (2002) was used as a guide to inform the parameter values used. Figure 39 shows the starting model, the dimensions were namely 286km (E-W), 196km (N-S) and 51.7km (0-Z). The 3D model visualizer is a software from Meqbel, (2009), and is called 3D Grid.

Table 6: Input and output parameters used to create the initial and resulting model files for both 3D inversion models.

Inversion model	**MODEL 1**	**MODEL 2**

Inversion type	Full impedance + tipper	Full impedance only
DATE FILE PARAMETERS		
Period range	10^{-5}s – 10^{2}s	10^{-5}s – 10^{2}s
Periods per decade	5	5
Period buffer factor (interpolation factor)	2	2
Impedance error type	Floor Egbert (% of $\sqrt{z_{xy} \times z_{yx}}$)	Floor Egbert (% of $\sqrt{z_{xy} \times z_{yx}}$)
Impedance error value	10%	10%
Tipper error type	Floor absolute	Floor absolute
Tipper error value	0.1	0.1
MODEL FILE PARAMETERS		
Cell size (east-west)	5000 m	5000 m
Cell size (north south)	5000 m	5000 m
Padding cells (north south)	3	3
Padding cells (east-west)	3	3
Padding (Z/Depth)	2	2
Padding increase factor vertical	1.6	1.6
Padding increase factor horizontal	1.9	1.9
Padding method	Stretch	Stretch

Resistivity initial value	100 Ω.m	100 Ω.m
No. of layers (depth)	60	60
First layer thickness	50 m	50 m
Target depth	40 000 m	40 000 m
Maximum depth of grid	51 644 m	51 644 m
COVARIANCE FILE PARAMETERS		
Smoothing (east-west)	0.6	0.6
Smoothing (north south)	0.6	0.6
Smoothing (depth)	0.6	0.6
INVERSION OUTPUT PARAMETERS		
Duration of inversion	14 hours	11 hours
Resulting RMS	2.52	2.61
Number of iterations	203	182

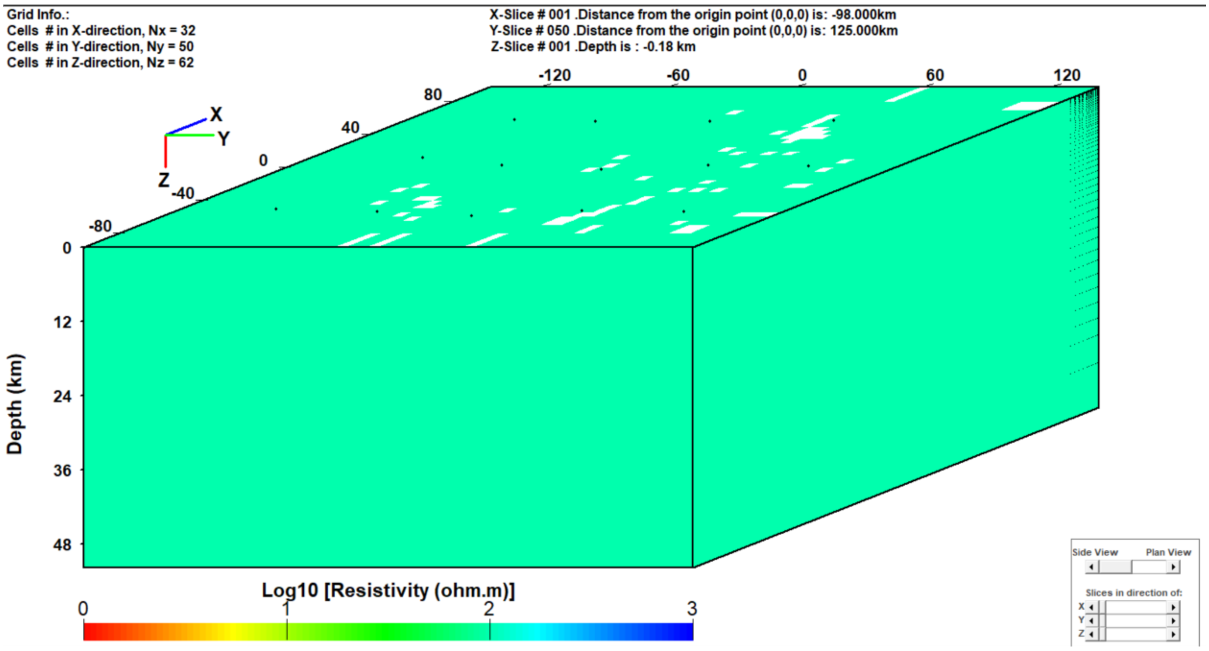

Figure 39: Image showing the starting model used for the 3D inversion. The model had a starting resistivity of 100ohm.m. The black dots on the surface of the model indicate that location of the MT stations. Topography of the region was also added on the model to adjust and correct for the elevations on surface (hence the white cells on the model surface).

To accommodate the intensive computational requirements involved in the full 3-D MT inversion tensor plus tipper data, a cluster had to be used, which was based at the Electrical Engineering Department at the University of the Witwatersrand. Table 7 shows the specifications of the cluster.

Table 7: Table showing the cluster specifications at the Electrical Engineering Department at the University of the Witwatersrand.

Operating System	Ubuntu 20.04.6 LTS
MPI library	MPICH ver. 3.3.2
F90 version	gfortran ver. 9.4.0
Number of compute nodes	36
Compute node CPU	Intel(R) Core (TM) i7-3770 CPU @ 3.40GHz
Compute node memory	32 GByte

Network interconnect	Ethernet 1Gbps

It is important to note that there were multiple inversion models that ran, mainly to determine what would be the right cell size and initial parameters that would produce the best results in the least amount of time to avoid frequent restarts due to power cuts. Initially the inversion models would run for a week (7 days) and with power cuts frequently up to four times a day for two hours (max down time of 8 hours a day), that meant having a lot more restarts and therefore further increasing the length of the job. It was then observed that smaller cells sizes, larger number of cells, high initial resistivity values, large number of period points taken per decade were one of the factors leading to a longer duration for the inversion job. Therefore, the final inversion models had initial parameters that produced the best results in a shorter span of time given the circumstances.

The first inversion model (model 1) used the full MT impedance tensor plus the tipper. This inversion took 14 hours and did 203 iterations with an RMS of 2.52. The root mean square (rms) error indicates the level of misfit between observed and modelled responses. Lower RMS values signify better agreement and higher confidence in the inverted model. Higher RMS values suggest larger discrepancies and potential issues like noise or model limitations. Figure 40 shows the resulting 3D MT inversion result. The model shows regions of low resistivity, with low resistivity regions being mapped at depths up to 45 km below surface.

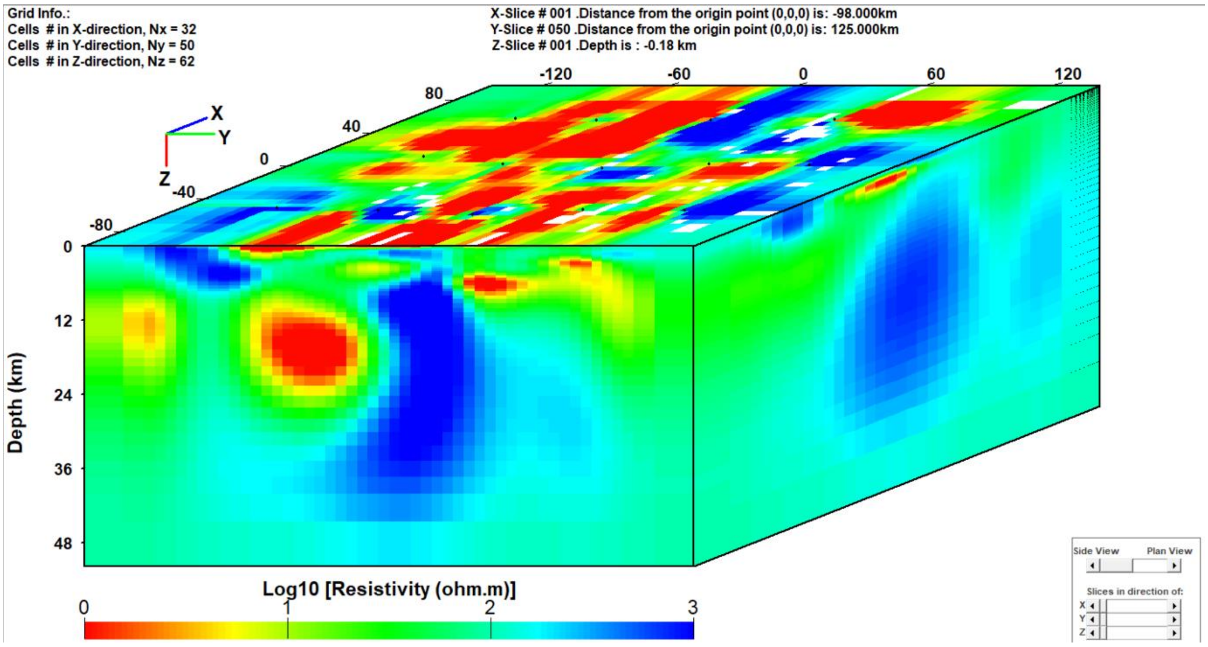

Figure 40: 3D perspective view of the MT inversion results titled model1, using the full impedance tensor plus tipper. The resulting RMS was 2.52 which took a total of 14 hours and 203 iterations. The x-direction on the diagram is the geographic north.

The second inversion model used the full MT impedance tensor only. This inversion model had two restarts (due to power cuts). The first part of the job took 4 hours and ran 88 iterations with an RMS value of 2.76, the second part (restart) took 7 hours and ran 94 iterations with an RMS of 2.61. Figure *41* shows the resulting 3D MT inversion result. Both the impedance + tipper (model 1) and impedance only (model 2) models look similar with Figure 40 showing a higher intensity of the conductivity and resistivity features. The Figure 40 model has a smaller RMS value and more iterations than the Figure 41 model, therefore the inversion model that used the full MT impedance tensor and tipper (model 1) will be used as the official results that will be interpreted and integrated moving forward.

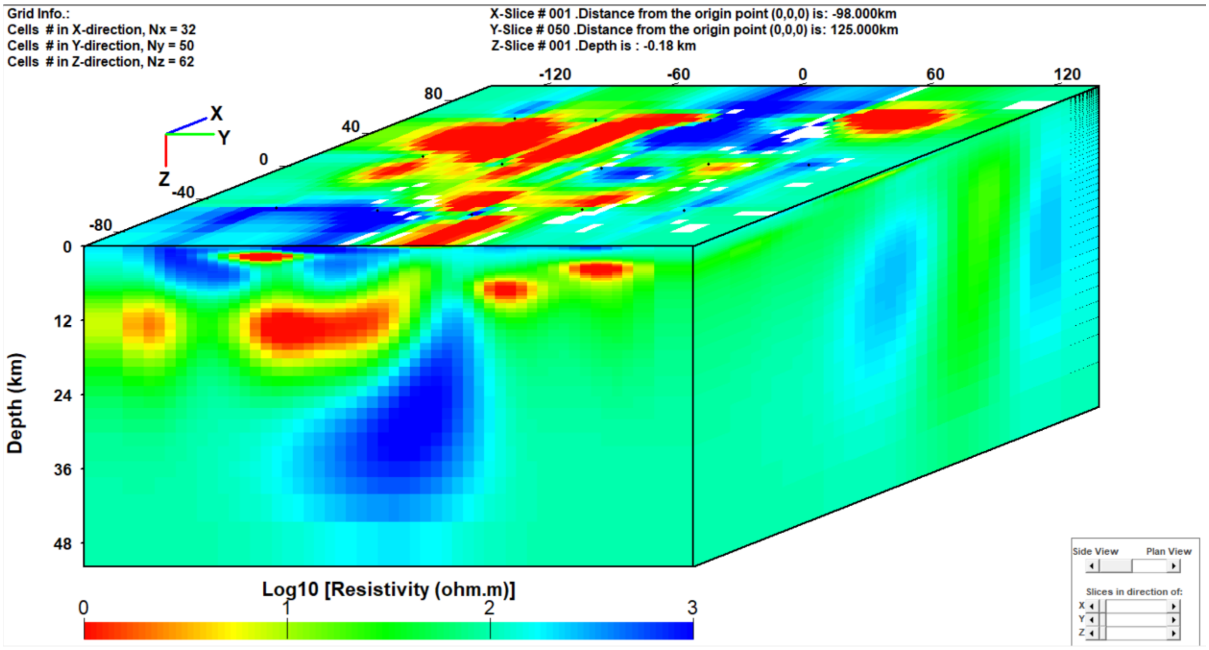

Figure 41: 3D perspective view of the MT inversion result, using the full impedance tensor only (model 2). The resulting RMS was 2.61 which took a total of 11 hours and 182 iterations. The x-direction on the diagram is the geographic north.

Figure 42 depicts an RMS map which shows the overall RMS values of each station, with 90% of the stations showing an overall RMS between 1 and 3. However station NAM165 appears to have a relatively high RMS value, reaching up to 5, this also happens to be the same station that showed a 600 km penetration depth in Figure 34 and was suggested to be a very resistive region. When looking at the RMS plots for the full impedance (Full Z), the full Tipper (Full Tz), and the Z_{xx}, Z_{yy}, Z_{xy}, Z_{yx}, T_{zy}, T_{zx} components at each station (see Appendix B: Total RMS Plots), we see that the total RMS values vary with each impedance and tipper component. Station NAM165 appears to have relatively high RMS values for the Z_{xx}, and Z_{xy} impedance tensor components only. Both components of these impedance tensors have the electrical field in the x direction as a similarity. This suggests that the high RMS value either relates to noisy data in the x direction of the electric current coming from the equipment, or there is a feature (cultural or geological) that is disrupting the flow of electric current in the x-direction in that region. When also comparing the total RMS plots of the Full Impedance tensor plus tipper with the total RMS plots of the Full Impedance tensor only, we observe they are almost identical. This shows that deciding to use the inversion model of the full impedance tensor plus tipper instead of the model with only the impedance tensor would not have made a significant difference.

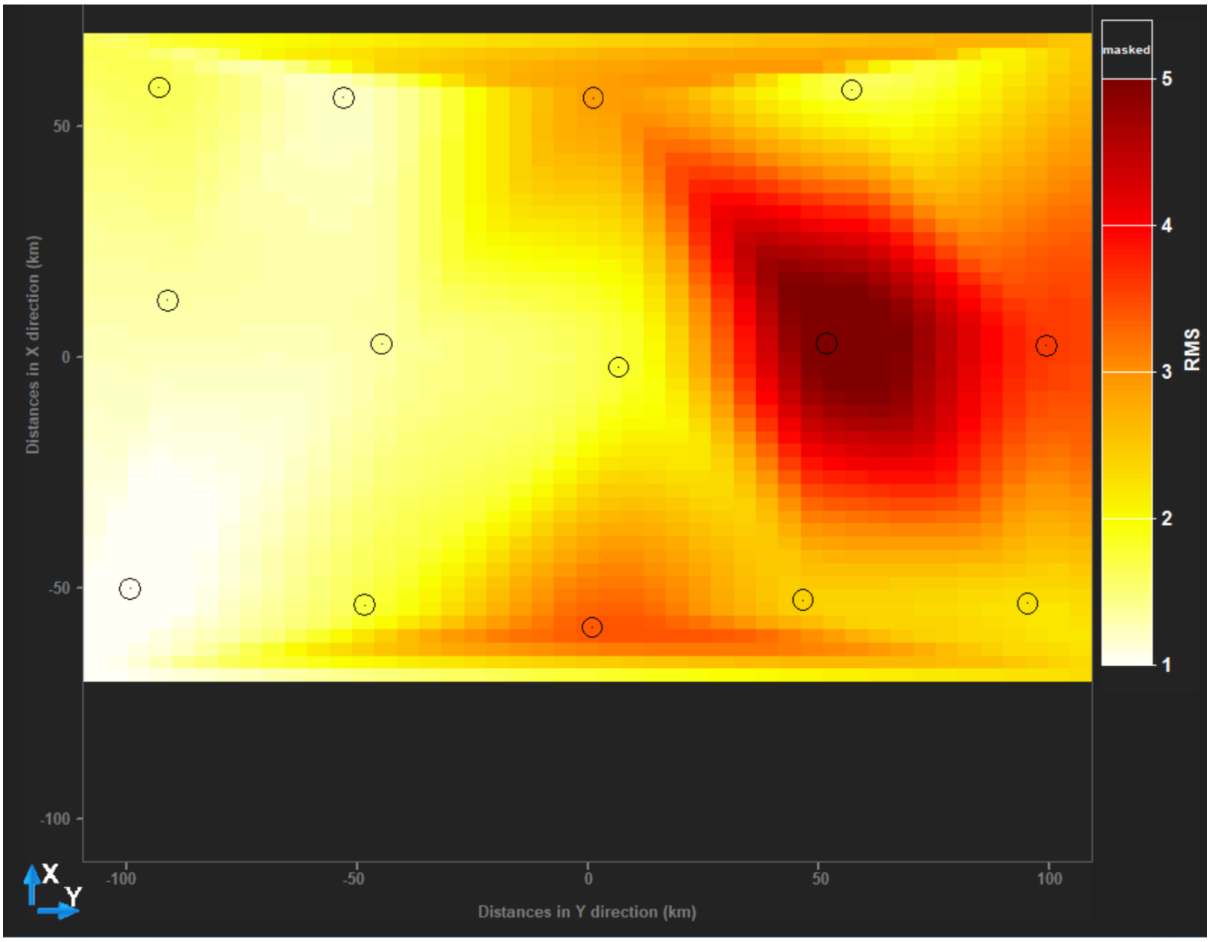

Figure 42: RMS value map of all of the MT stations used in the 3D inversion.

To further interrogate the integrity and quality of the inversion model. Inversion fit plots were plotted for each (see Appendix C: Inversion Fit Plots). What can immediately be observed from these plots is that the inversion program was able to fit the Z_{xy} and Z_{yx} components better than the Z_{xx} and Z_{yy} components for both the apparent resistivity and phase plots. Looking at the fit for station NAM165, it can be observed that the inversion software struggled to fit at longer periods due to a sudden smooth increase in the apparent resistivity, this shows that the failure to properly fit the data was mainly due to a change in the geoelectric structure and less likely due to bad data points. Based on the analyses, it can be concluded that the inversion model produced a reliable geoelectric structural model which can be used for interpretation and data integration. What can be suggested in future to compare the results is producing an inversion model using only the Z_{xy} and Z_{yx} components of the impedance tensor and determining if there is any improvement in the data/model.

To sufficiently analyse the 3D inversion model. Slices were taken at various directions. For the purpose of this research, three types of slices from the model will be discussed. A surface map slice, 3 cross-sectional slices that are along the three profiles previously mentioned, and a cross-sectional slice that is along the seismic line used for this research.

Surface map slice

Depth map slices were extracted from the 3D inversion model. Slices were extracted from surface (-0.183km) to 51.6km below surface (see Appendix D: Depth MT Inversion Model Slices). For the purposes of this section only the surface map slice will be discussed as shown in Figure 43.

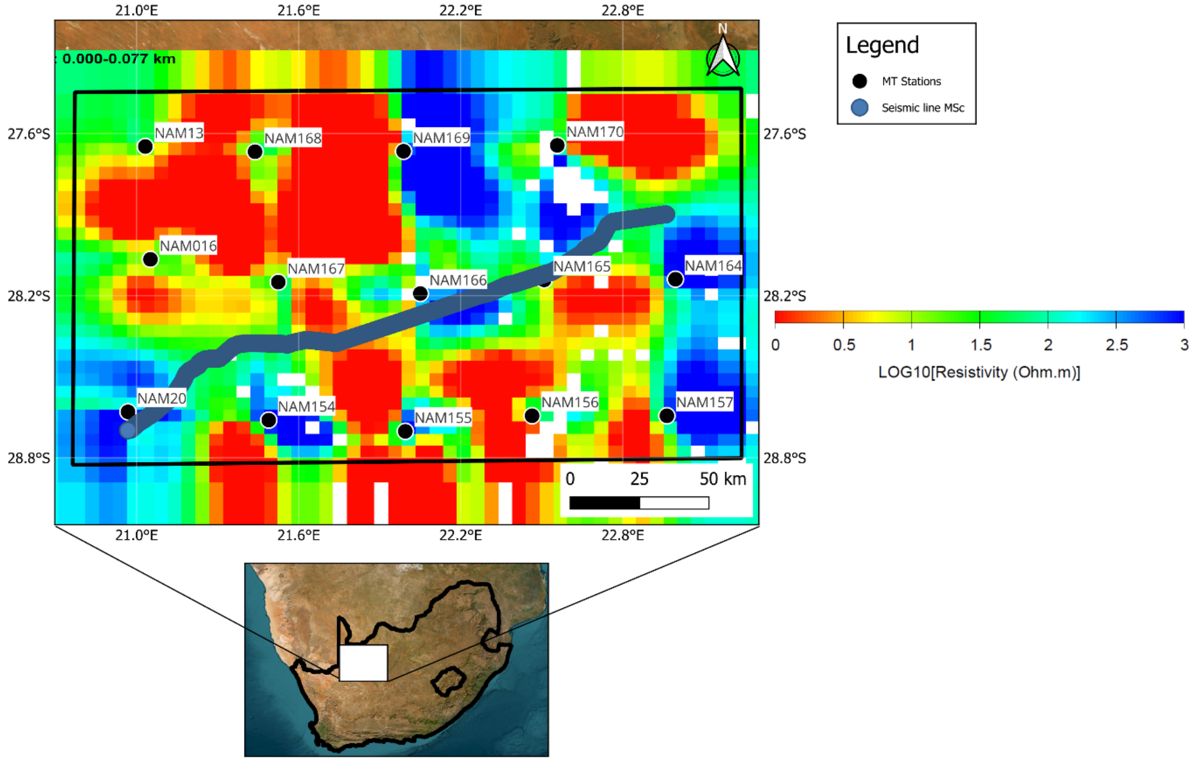

Figure 43: Google Earth surface (depth -0.18 km) resistivity map of the 3D inversion model covering the study area and showing the various local towns locations. The black stars indicate the locations of the 14 MT stations. The black line indicates the location of the SAGS-02-91 seismic line.

Profile cross sectional slices

X-direction cross section slices were extracted from the 3D inversion model. Slices were extracted for every 5 km. For the purposes of this section only the 3 profiles mentioned earlier will be discussed.

Figure 44 shows cross sectional slices of the three profiles mentioned in previous sections. Figure 44a represents profile 1, the cross section shows a concave conductive boundary belt that separates two resistive regions, the concave conductive boundary belt starts from surface and transcends up to approximately 30 km below surface. This conductive boundary also shows three relatively high conductive anomalies along the eastern region of the belt. Figure 44b represents profile 2. The cross section shows the same conductive belt as shown in profile 1 but there is a conductive region from the between 25 km to 50 km depth in the western region that appears to penetrate through the conductive belt and reaches the surface. Figure 44c represents profile 3, the cross section shows a regionally resistive region with conductive anomalies appearing at approximately 15 km below surface, below stations NAM154, NAM156, and NAM157.

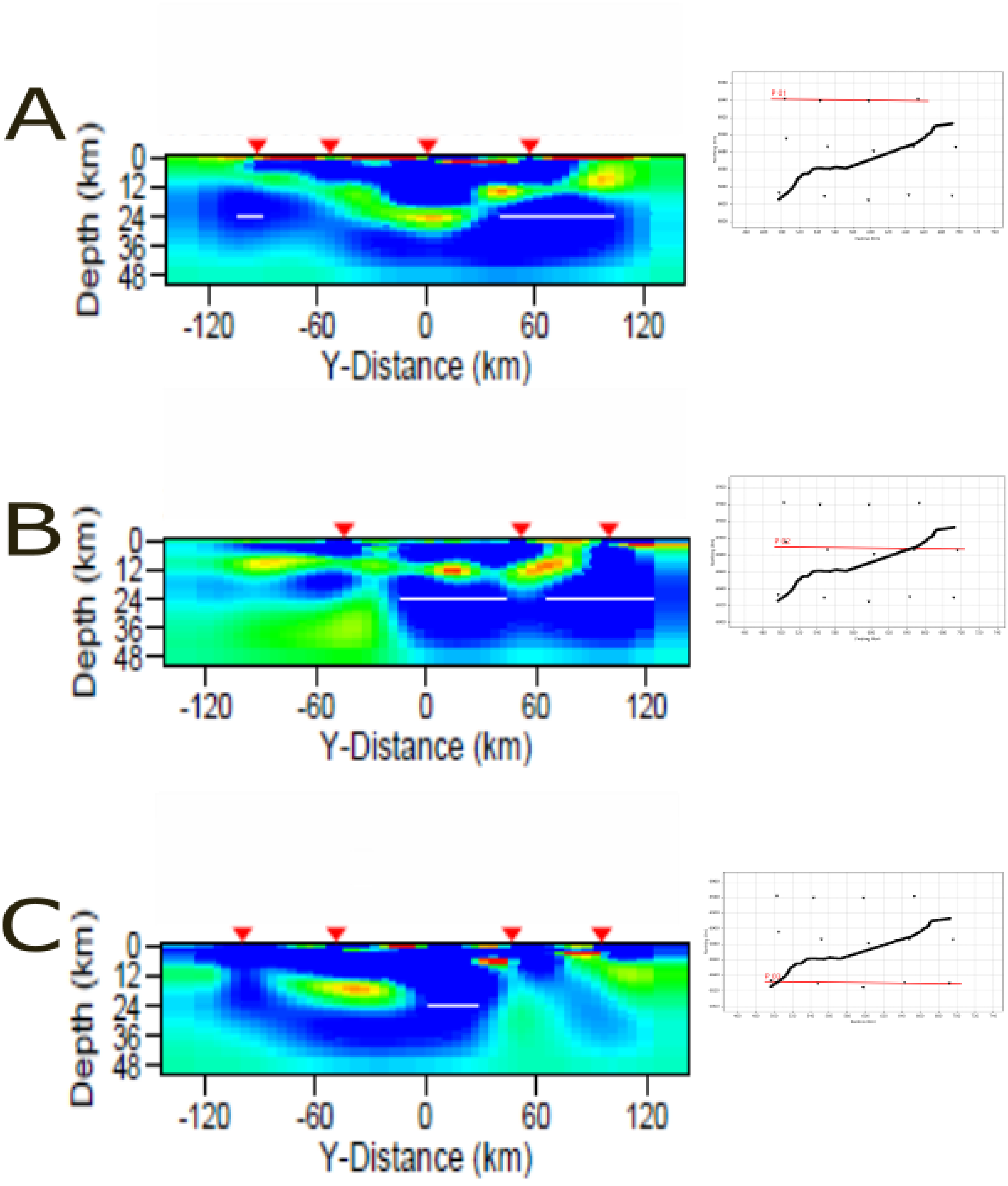

Figure 44: Resistivity cross sectional slices of the three profiles mentioned in previous sections. (A) represents profile 1, (B) represents profile 2, (C) represents profile 3. The red triangles on top of each profile indicates the location of the respective MT station. The seismic line (black line), MT stations (black dots) and profile (red line) are shown on the right.

MT-Seismic line slice

A cross-section extracted from the 3D MT inversion models showing the electrical resistivity structures is extracted along the existing seismic line SAGS-02-91 in Figure 45 and Figure 46.

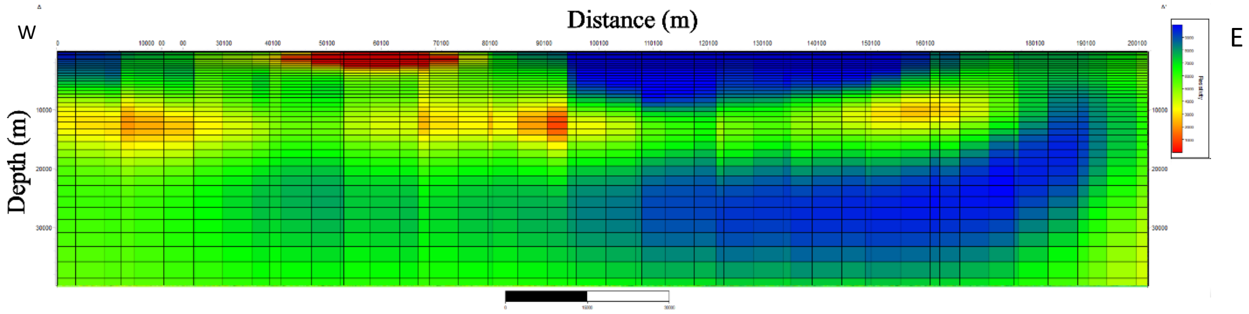

Figure 45: Image showing a 2D section of the impedance tensor only 3D MT inversion mode (model 2) along the SAGS-02-91 seismic line.

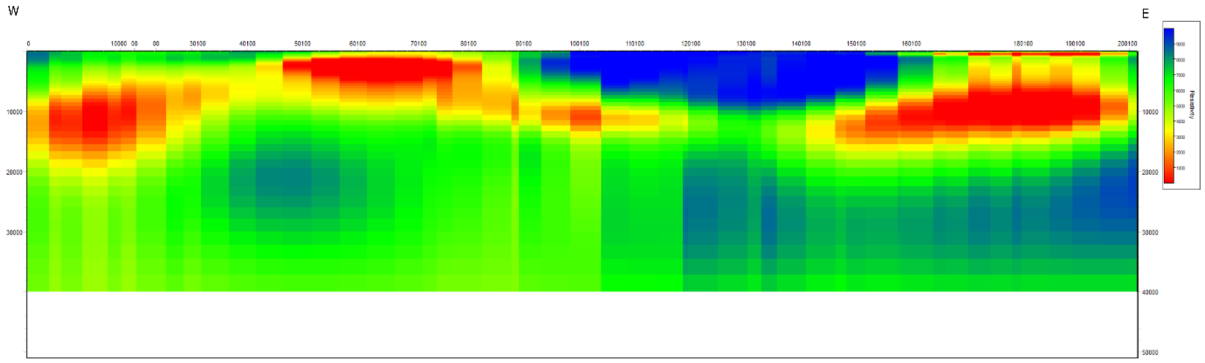

Figure 46: Image showing a 2D section of the impedance plus tipper 3D MT inversion model (model 1) along the SAGS-02-91 seismic line.

When both impedance and tipper data are used in inversion, the inversion process can potentially provide more detailed information about subsurface resistivity structures, especially in regions where there are significant lateral variations or anisotropy. This is because it uses information about both the magnitude and phase of the electric and magnetic fields at different frequencies. When using only the impedance tensor, the inversion relies solely on the measurements of the relationship between electric and magnetic fields at different frequencies. This means that in regions where there are significant lateral variations or anisotropy, the inversion process may be more challenging and may result in less resolved models. We see this when comparing model 1 and model 2, similar electrical resistivity responses can be see in both models, however model 1 produces more detailed and stronger responses. This shows that for this dataset, incorporating both impedance and tipper data leads to more robust and detailed model in the 3D inversion compared to using impedance tensor data alone. Therefore, model 1 will be used for intepretation and integration.

The MT inversion for model 1 shows both resistive and conductive zones, labelled A to F in Figure 47. Zone A depicts a conductive anomaly of < 200 Ω.m in the west part of the transect from depths between 5 km to 20 km. Zone B depicts a resistive anomaly of approximately 900 Ω.m, the anomaly is circular and stands out on its out from depths between 15 km to 30 km. Zone C depicts a conductive anomaly of < 200 Ω.m which appears to be dipping easterly from near surface (<1 km) to approximately 15 km in depth. Zone D depicts a highly resisitive anomaly of >1000 Ω.m near the middle of the transect from depth between the surface to approximately 10 km below surface. Zone F depicts a conductive anomaly of < 200 Ω.m which appears to be dipping westerly from near surface (<3 km) to approximately 15 km in depth. Zone E and G depicts a continuous resistive anomaly of approximately 850 Ω.m. This feature stretches from the eastern boundary of the transect to near the centre of the transect and it can be observed from depths between aprroximately 18 km to 40 km.

Anomally B, E and G appear to be connected, forming a resistive structure that has a less resistive region between it. This belt is approximately 10 km thick and appears in the upper crust (up to 15 km deep).

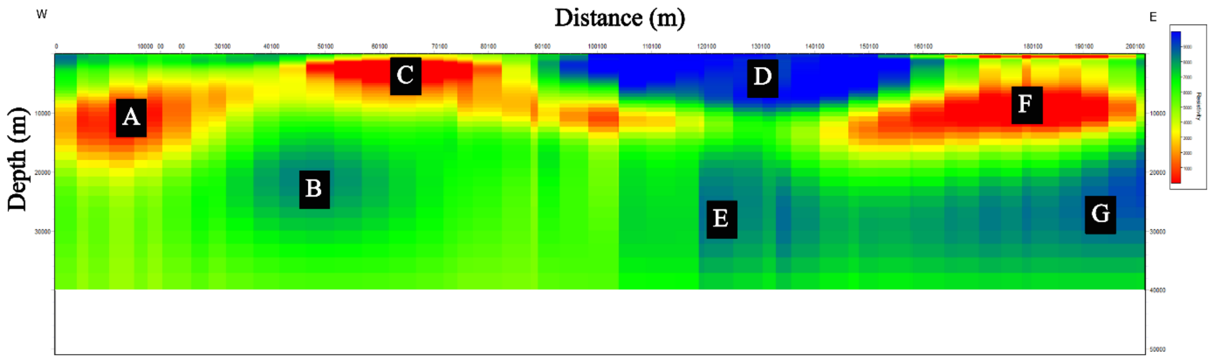

Figure 47: 2D section of the impedance plus tipper 3D MT inversion model (model 1) along the SAGS-02-91 seismic line, labelled from A-G for interpretation.

Chapter 6. Discussion

A qualitative description of some visually correlatable features

A basic interpretation is made here of the SAGS-02-91 reflection seismic profile in Figure 48. Referring to reflectors that are visible starting with the ones' marked A and B. The two features are lens-like and appear to have been displaced vertically between each other along the blue line marked between them, these reflectors appear between 10 km and 30 km below surface. The reflector marked C appears to be a lens-like feature with a dense number of reflectors present on it. This feature indicates that it could be a body with a high density or velocity contrast or both. The reflector also appears to have a discontinuity marked by a blue line east of it and it appears at approximately 20 km below surface. The reflectors marked D appear to be layered, the most distinct layered reflectors are shown with a black line. The first black line from the surface going down indicates a possibility of a boundary between two geological structures that have high density or seismic velocity contrast. These layers appear to be dipping in the westerly direction.

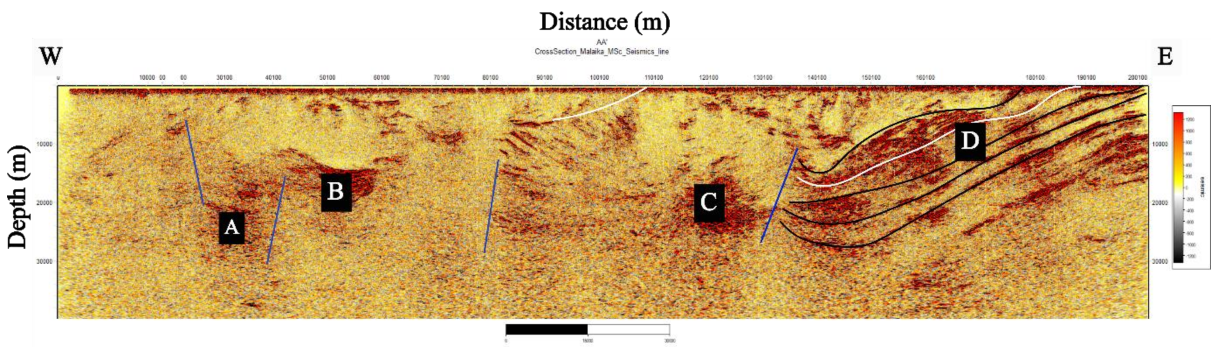

Figure 48: Interpreted migrated SAGS-02-91 reflection seismic profile along the Kheis Terrane Transact labelled from A-D. The blue lines represent interpreted fault lines, the black lines represent interpreted lithological structures, and the white lines represent interpreted thrust fault features.

Before discussing the overlaying of MT and seismic data, it must be emphasized that due to the geology of the Kheis-Namaqua Provinces boundary constituting thrusted and highly metamorphosed terrains intruded by various granite complexes, the observed reflection seismic will mainly highlight the gross structure of the Kheis Terrane due to the Kheis-Namaqua Provinces' geologically complex and poor density and seismic velocity contrasts.

The interpretation of the seismic and MT overlain profile in Figure 49 for these sections follows the clearly marked black lines, blue lines and zones labelled from A-G. The conductive region in zone A appears to be separated from zone C by a possible shear zone or fault (blue line) between them which is shown through the north-south displacement of the reflector package in zone B. Zone D is a very resistive structure that appears to be structurally complex due to the complex and the random nature the seismic reflectors appear. The structure in Zone D appears to be extending from surface, as there is no evidence that shows it may have diapirically risen from the subsurface, this suggestion is supported by a visible discontinuous conductive layer in zone C and F that appears to act like a base for the structure in zone D. This suggests that zone D is a resistive quartzite cover that was deposited after the formation of zone C and F. Zone F shows layered conductive structures that are dipping westerly. The layers appear to end at a fault feature (marked by a white dashed line) which also separates it from zone E.

Figure 49, shows the overlapped MT and seismic profiles with black and white dashed linear lines marked to illustrate prominent seismic reflectors and zones marked from A-G to show the major resistive and conductive anomalies. What is most notable is that some regions that have a dense number of reflectors correlate with the location of the resistive anomalies, this can be seen in zone B, D and E. It can also be observed that the conductive and resistive anomalies appear to show the boundaries and the extent of these seismic reflectors. We see this in zone B where the dense lens-like reflector package is surrounded by a slightly resistive anomaly, this is visible in zone F as well where the linear reflector packages marked in black mainly lay within the conductive anomaly region. The top black line also appears to portray the boundary between the resistive anomaly at zone D and the conductive anomaly at zone F. The bottom black line appears to portray the boundary between the conductive anomaly at zone F and the resistive anomaly at zone G. This is part of the first evidence that validates the MT inversion profile and shows that it correlates with the seismic profile along it.

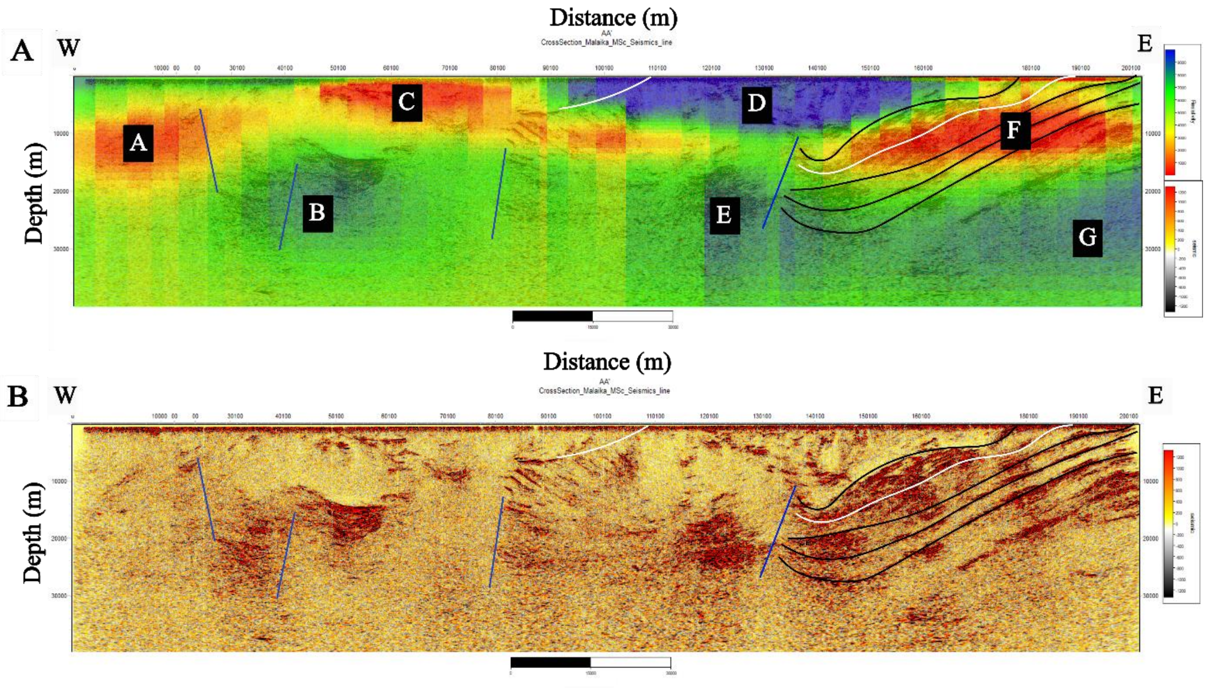

Figure 49: A) 2D section of the 3D MT inversion model (model 1) along the seismic line, with the seismic data overlain. B) Interpreted seismic section. From the seismic interpretation: the blue lines represent interpreted fault lines, the black lines represent interpreted lithological structures, and the white lines represent interpreted thrust fault features. Various zones are marked from A-G to show major resistive and conductive anomalies.

It is important to note that, when interpreting the seismic profile alone, one would interpret the reflector packages in zone C and F *(see Figure 49)* as a continuous structure, this is also true for the reflector packages in zone B and E. However, the MT data shows that the above listed zones may not be continuous structures, however further processing will need to be done to confirm whether the structures are well resolved. In the case for zone C and F, they both portray a conductive anomaly but there is a gap between them in the resistivity structure. The same can be said for zones B and E, where zone B is shown to be an isolated resistive circular structure, and zone E also appears to be and isolated resistive structure. This shows that the MT inversion profile helps in observing boundaries of prominent seismic reflectors. This is important as it will help delineate geological structures that may appear continuous in seismic profile but are in fact completely different and discontinuous geological features shown through the difference in their resistivity and conductivity response. It is also important to validate that such gaps are reliable features in the inversion and not just artefacts.

Where the MT data fails in showing possible locations of faults, seismics appears to map those structures well. This is indicated with blue lines on the seismic reflector packages *(see Figure 49)*. The resistivity profile does not show any displacements in the structures. Integrating seismic and MT data together can prove to be advantageous as the disadvantages in interpreting seismic data can be mediated by using MT data and the disadvantages in interpreting MT data can be mediated by using seismic data.

Figure 50 shows the regional geology map of the study area along the SAGS-02-91 seismic line. This map along with descriptive key below it will be used as reference when describing the geology in this section.

The 3D MT inversion was overlain with regional magnetic data over the region. The first derivative of the magnetic data in Figure 51a illustrates persistent southwest-northeast lineaments from the centre to the east of the seismic profile. These lineaments appear to change direction and become less coherent along the western region of the seismic profile. The total magnetic intensity map in Figure 51b appears to delineate the volcanic rocks of the Olifansthoek Group and sediments of the Kalahari Group by showing a strong magnetic signature for the volcanic rocks and relatively low magnetic signature for the sediments *(see Figure 50 and Figure)*. Along the large area covered by the Kalahari sediments along the middle of the seismic profile, weaker/broader magnetic signatures are observed which can be associated with buried rocks of the Brulpan and Wilgenhoutsdrift Group *(see Figure 50 and Figure)*.

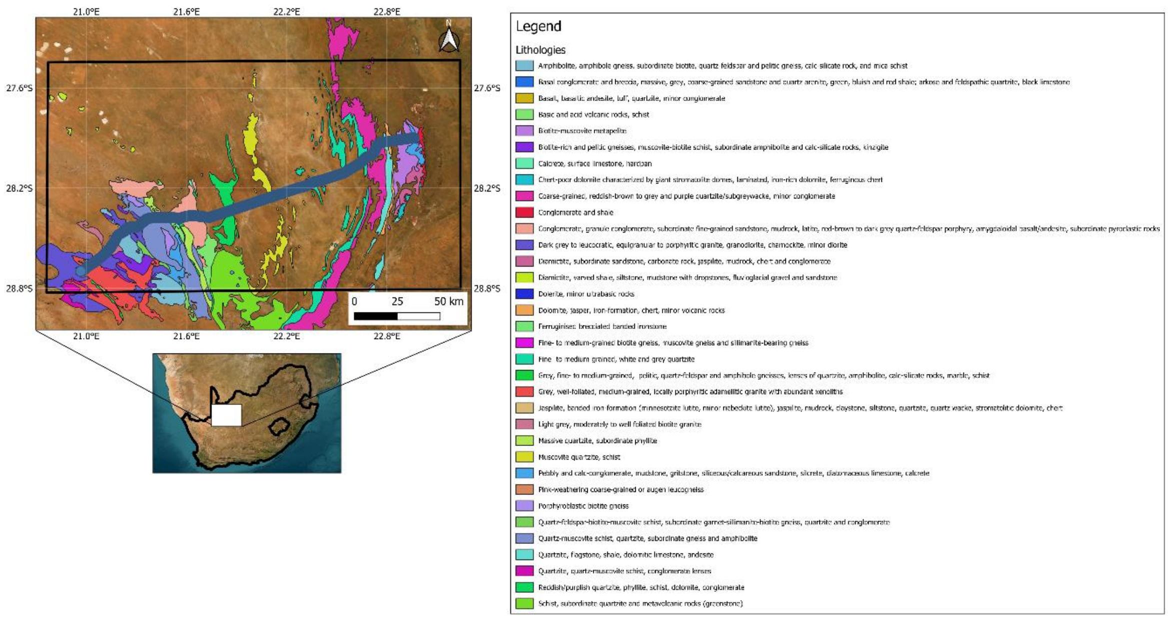

Figure 50: Regional geology map of area along the seismic line. The blue line represents the seismic line. The legend shows the geological lithology of each coloured region.

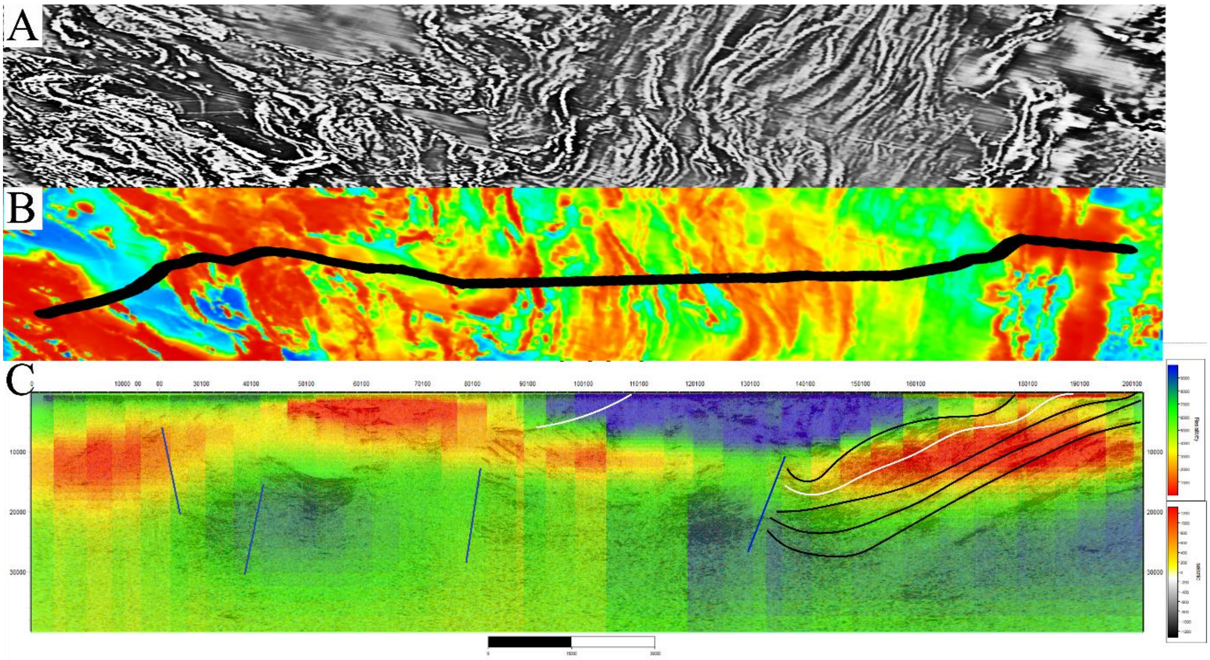

Figure 51: MT and Seismic profile interpretation integrated with magnetic data over the region.: A) The vertical derivative magnetic map along the seismic line, B) The total magnetic intensity magnetic map along the seismic line (black line), C) The integrated and interpreted seismic and MT profile.

Figure 52 shows the depth slice/top view of the MT inversion model integrated with the total magnetic intensity magnetic map. The two datasets appear to have a strong correlation, validating the MT inversion model. White lines have been marked along the black seismic line of the map to indicate possible geological structures which corelate in both the MT map and magnetic map.

When overlaying MT and magnetic data, we see that the magnetic data shows a variety of lineaments. The MT data then assists in separating and grouping these lineaments in terms of their conductivity and resistivity signatures. The MT data do this by delineating boundaries of these groups of linear features, which also appear to correlate with the linear features of the magnetic data as shown with the white lines on Figure 52. This will assist in proposing the various subdivisions of the rocks forming the Kheis Terrane.

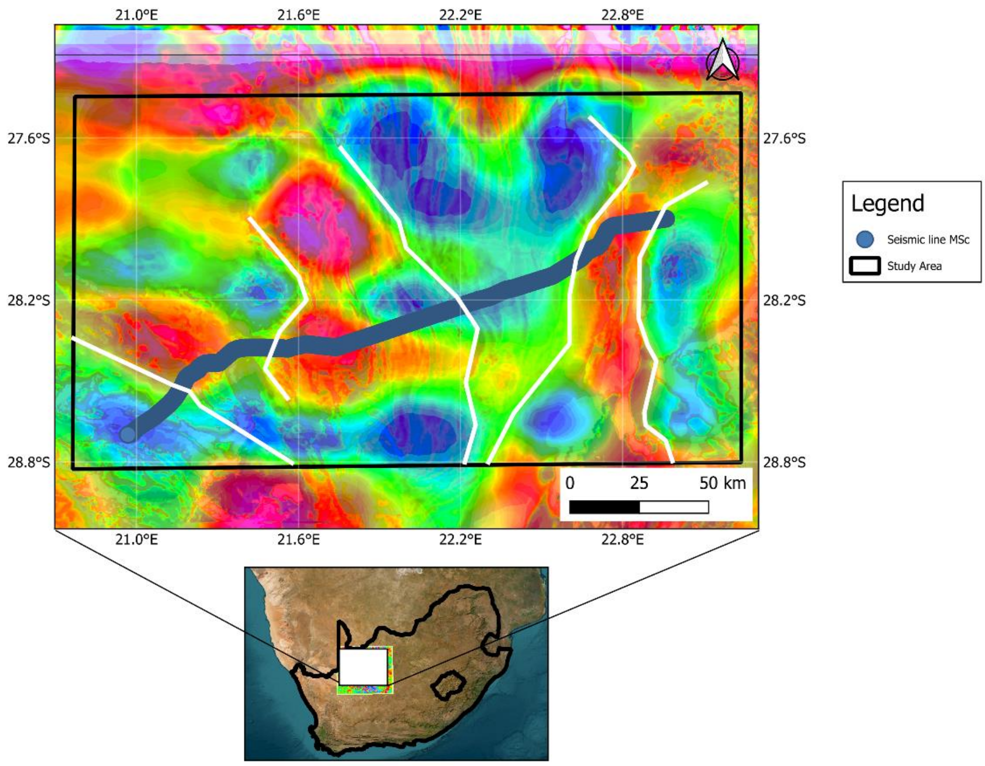

Figure 52: MT surface (depth -0.183 km) slice integrated with the magnetic map. The white line represents features that correlates with both the MT and magnetic data. The blue line indicates the seismic line location.

The MT inversion model has now been validated through its correlation with the seismic and magnetic data. The integration of the MT data with seismic and magnetic data has successfully provided insight on the possible geological structures in the subsurface and surface of the Kheis Terrane. Using geological data and information provided by van Niekerk & Beukes (2019), the geophysical data were integrated and intepreted further with geological data and produce geological models of the Kheis Terrane.

Geological model

Figure 53 depicts the proposed geology section, based on the MT and magnetic integration. The labelling of the regions was adapted from Van Niekerk and Beukes, (2019) suggestions and their intepretation of the magnetic map. The map has a dashed line towards the end of the boundary between the Areachap Group and the Kaaien Terrane, this is to suggest that along that region the rocks of the Areachap Group either merge with the Kaaien Terrane or they disappear. This proposed geological map supports Van Niekerk and Beukes, (2019) suggestion of the presence of a transitional contact between the rocks of the Volop Formation and Groblershoop Group. This contact is shown on Figure 53 as the boundary between the Groblershoop Group and the Olifantshoek Group. The geological map also supports the presence of an unconformable contact between the Wilgenhoutsdrif Group and the underlying Groblershoop Group. This contact suggest a significant gap or interruption in the geological sequence, therefore this contact is proposed to be the Brakbosch Fault which seperates the Areachap Group from the Kaaien Terrane which are suggested to be from different geological periods. This geological model provides the important subdivisions of the region around the Kheis Terrane and also maps the Kheis Terrane to be between the western boundary of the Kaaien Terrane and the eastern boundary of the Olifantshoek Group.

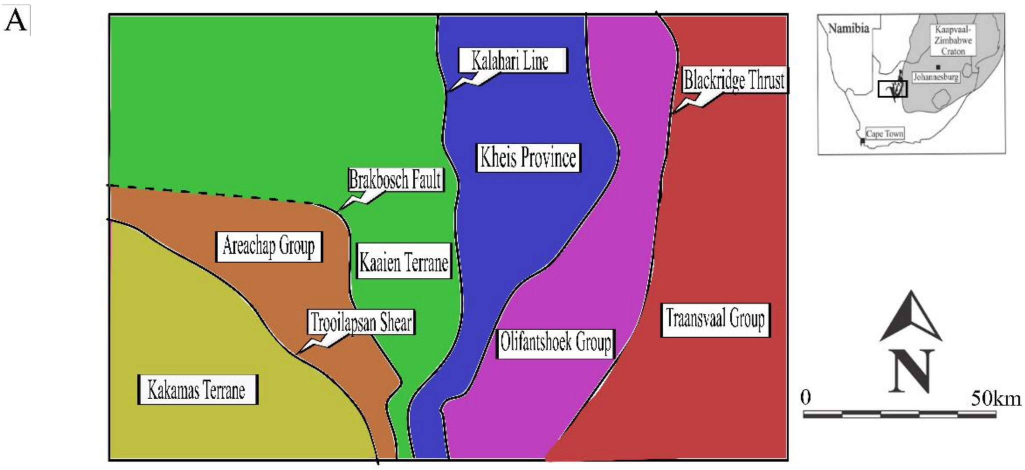

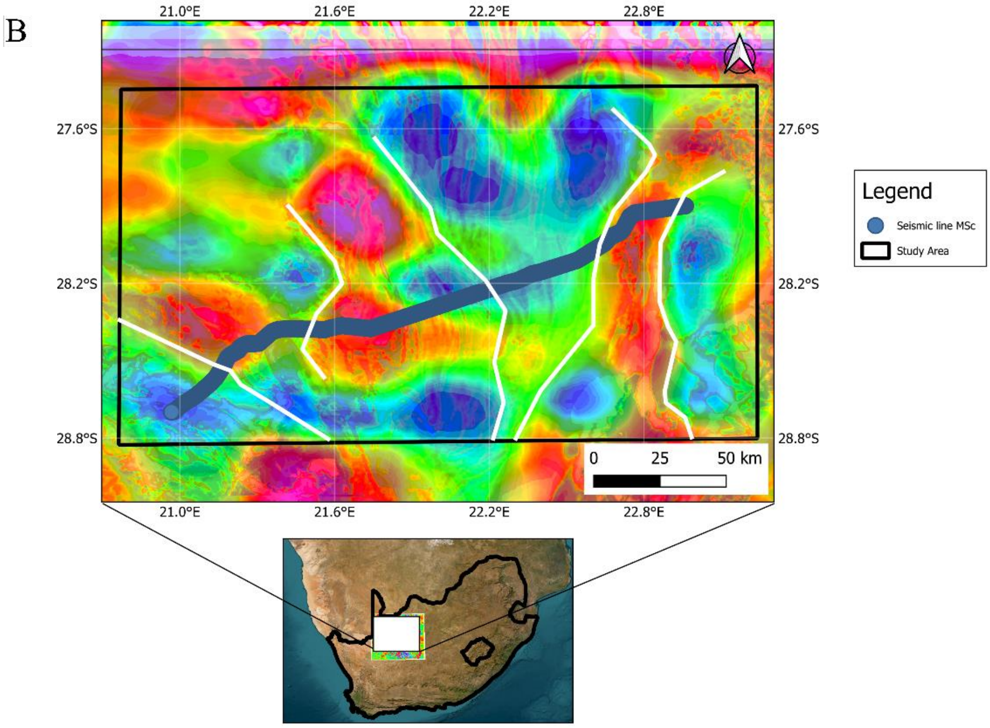

Figure 53: A) Proposed interpreted geology map of the study area. B) The integrated and interpreted MT and magnetic data that was used to create the proposed geological map.

Figure 54 depicts the proposed geological cross-sectional model of the region across the Kheis Terrane based on integrated MT, seismic and geological data, as well as geological models proposed by Thomas et al. (1994); Cornell & Pettersson (2007); van Niekerk & Beukes (2019). Starting from east to west, the model shows a granitic base of the Kaapvaal Craton, which is then overlain by the volcanic rocks of the Traansvaal Group. This region of volcanic rocks is supported by a visible high conductivity region in the same area on the MT section. The Traansvaal Group rock are then overlain by the

Olifantshoek Group rocks which are bounded by the Blackridge Thrust between them and signify a terrane boundary which separates the start of the Kheis Terrane in the Olifantshoek Group and the end of the Kaapvaal Craton in the Traansvaal Group. This thrust fault is supported by a dense linear reflector package in the seismic section which suggests thrusting may have occurred in that region. Overlaying the Olifantshoek Group is the Groblershoop Group. Based on the model the Kheis Province comprises of the Olifantshoek and the Groblershoop Group. The frequent quartzite layers of the Groblershoop Group have a high resistive signature on the MT section that is bowl shaped. Next to the Groblershoop Group is the Wilgenhoutsdrif Group. The volcanic and sedimentary rocks of the Wilgenhoutsdrif Group appear with an easterly dipping conductive narrow strip on the MT section. This suggests that the Wilgenhoutsdrif Group rocks lie in a syncline sitting below the Groblershoop Group sediments. After the Wilgenhoutsdrif is the Areachap Terrane which is bounded by the Brakbosch Fault and Trooilspan Shear zone which are relfected on the seismic section. This region is also known to be associated with intrusions of granite, this observation can be supported as the seismic section shows dense lense like reflector packages, while the MT section shows a resistive anomaly in the same region. Next to the Areachap Terrane is the Kakamas Terrane which is suggested to be shown with the conductive westerly dipping layer on the MT section and it overlays the Bushmanland Terrane. The top layer is intepreted to be the Kalahari sediment cover which is visble on the seismic section.

Van Niekerk and Beukes (2019) suggestions are further supported, firstly by confirming that the Kheis Supergroup comprises of the Olifantshoek-, Groblershoop-, and Wilgenhoutsdrift Groups. Secondly by supporting the suggestion that the Blackridge fault serves as the genuine terrane boundary separating the Kheis Terrane from the Kaapvaal Craton rocks.

Folding appears to be evident in the Kheis Terrane, which suggests that theory of the Namaqua Natal Metamorphic Complex coliding with the Kaapvaal Craton in what is termed as the ‘Kheis Event’ could most likely have occurred, creating a highly metamorphosed, faulted and folded wedge termed the Kheis Terrane.

Based on this model, the Kaapvaal Craton can be suggestted to interlock the Kheis Terrane, which therefore suggests a collison event that may have occurred between the NNMP and Kaapvaal Craton.

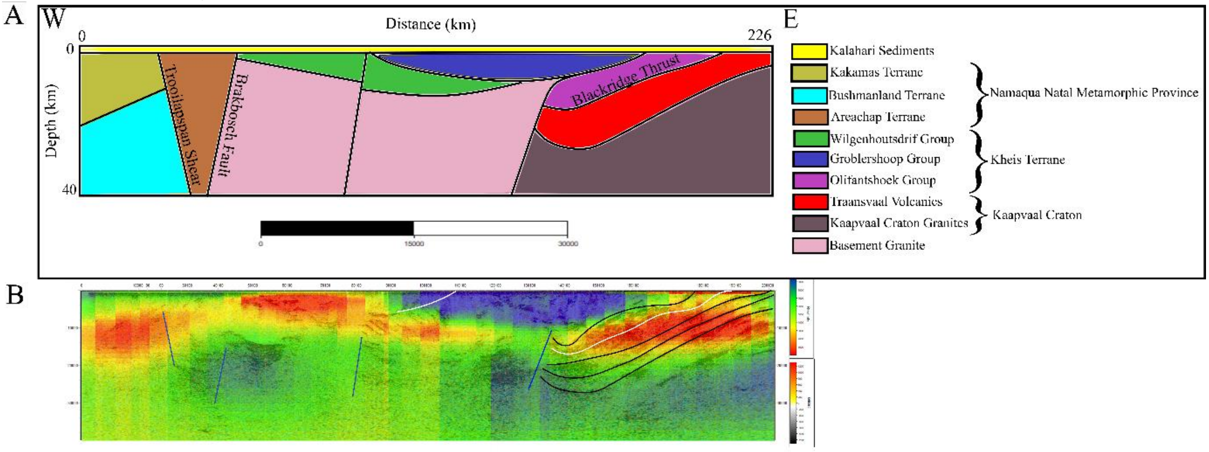

Figure 54: A) Proposed geological cross section of the Kheis Terrane. The white lines indicate proposed regions of faulting or shear zones, some of these regions represent boundaries between difference geological units. B) The integrated and interpreted MT and seismic sections used to create the geological model.

Chapter 7. Conclusions and Recommendations

In conclusion, the preliminary analysis of the magnetotelluric (MT) dataset has provided valuable insights into the subsurface characteristics of the study area, the Kheis Terrane. The investigation of apparent resistivity plots, phase values, and penetration depth has revealed the subsurface heterogeneity due to 3D electrical structures. This is particularly evident in the diagonal components (Zxx and Zyy) of the impedance tensor, suggesting sensitivity to subsurface heterogeneity and anisotropy.

The phase tensor analysis has further supported the notion of 2-D and 3-D structures in the subsurface. The orientation of the phase tensor ellipse indicates complex geological features facing different directions, and the skew angle values reveal non-orthogonality between major and minor axes, indicating structural complexity.

The calculated strike angles from multiple methods consistently suggest a strike direction of approximately 75° NW or 15° West of North. The dimensionality analysis using the WALDIM code has shown a variety of dimensions at different periods, indicating a structurally complex subsurface with evidence of galvanic distortion and electric anisotropy, as well as a dominance of 3-D structures.

Based on these findings, a 3-D inversion approach using all four impedance tensor components (Zxx, Zyy, Zxy, Zyx) and tipper data has been employed to model the electric resistivity structure of the Kheis Terrane. The inclusion of all components and tipper data is expected to yield more reliable results, given the complex nature of the subsurface.

Despite challenges such as power cuts causing job restarts, the inversion models have been successfully generated. The resulting 3-D MT inversion model depicts regions of high conductivity and low resistivity, with notable variations in the geological structure. The integration of seismic and magnetic data has further validated the MT inversion model, revealing correlations with seismic reflectors and linear features.

This integrated approach has allowed for the development of a proposed geological model for the Kheis Terrane, supporting previous geological interpretations. The geological cross-sectional model showcases the structural complexity of the region, with evidence of thrusting, folding, and the presence of different terranes. It supports the theory of the 'Kheis Event,' suggesting the collision of the Namaqua Natal Metamorphic Complex with the Kaapvaal Craton.

The investigation of the nature of the boundary (geometry and depth extent) between the Kheis Province and the western edge of the Kaapvaal Craton shows that the boundary is approximately between 20 km to 30 km at depth. And the depth extent of the Kheis Terrane is approximately 20 km deep.

Future studies in the area could collect more MT data specifically along the seismic line. An increase in the density of MT stations along the seismic will improve the dataset as it would allow to produce a 2D inversion model. This will allow for a better delineation of possible faults which may have not been visible in this study. Conducting a resolution test on the model would also be helpful, in order to analyse any overlapping induction spheres, helping the inversion to not put artefacts in the spaces between the stations. Further extensions to this research could be conducting a joint inversion with MT and seismics to further improve the dataset. To confirm the findings made by this research more physical properties studies on the region will be done, drilling is recommended to confirm the depth extent of the Kheis Terrane and possible economic mineralization of iron and manganese deposits along the eastern region of the Kheis Terrane.

Overall, the successful integration of MT, seismic, and magnetic data with geological models has improved our understanding of the subsurface geology of the Kheis Terrane. These findings provide a solid foundation for further geological research and exploration in the region, enhancing our knowledge of the Earth's complex geological history.

References

Bahr, K. (2007). Galvanic Distortion. In D. Gubbins & E. Herrero-Bervera (Eds.), *Encyclopaedia of Geomagnetism and Palaeomagnetism* (pp. 277–278). Springer Netherlands. https://doi.org/10.1007/978-1-4020-4423-6_103

Boardman, L. G., & Visser, D. J. L. (1958). *The geology and mineral deposits of the Griquatown area, Cape Province (Sheet 175 Geology 125K Explanation)*.

Bostik, F. X. (1977). A simple almost exact method of MT analysis. *Workshop on Electrical Methods Geothermal Exploration*.

Cagniard, L. (1953). BASIC THEORY OF THE MAGNETO-TELLURIC METHOD OF GEOPHYSICAL PROSPECTING. *GEOPHYSICS*, *18*(3), 605–635. https://doi.org/10.1190/1.1437915

Caldwell, T. G., Bibby, H. M., & Brown, C. (2004). The magnetotelluric phase tensor. *Geophysical Journal International*, *158*(2), 457–469. https://doi.org/10.1111/j.1365-246X.2004.02281.x

Cornell, D. H., & Pettersson, A. (2007). Ion probe zircon dating of metasediments from the Areachap and Kakamas Terranes, Namaqua-Natal Province and the stratigraphic integrity of the Areachap Group. *South African Journal of Geology*, *110*(4), 575–584. https://doi.org/10.2113/gssajg.110.4.575

De Beer, J. H. (1978). THE RELATIONSHIP BETWEEN THE DEEP ELECTRICAL RESISTIVITY STRUCTURE AND TECTONIC PROVINCES IN SOUTHERN AFRICA PART 2. RESULTS OBTAINED BY MAGNETOMETER ARRAY STUDIES by. *Trans. Geol. Soc. S. Afr*, *81*, 143–154.

De Beer, J. H., & Meyer, R. (1984). Geophysical characteristics of the Namaqua-Natal Belt and its boundaries, South Africa. *Journal of Geodynamics*, *1*(3–5), 473–494. https://doi.org/10.1016/0264-3707(84)90020-6

De Beer, J., & Stettler, E. (2015). The Beattie Magnetic Anomaly. In Johan. H. De Beer (Ed.), *The History of Geophysics in Southern Africa* (1st ed., pp. 147–155). African Sun Media.

Egbert, G. D., & Kelbert, A. (2012). Computational recipes for electromagnetic inverse problems. *Geophysical Journal International*, *189*(1), 251–267. https://doi.org/10.1111/j.1365-246X.2011.05347.x

Fourie, S., & Cole, P. (2000). Gravity map of the Republic of South Africa. *Council for Geoscience*.

Hanson, R. E. (2003). Proterozoic geochronology and tectonic evolution of southern Africa. *Geological Society, London, Special Publications*, *206*(1), 427–463. https://doi.org/10.1144/GSL.SP.2003.206.01.20

Jacobs, J., Thomas, R. J., & Weber, K. (1993). Accretion and indentation tectonics at the southern edge of the Kaapvaal craton during the Kibaran (Grenville) orogeny. *Geology*, *21*(3), 203. https://doi.org/10.1130/0091-7613(1993)021<0203:AAITAT>2.3.CO;2

Johnson, M. R., Anhaeusser, C. R., & Thomas, R. J. (2006). *The geology of South Africa*. The geology of South Africa. Geological Society of South Africa, Johannesburg/Council for Geoscience, Pretoria.

Kelbert, A., Meqbel, N., Egbert, G. D., & Tandon, K. (2014). ModEM: A modular system for inversion of electromagnetic geophysical data. *Computers and Geosciences*, *66*, 40–53. https://doi.org/10.1016/j.cageo.2014.01.010

Keller, George. V, & Frischknecht, Frank. C. (1966). *Electrical methods in geophysical prospecting*. Oxford, New York, Pergamon Press.

Kirkby, A., Zhang, F., Peacock, J., Hassan, R., & Duan, J. (2019). The MTPy software package for magnetotelluric data analysis and visualisation. *Journal of Open Source Software*, *4*(37), 1358. https://doi.org/10.21105/joss.01358

Krieger, L., & Peacock, J. R. (2014). MTpy: A Python toolbox for magnetotellurics. *Computers & Geosciences*, *72*, 167–175. https://doi.org/10.1016/j.cageo.2014.07.013

Lilley, F. E. M. (1993). Magnetotelluric analysis using Mohr circles. *GEOPHYSICS*, *58*(10), 1498–1506. https://doi.org/10.1190/1.1443364

Mackie, R. (2002). *Multi-Dimensional Magnetotelluric Modelling and Inversion*.

Martí, A., Queralt, P., & Ledo, J. (2009). WALDIM: A code for the dimensionality analysis of magnetotelluric data using the rotational invariants of the magnetotelluric tensor. *Computers and Geosciences*, *35*(12), 2295–2303. https://doi.org/10.1016/j.cageo.2009.03.004

Martí, A., Queralt, P., Ledo, J., & Farquharson, C. (2010). Dimensionality imprint of electrical anisotropy in magnetotelluric responses. *Physics of the Earth and Planetary Interiors*, *182*(3–4), 139–151. https://doi.org/10.1016/j.pepi.2010.07.007

Meqbel, N. M. M. (2009). *The electrical conductivity structure of the Dead Sea Basin derived from 2D and 3D inversion of magnetotelluric data*.

Muller, M. R., Jones, A. G., Evans, R. L., Grütter, H. S., Hatton, C., Garcia, X., Hamilton, M. P., Miensopust, M. P., Cole, P., Ngwisanyi, T., Hutchins, D., Fourie, C. J., Jelsma, H. A., Evans, S. F., Aravanis, T., Pettit, W., Webb, S. J., & Wasborg, J. (2009). Lithospheric structure, evolution and diamond prospectivity of the Rehoboth Terrane and western Kaapvaal Craton, southern Africa: Constraints from broadband magnetotellurics. *Lithos*, *112*, 93–105. https://doi.org/10.1016/j.lithos.2009.06.023

Niblett, E. R., & Sayn-Wittgenstein, C. (1960). VARIATION OF ELECTRICAL CONDUCTIVITY WITH DEPTH BY THE MAGNETO-TELLURIC METHOD. *GEOPHYSICS*, *25*(5), 998–1008. https://doi.org/10.1190/1.1438799

Palacky, G. J. (1988). Resistivity characteristics of geologic targets. In E. B. Neitzel (Ed.), *Electromagnetic methods in applied geophysics* (pp. 52–129). Society of Exploration Geophysicists.

Parkinson, W. D. (1959). Directions of Rapid Geomagnetic Fluctuations. *Geophysical Journal International*, *2*(1), 1–14. https://doi.org/10.1111/j.1365-246X.1959.tb05776.x

Simpson, Fiona., & Bahr, Karsten. (2005). *Practical magnetotellurics*. Cambridge University Press.

Stettler, E., Fourie, S., & Cole, P. (2000). *Total Magnetic Field Intensity map of South Africa.*

Stettler, E. H., Prinsloo, J., & Hauger, M. E. (1998). A geophysical transect between Avondale on the Kheis tectonic province and Keimoes on the Namaqua Metamorphic Province, South Africa. *Southern African Geophysical Review*, *2*, 83–93.

Stettler, E. H., Prinsloo, J., Hauger, M. E., & Du Toit, M. C. (1999). A crustal geophysical model for the Kheis Tectonic Province, South Africa based on magnetotellurics, reflection seismic, gravity and magnetic data sets. *South African Geophysical Review*, *3*, 54–68.

Swift, Charles. M. (1967). *A magnetotelluric investigation of an electrical conductivity anomaly on the Southwestern United States* [Massachusetts Institute of Technology]. http://libraries.mit.edu/docs

Thomas, R. J., Cornell, D. H., Moore, J. M., & Jacobs, J. (1994). Crustal evolution of the Namaqua-Natal Metamorphic Province, southern Africa. *J.Geol*, *1*, 8–14.

Tikhonov, A. N. (1950). ON DETERMINING ELECTRICAL CHARACTERISTICS OF THE DEEP LAYERS OF THE EARTH'S CRUST. *Magnetotelluric Methods*, *5*, 2–3.

Tinker, J., Wit, M. DE, & Grotzinger, J. (2002). Seismic Stratigraphic Constraints on Neoarchean-Paleoproterozoic Evolution of the Western Margin of the Kaapvaal Craton, South Africa Maarten de Wit. *SOUTH AFRICAN JOURNAL OF GEOLOGY*, *105*, 107–134. http://www.ciw.edu/mantle/kaapvaal

Unrug, R. (1992). THE SUPERCONTINENT CYCLE AND GONDWANALAND ASSEMBLY: COMPONENT CRATONS AND THE TIMING OF SUTURING EVENTS. *J. Geodynamics*, *16*(4), 215–240.

Van Niekerk, H. S. (2006). *The origin of the Kheis Terrane and its relationship with the Archean Kaapvaal Craton and the Grenvillian Namaqua Province in southern Africa*. University of Johannesburg.

van Niekerk, H. S., & Beukes, N. J. (2019). Revised definition/outline of the Kheis Terrane along the western margin of the Kaapvaal Craton and lithostratigraphy of the newly proposed Keis supergroup. *South African Journal of Geology*, *122*(2), 187–220. https://doi.org/10.25131/sajg.122.0014

Von Backstrom, J. W., & De Villiers, J. (1972). *The geology along the Orange River Valley between Onseepkans and the Richtersveld*.

Weaver, J. T., Agarwal, A. K., & Lilley, F. E. M. (2000). Characterization of the magnetotelluric tensor in terms of its invariants. *Geophysical Journal International*, *141*(2), 321–336. https://doi.org/10.1046/j.1365-246x.2000.00089.x

Appendix

Appendix A: Raw Edi Plots

This appendix contains raw edi plots depicting apparent resistivity and phase curves of all 15 MT stations. These plots also depict curves of all four components (Z_{xx}, Zyy, Zxy, Zyx).

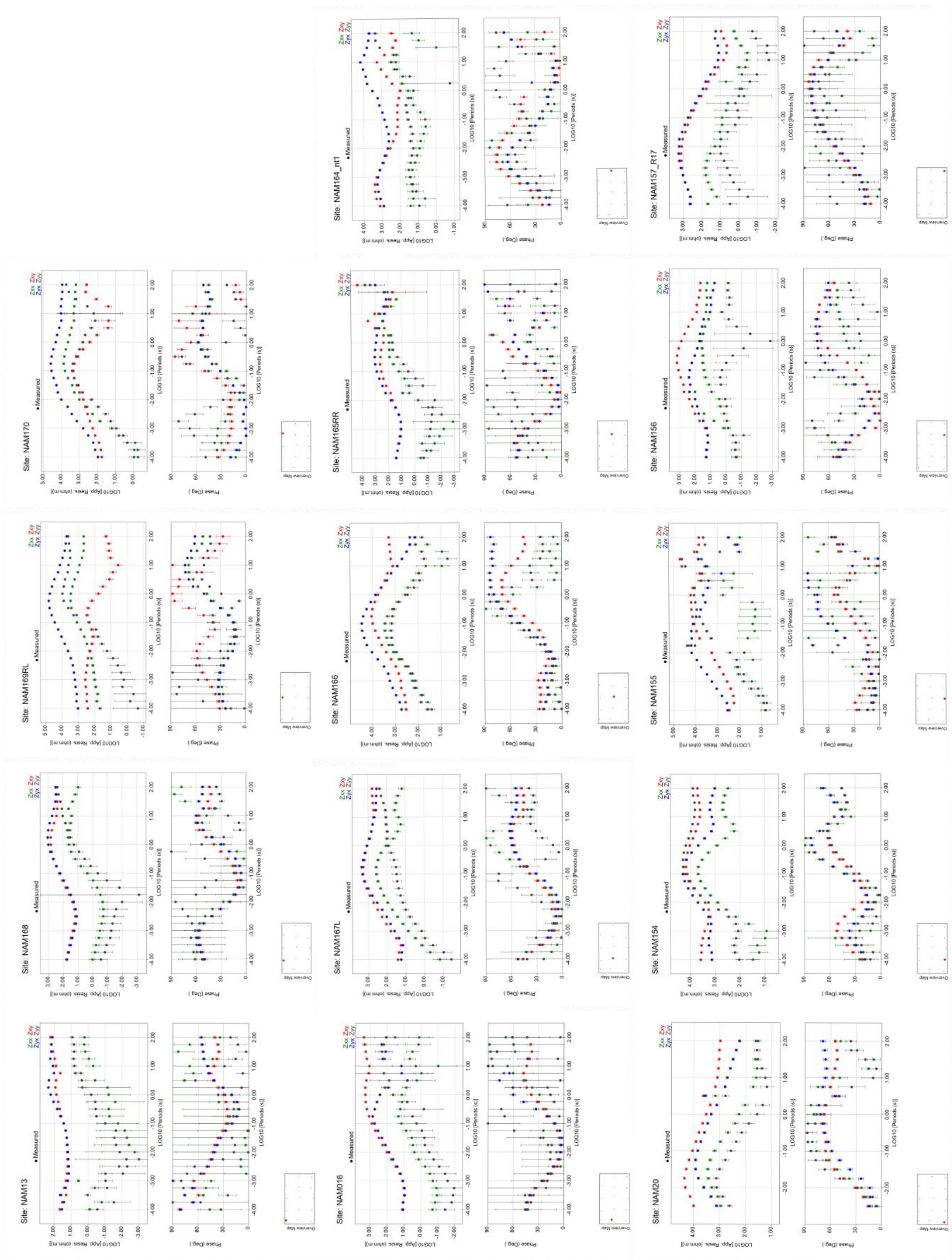

Appendix B: Total RMS Plots

This appendix shows the Total RMS plots of each station for the full impedance (Full Z), the full Tipper (Full Tz), and the Z_{xx}, Z_{yy}, Z_{xy}, Z_{yx}, T_{zy}, T_{zx} components.

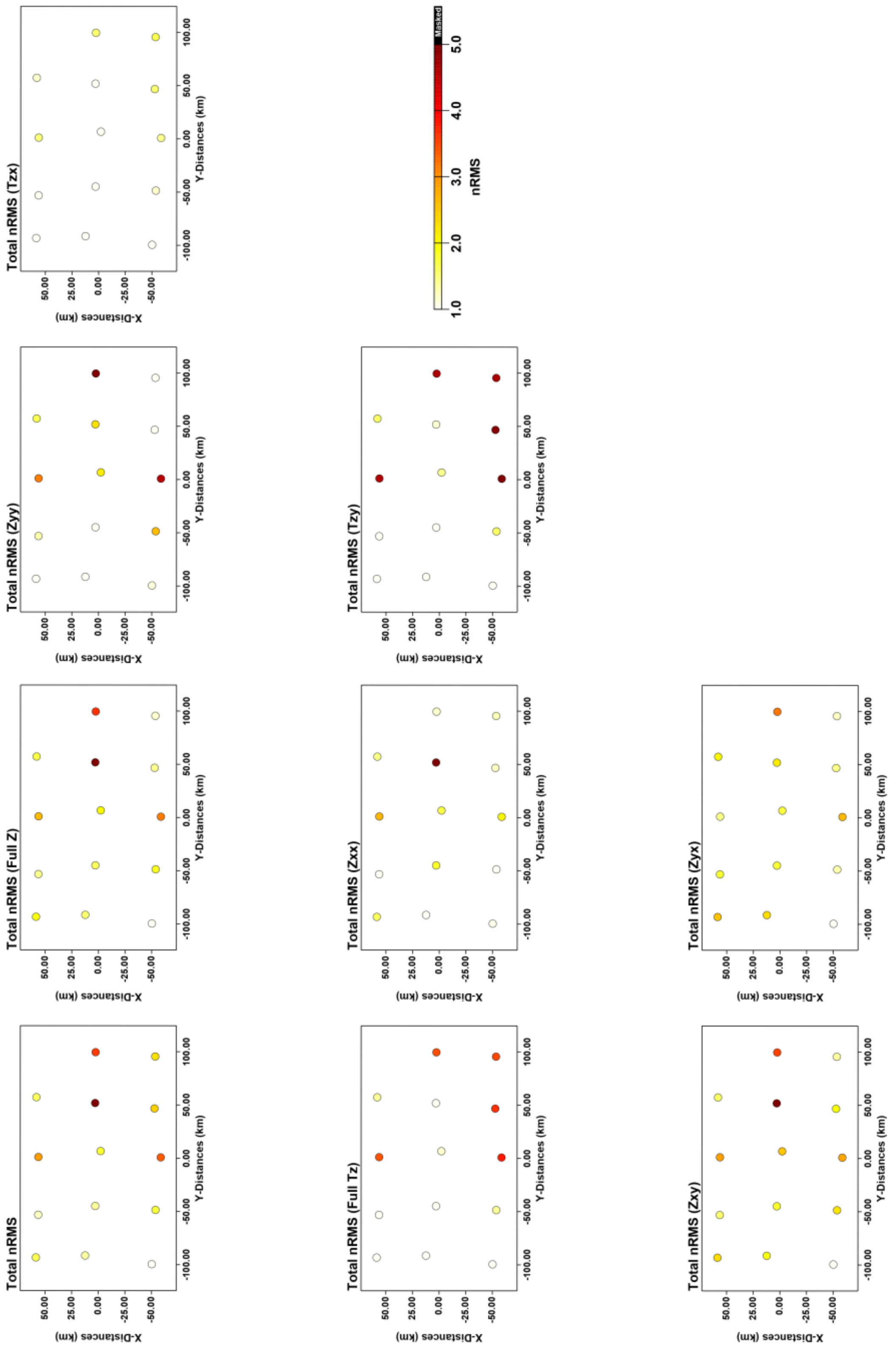

Appendix C: Inversion Fit Plots

This appendix shows the inversion fit plots of all stations in each component for the apparent resistivity and phase value curves. The plots show a comparison between the predicted and measured values.

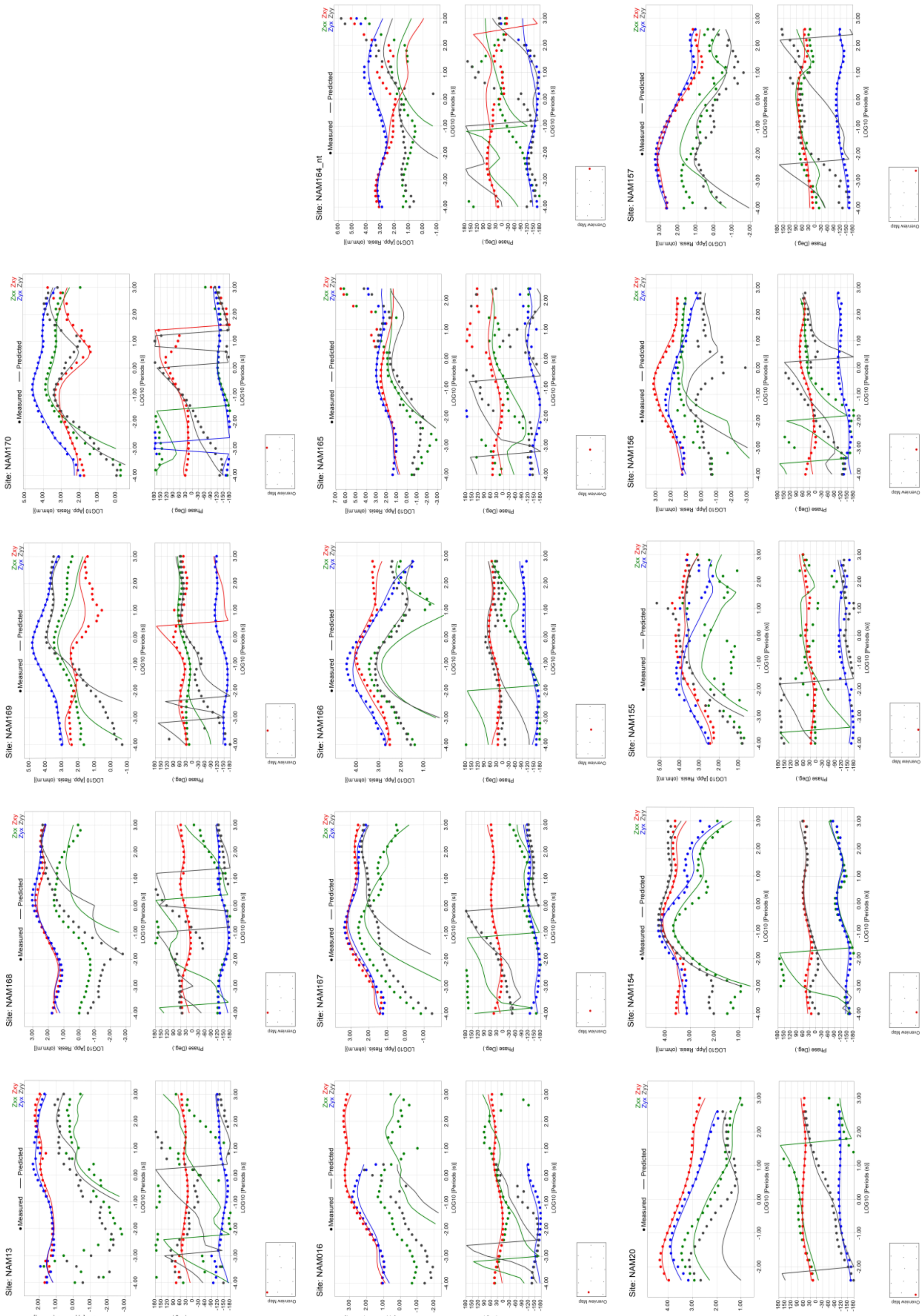

Appendix D: Depth MT Inversion Model Slices

This appendix shows depth slices of the 3D MT Inversion model. Slices were extracted for every 60m from surface (-0.183km) to 51.6km below surface. The x-direction is considered to be north.

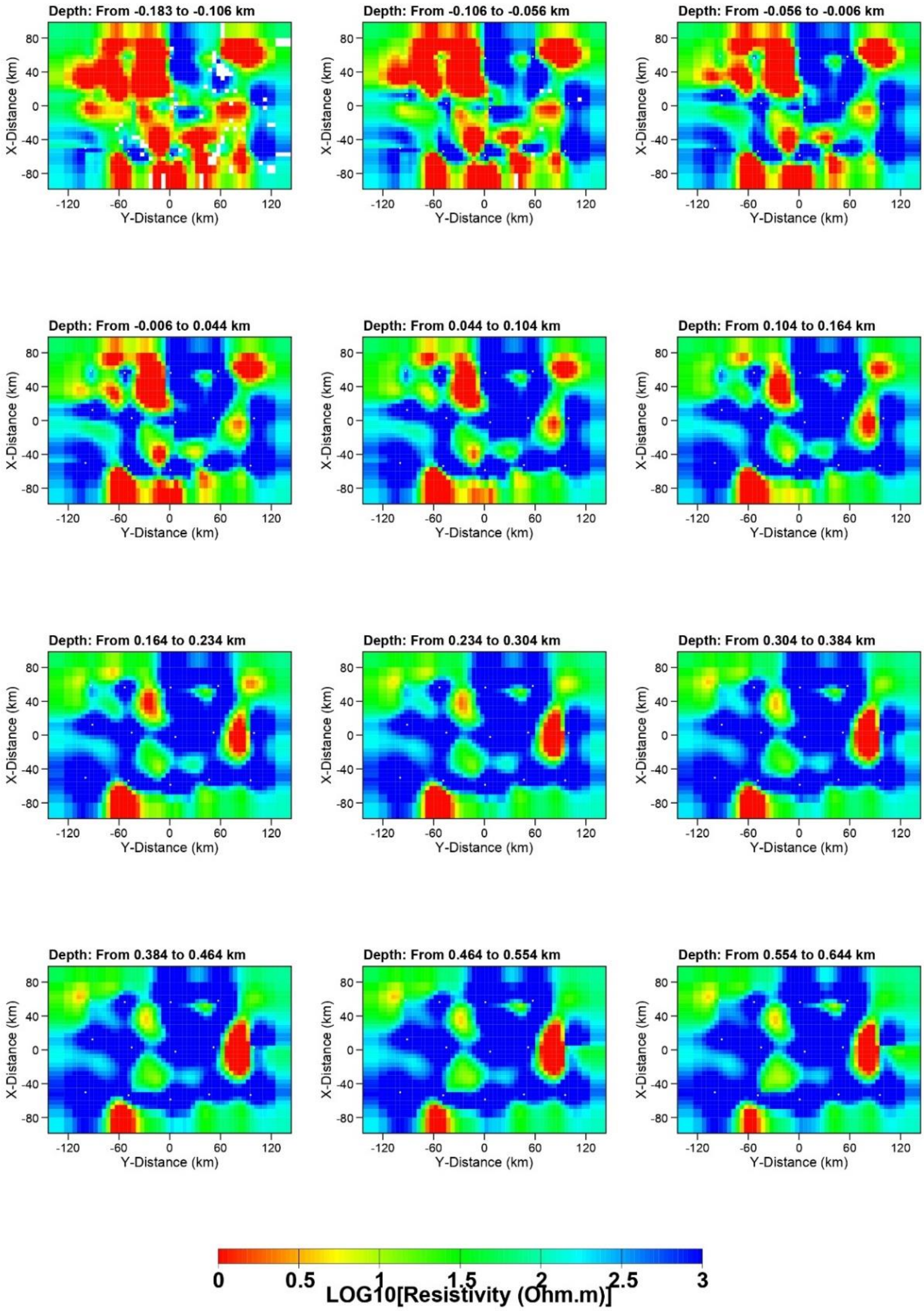

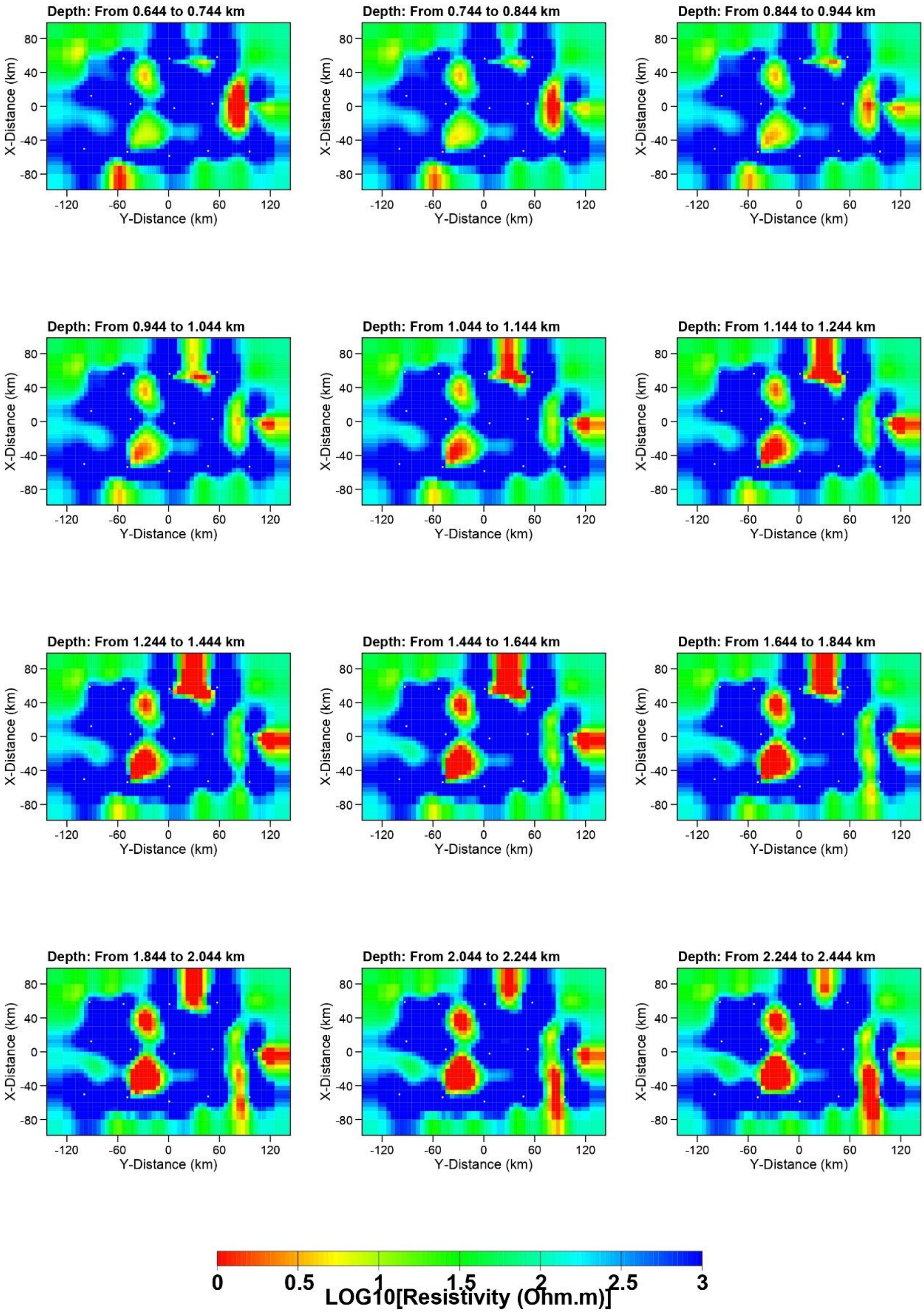
Depth: From 0.644 to 0.744 km
Depth: From 0.744 to 0.844 km
Depth: From 0.844 to 0.944 km
Depth: From 0.944 to 1.044 km
Depth: From 1.044 to 1.144 km
Depth: From 1.144 to 1.244 km
Depth: From 1.244 to 1.444 km
Depth: From 1.444 to 1.644 km
Depth: From 1.644 to 1.844 km
Depth: From 1.844 to 2.044 km
Depth: From 2.044 to 2.244 km
Depth: From 2.244 to 2.444 km
X-Distance (km)
Y-Distance (km)
80
40
0
-40
-80
-120
-60
0
60
120
0
0.5
1
1.5
2
2.5
3
LOG10[Resistivity (Ohm.m)]

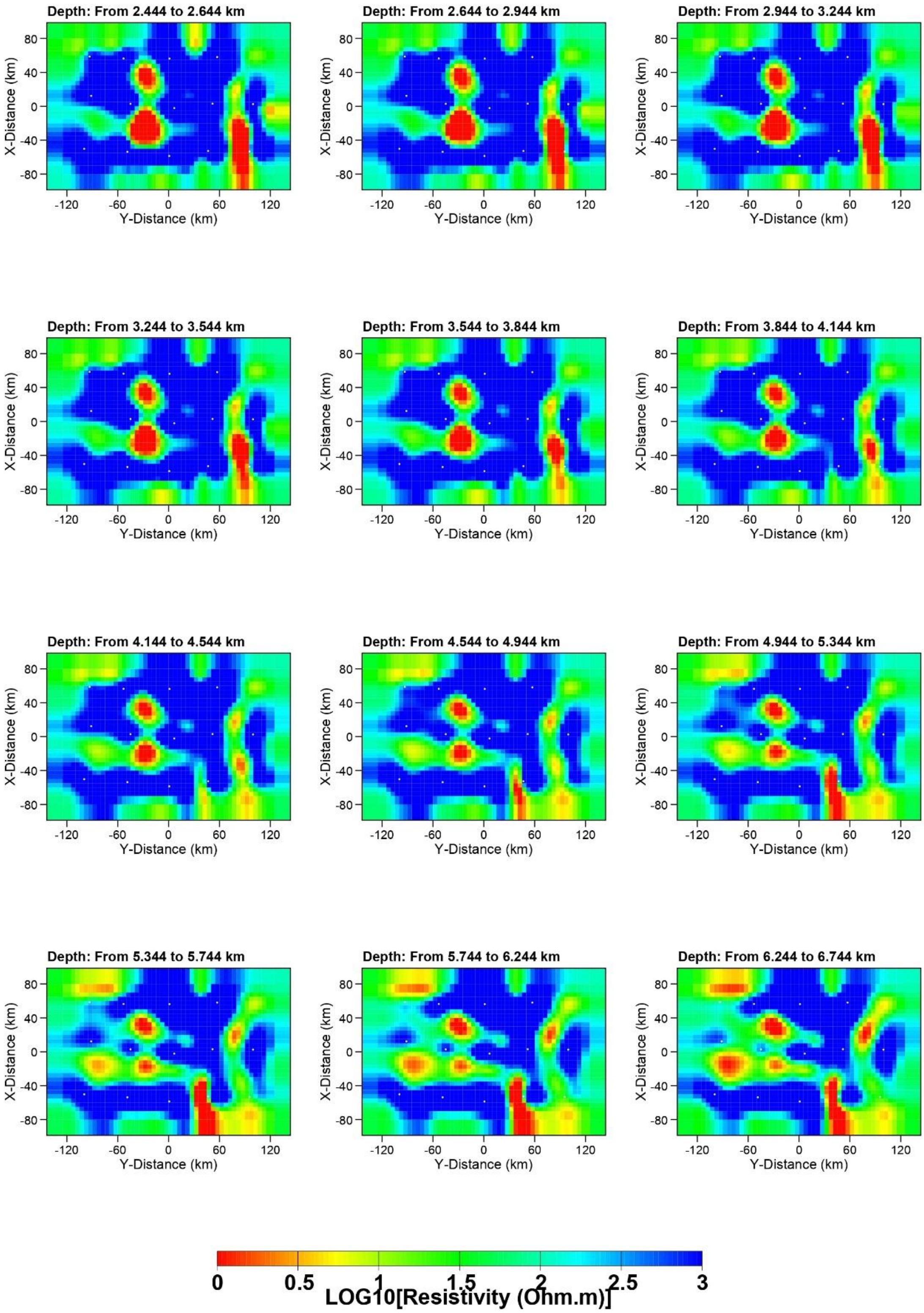

Depth: From 2.444 to 2.644 km
Depth: From 2.644 to 2.944 km
Depth: From 2.944 to 3.244 km
Depth: From 3.244 to 3.544 km
Depth: From 3.544 to 3.844 km
Depth: From 3.844 to 4.144 km
Depth: From 4.144 to 4.544 km
Depth: From 4.544 to 4.944 km
Depth: From 4.944 to 5.344 km
Depth: From 5.344 to 5.744 km
Depth: From 5.744 to 6.244 km
Depth: From 6.244 to 6.744 km
X-Distance (km)
80
40
0
-40
-80
Y-Distance (km)
-120
-60
0
60
120
0
0.5
1
1.5
2
2.5
3
LOG10[Resistivity (Ohm.m)]

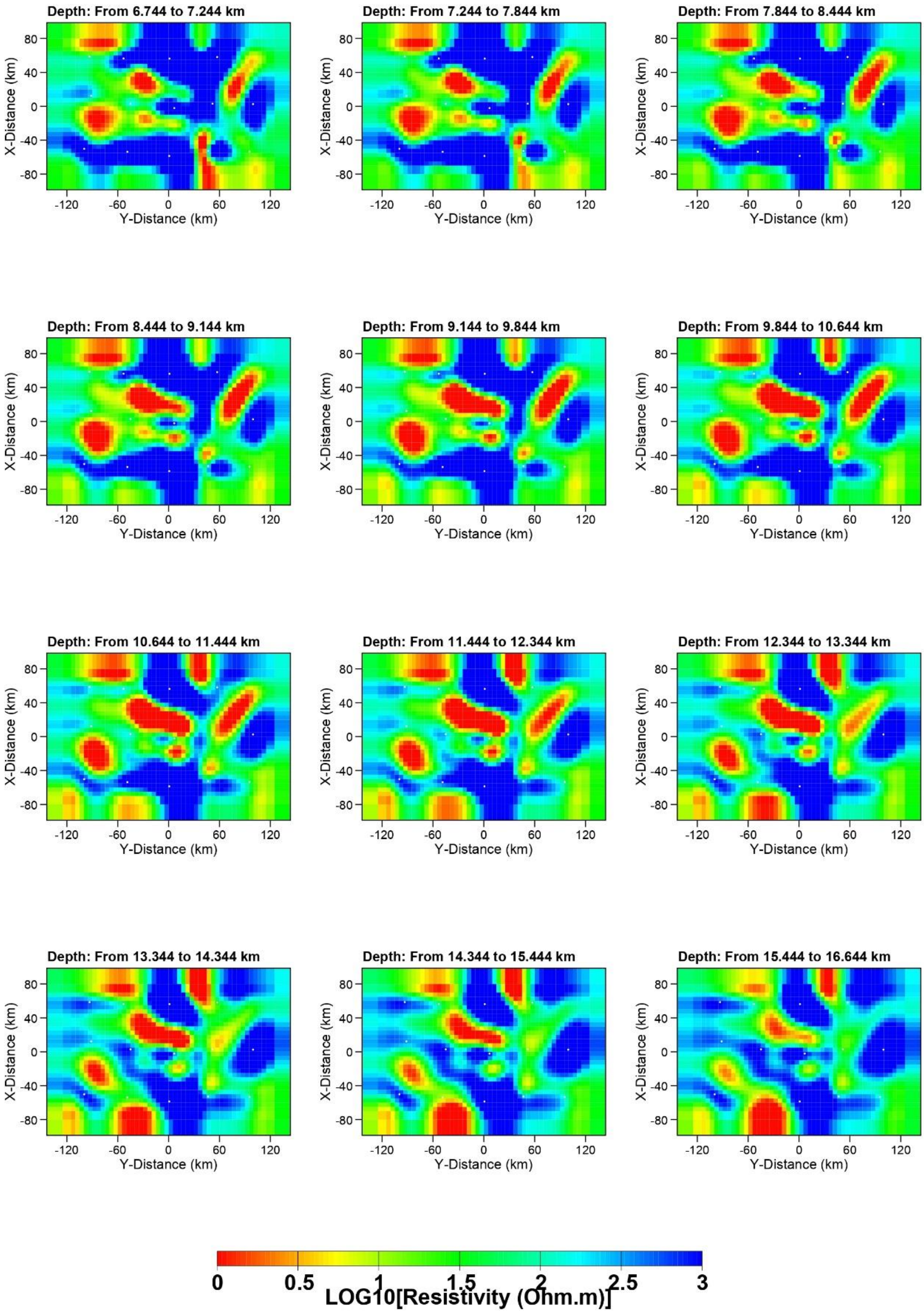
Depth: From 6.744 to 7.244 km
Depth: From 7.244 to 7.844 km
Depth: From 7.844 to 8.444 km
Depth: From 8.444 to 9.144 km
Depth: From 9.144 to 9.844 km
Depth: From 9.844 to 10.644 km
Depth: From 10.644 to 11.444 km
Depth: From 11.444 to 12.344 km
Depth: From 12.344 to 13.344 km
Depth: From 13.344 to 14.344 km
Depth: From 14.344 to 15.444 km
Depth: From 15.444 to 16.644 km
X-Distance (km)
Y-Distance (km)
80
40
0
-40
-80
-120
-60
0
60
120
0
0.5
1
1.5
2
2.5
3
LOG10[Resistivity (Ohm.m)]

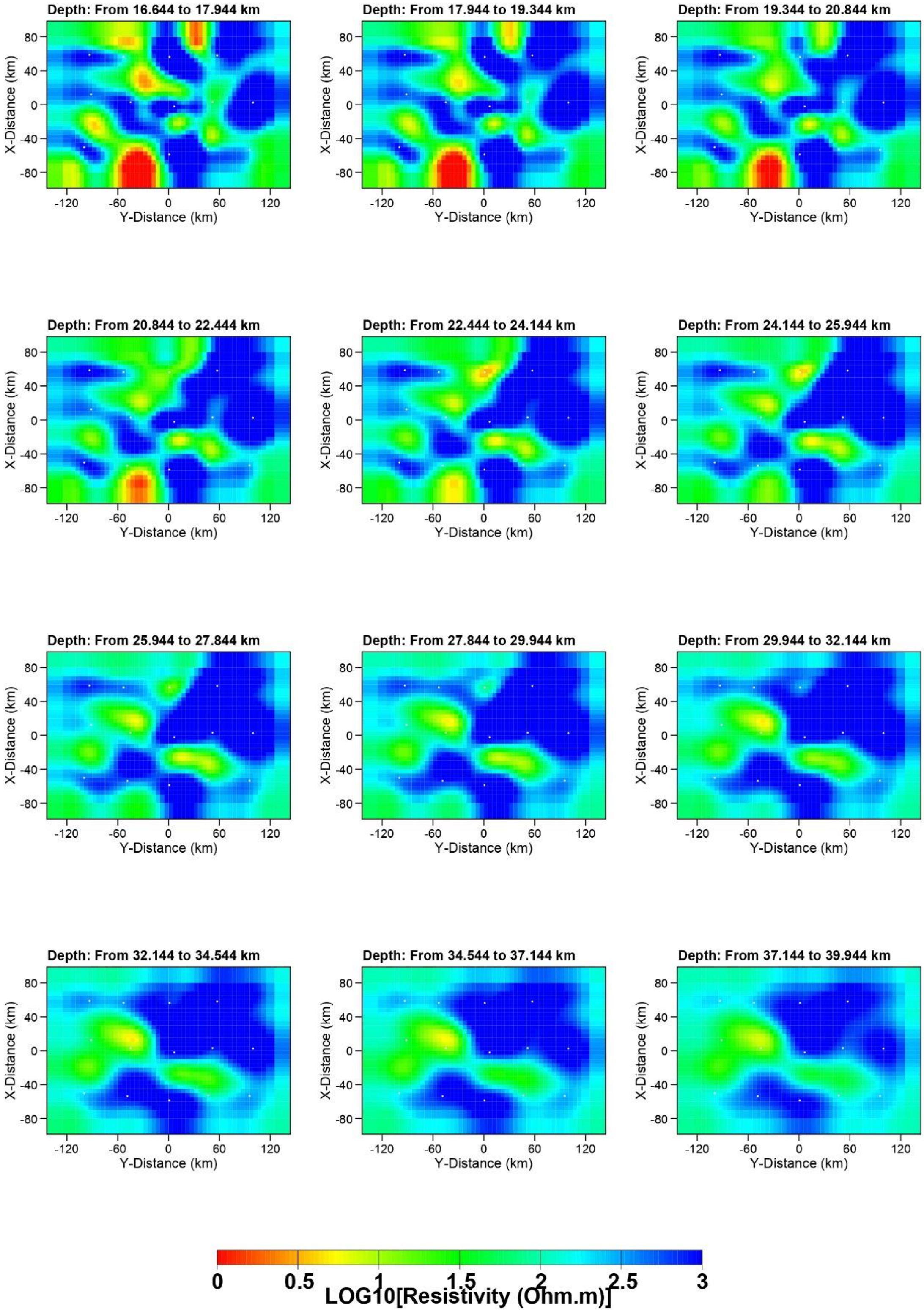

Depth: From 16.644 to 17.944 km
Depth: From 17.944 to 19.344 km
Depth: From 19.344 to 20.844 km
Depth: From 20.844 to 22.444 km
Depth: From 22.444 to 24.144 km
Depth: From 24.144 to 25.944 km
Depth: From 25.944 to 27.844 km
Depth: From 27.844 to 29.944 km
Depth: From 29.944 to 32.144 km
Depth: From 32.144 to 34.544 km
Depth: From 34.544 to 37.144 km
Depth: From 37.144 to 39.944 km
X-Distance (km)
80
40
0
-40
-80
Y-Distance (km)
-120
-60
0
60
120
0
0.5
1
1.5
2
2.5
3
LOG10[Resistivity (Ohm.m)]

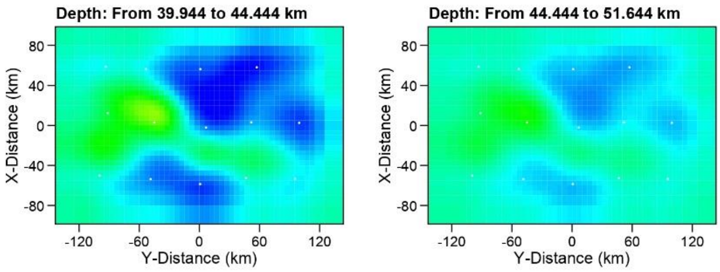
Depth: From 39.944 to 44.444 km
Depth: From 44.444 to 51.644 km
X-Distance (km)
Y-Distance (km)
80
40
0
-40
-80
-120
-60
0
60
120


0
0.5
1
1.5
2
2.5
3
LOG10[Resistivity (Ohm.m)]

Appendix E: X-Direction MT Inversion Model Slices

This appendix shows X-direction slices of the 3D MT Inversion model. Slices were extracted for every 5 km. The x-direction is north.

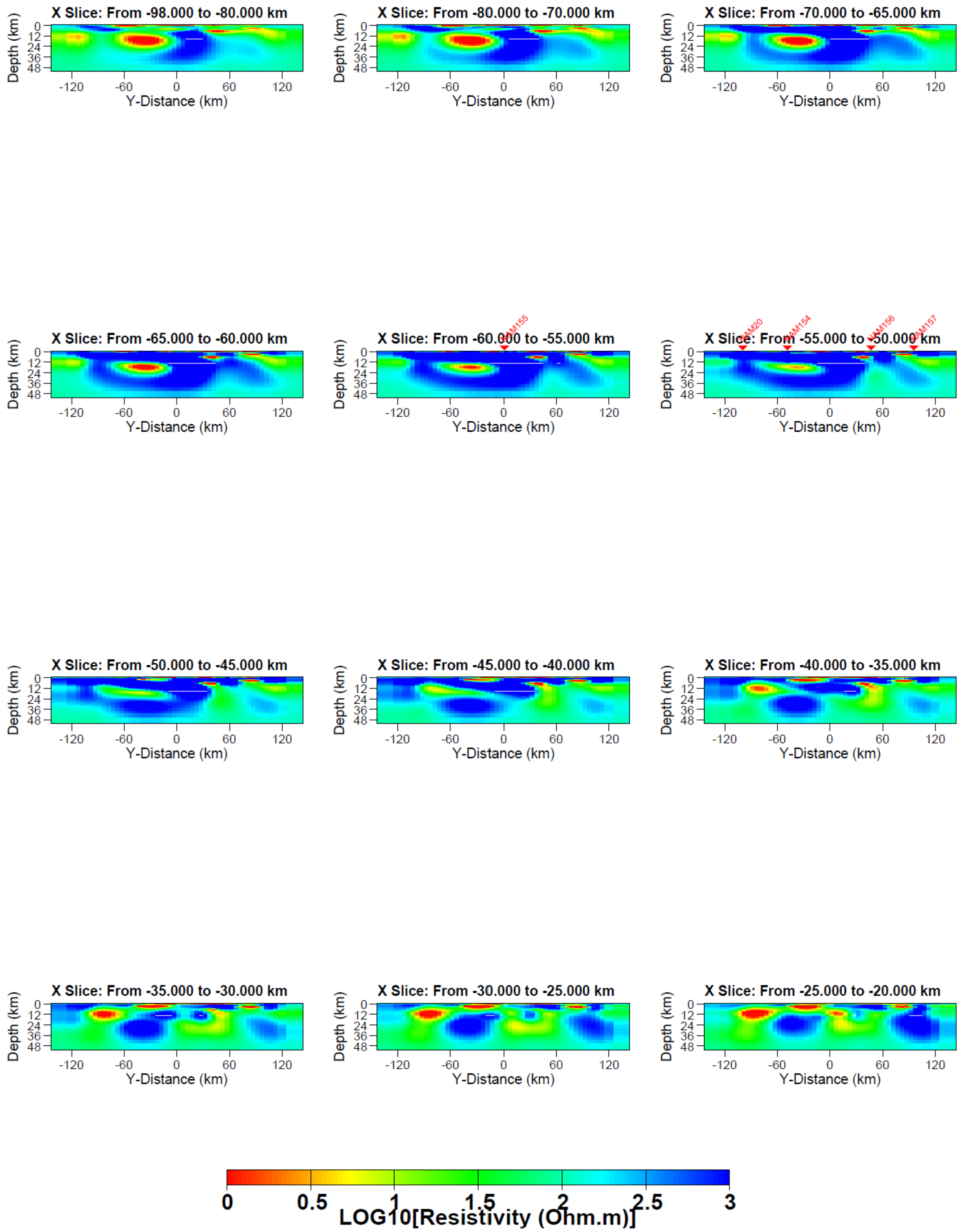

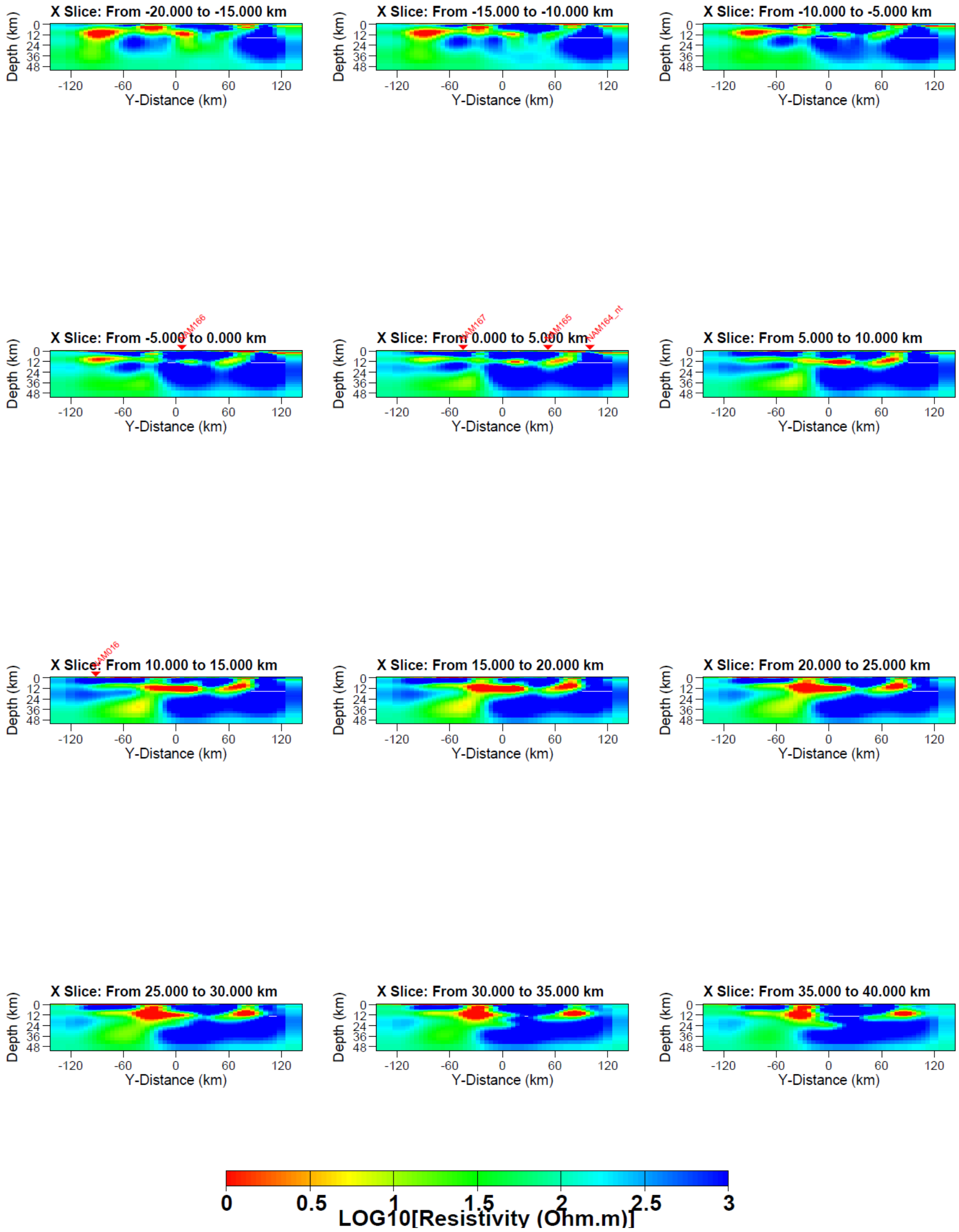
X Slice: From -20.000 to -15.000 km
X Slice: From -15.000 to -10.000 km
X Slice: From -10.000 to -5.000 km
X Slice: From -5.000 to 0.000 km
X Slice: From 0.000 to 5.000 km
X Slice: From 5.000 to 10.000 km
X Slice: From 10.000 to 15.000 km
X Slice: From 15.000 to 20.000 km
X Slice: From 20.000 to 25.000 km
X Slice: From 25.000 to 30.000 km
X Slice: From 30.000 to 35.000 km
X Slice: From 35.000 to 40.000 km
Depth (km)
0
12
24
36
48
Y-Distance (km)
-120
-60
0
60
120
0
0.5
1
1.5
2
2.5
3
LOG10[Resistivity (Ohm.m)]

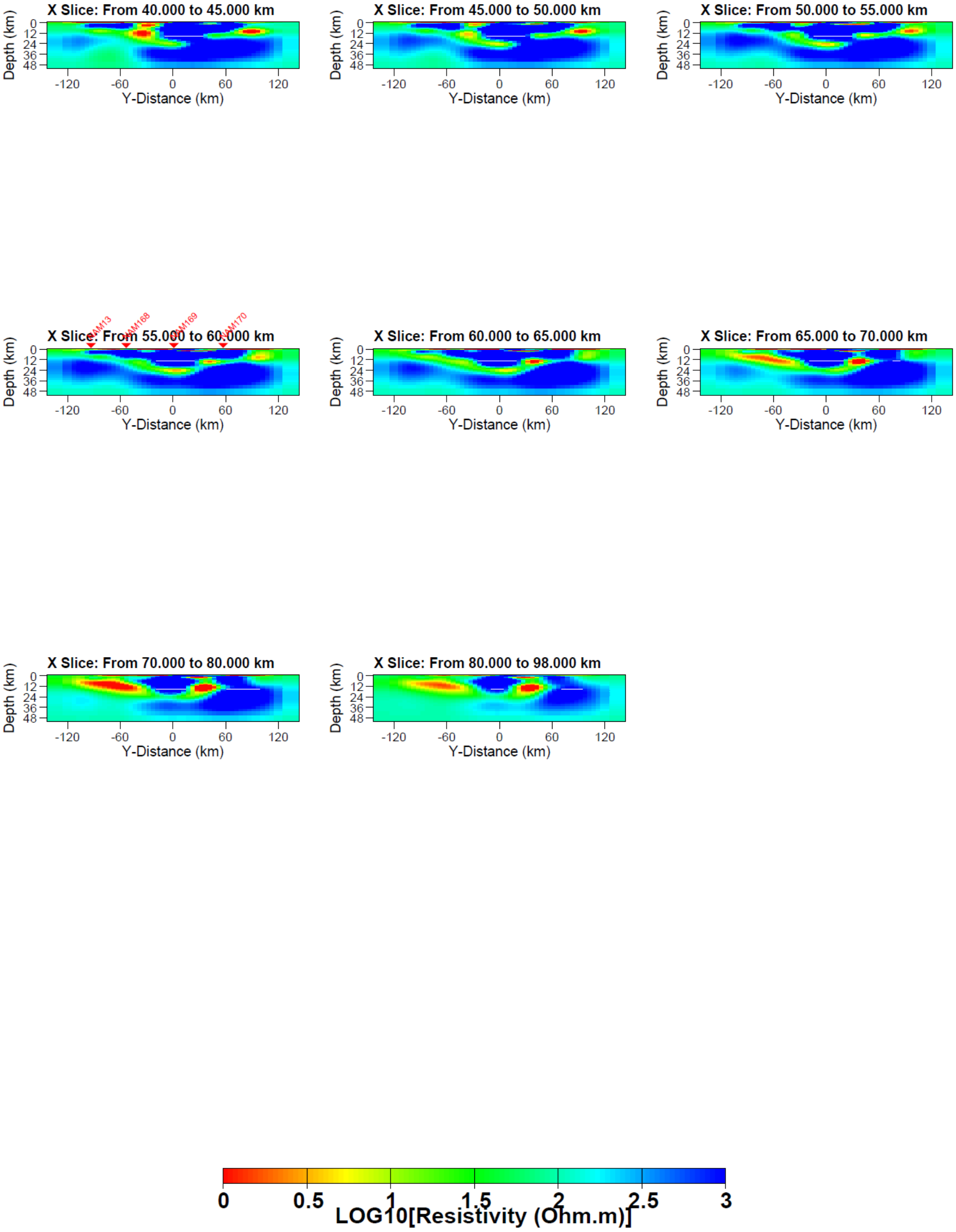
X Slice: From 40.000 to 45.000 km
X Slice: From 45.000 to 50.000 km
X Slice: From 50.000 to 55.000 km
X Slice: From 55.000 to 60.000 km
X Slice: From 60.000 to 65.000 km
X Slice: From 65.000 to 70.000 km
X Slice: From 70.000 to 80.000 km
X Slice: From 80.000 to 98.000 km
Depth (km)
0
12
24
36
48
-120
-60
0
60
120
Y-Distance (km)
0
0.5
1
1.5
2
2.5
3
LOG10[Resistivity (Ohm.m)]